EUROPEAN ORGANIZATION FOR NUCLEAR RESEARCH

CERN/EF 90-3
30 January 1990

HOLOGRAPHY OF PARTICLE TRACKS IN THE FERMILAB 15-FOOT BUBBLE CHAMBER

E-632 Collaboration(*)

ABSTRACT

During a quadrupole-triplet neutrino experiment with the 15-Foot Bubble Chamber at Fermilab, a large number of events was recorded on ~ 110,000 good holograms, which were taken simultaneously with the conventional three-view photographs. The holograms show an important improvement of the resolution, which allows a study of event vertices in a large volume with greatly improved precision. The experimental set-up, including an innovative pulse stretching circuitry for a powerful holographic laser, an optical relay system for the laser beam transport, and an on-line monitoring system for this beam are described. The experience with the operation of the system, and preliminary results obtained during the study of holograms with the newly developed real- and virtual-image replay machines, will be discussed.

Submitted to Nuclear Instruments and Methods in Physics Research

---

(*) Berkeley, Birmingham, Brussels (ULB-VUB)/Antwerp, CERN, Chandigarh, Fermilab, Hawaii, Illinois Institute of Technology, Imperial College London, Jammu, Munich (MPI), Oxford, Rutgers, Rutherford Appleton Laboratory, Saclay, Stevens Institute of Technology, Tufts

EF/4702F/GGH

H. Bingham, J. Lys
University of California,
Berkeley, CA 94720, USA

L. Verluyten[(*),(&)], S. Willocq[1]
Interuniversity Institute for High Energies (ULB-VUB),
B-1050 Brussels, Belgium
and
Fermilab,
Batavia, IL 60510, USA

J. Moreels
Interuniversity Institute for High Energies (ULB-VUB),
B-1050 Brussels, Belgium

K. Geissler, G.G. Harigel, D.R.O. Morrison
CERN,
CH-1211 Geneva 23, Switzerland

F. Bellinger[2], H. Bjelkhagen[3], H. Carter, J. Ellermeier, J. Foglesong,
J. Hawkins, J. Kilmer, T. Kovarik, W. Smart, J. Urbin, L. Voyvodic, E. Wesly[4],
W. Williams
Fermilab,
Batavia, IL. 60510, USA

R.J. Cence, M.W. Peters
University of Hawaii,
Honolulu, HI. 96822, USA

R.A. Burnstein, R. Naon
Illinois Institute of Technology,
Chicago, IL. 60616, USA

P. Nailor[5]
Imperial College,
London SW7, UK

M. Aderholz
Max-Planck-Institut für Physik und Astrophysik
D-8000 München 40, FRG

G. Corrigan[6]
University of Oxford,
Oxford OX1 3RH, UK

R. Plano
Rutgers University,
New Brunswick, NJ. 08903, USA

R.L. Sekulin, S. Sewell[7]
Rutherford Appleton Laboratories,
Didcot OX110QX, UK

E.B. Brucker
Stevens Institute of Technology,
Hoboken, NJ. 07030, USA

H. Akbari[8], R.H. Milburn, D. Passmore, J. Schneps
Tufts University,
Medford, MA. 02155, USA

(*) Also Universitaire Instelling Antwerpen, B-2610 Wilrijk, Belgium
1 Now at Tufts University, Medford, MA. 02155, USA
2 Now at Argonne National Laboratory, Argonne, IL. 60439, USA
3 Now at Northwestern University, Evanston, IL. 60208, USA
4 Now with Lake Forest College, Lake Forest, IL 60045, USA
5 Now with Scientific Generics, Cambridge, UK
6 Now with Tessella Support Services Ltd., Abingdon, UK
7 Now with Autofile Ltd., Slough, UK
8 Now at Johns Hopkins University, Baltimore, MD. 21218, USA
(&) Researcher IIKW, Brussels, Belgium

1. INTRODUCTION

Holography offers the possibility of photographing large volumes with better resolution than obtainable with conventional optics. This is of particular interest for the study of elementary particle interactions in gaseous or liquid detectors, where one searches for rare interactions with short lifetimes (i.e. short track lengths). The feasibility of this technique had been demonstrated for the first time in a 120-cm^3 bubble chamber (Berne Infinitesimal Bubble Chamber BIBC [1]). The exposure of a 2-ℓ chamber (HOlographic Bubble Chamber HOBC [2]) in a hadron beam at CERN resulted in 40,000 holograms, which were analyzed. However, bubble chambers operated in neutrino beams are the most useful applications of this technique [3, 4]. In the large cryogenic bubble chambers [3] the aim is to holograph bubbles in a volume of up to several cubic meters ~ 1 ms after their creation, when they have grown to only ~ 100 μm in diameter. These holograms supplement the conventional stereophotographs of particle tracks taken some ten milliseconds later, when the bubbles have grown to diameters of ~ 400 μm. These two techniques combine the advantages of a quick overall view, easy event recognition and track measurement in the conventional photographs, with the more detailed picture of the interesting event vertex region in the holograms.

The present paper describes the experience with holography in the 15-Foot Bubble Chamber at Fermilab, gained during a technical run (1984) and two physics runs (1985 and 1987/88). The Chamber was exposed to a quadrupole-triplet neutrino beam with 800 GeV/c protons from the Tevatron on the production target. In the second physics run, 293,060 conventional 3-view pictures and ~ 218,000 holograms, of which ~ 110,000 are useful for physics analysis, were recorded simultaneously. The analysis of these photographs and holograms is in progress and some preliminary results from the scanning of the holograms will be presented.

We limit ourselves here to a description of the modified single-beam holography. The basic idea had been developed by C. Baltay of Columbia University [3, 5] and was tested earlier in the Big European Bubble Chamber (BEBC) at CERN [6, 7]. First results from the application of this technique in the 15-Foot Bubble Chamber can be found in refs [8-11]. The main emphasis of this paper is on the technical aspects of the layout used in the second physics run and on the practical experience with this system. Descriptions of replay machines built for the analysis of these holograms are given in refs [12-16]. Features of two-beam illumination systems for large volume holography can be found in refs [17, 18].

In sect. 2, we describe the theory and design considerations of our modified single-beam technique, with emphasis on the layout of the illumination system, its adaption to the existing geometry of the 15-Foot Bubble Chamber, and on a variety of effects due to non-static conditions during the recording of holograms. In sect. 3, details are presented on the layout of the holographic system, including our modifications of the commercial holographic laser, the transport and monitoring of the laser beam, and the design of the dispersing lens. Also in this section are described the synchronisation of the laser pulse with the neutrino beam pulse, and a replay facility used during the run for the monitoring of the hologram quality. Sect. 4 gives an overview of our experience with the system during several months of running, concentrating on laser-induced boiling and how we reduced it to an acceptable level. Furthermore, preliminary results obtained during the replay of a small sample of holograms are given, which show that we achieved the expected resolution over a large volume. Sect. 5 contains a summary of our new developments and a brief outlook on further applications of the technique.

2. THEORY AND DESIGN CONSIDERATIONS OF THE MODIFIED SINGLE-BEAM TECHNIQUE

A hologram is formed by the interference of coherent light from a reference beam with the coherent light scattered by objects. In our case the objects are vapour bubbles with a refractive index of $\sim$ 1.0 in a liquid with an index of $\sim$ 1.088.

In two small bubble chambers, operated with liquids above room temperature [1, 2], a in-line, or Gabor-type illumination was used: an expanded parallel laser beam passes through the liquid onto the holographic film. Only a small part of this beam is diffracted by the bubbles and interference between the diffused and non-diffused waves produces fringes which are recorded by the emulsion. For HOBC [2], two-beam geometries were tested, where the reference beam did not pass through the medium to be holographed. These were unnecessarily complicated and did not improve the quality of track recording. Due to the layout of our existing 15-Foot Bubble Chamber, having a volume more than three orders of magnitude larger than that of the small chamber HOBC, we had to modify the standard holographic techniques.

We describe the experimental scheme (as used in the second physics run), in which the object and reference beam are combined in a new way. The laser beam enters the Bubble Chamber (fig. 1), filled with a 63/37 mole percent Ne/H_2-mixture, at its bottom through a specially designed aspheric diverging lens, which also serves as an entrance window. This lens - a sophisticated beam-splitter - is designed so that only a small part of the laser light goes through the liquid to a set of three concentric hemispherical windows (fisheye lenses) on the opposite side of the Chamber directly onto the film. This reference beam exposes completely the 70 mm holographic film format. The rest of the beam illuminates the tracks within a conical volume. The intensity of this object beam is designed to increase at large angles to partly compensate for the decrease of the light scattered by the bubbles at these angles. Some elementary formulas, together with estimates based on experience in the smaller bubble chambers, are given in ref [6]. The latter contains data on the optical resolution of such a system, the energy needed to illuminate a given volume, the ratio of intensities of object to reference beam (Beam Branching Ratio), and the required resolution of the photographic emulsion. These data will be re-evaluated in the context of our recent experience. A large coherence length, and a Gaussian-like spatial distribution (TEM_{oo}-mode) of the beam from the oscillator stage, together with a fairly uniform profile of the amplified laser beam over the aperture of the dispersing lens are important laser beam properties for our experiment.

In applying this modified single-beam technique to holography of tiny bubbles in a cryogenic multi-cubic-meter Bubble Chamber, several disturbing experimental effects had to be controlled. The most serious of these disturbances arise from: (a) excessive heating of the cryogenic liquid by the intense laser light, causing parasitic bubble creation and thereby unwanted scattered light, (b) vibration of the equipment during the mechanical expansion of the liquid, and (c) movement and growth of track bubbles during the laser illumination. Furthermore, (d) multiple scattering of the laser light from the Chamber wall, which is covered with a reflecting material (Scotchlite), can spoil the quality of the hologram, lower the contrast, and decrease the visible volume.

We give here some of the design considerations which govern the choices of laser energy, pulse length, and light distribution inside the Bubble Chamber needed to maximize the volume recorded in the hologram. These considerations also indicate hardware changes which help to achieve this goal.

2.1 Effect of Background Light (Noise) Hitting the Holographic Film

The information available to be recorded on the holographic film is the fringe pattern formed by the interference of the reference beam and the object beam (i.e. the light scattered by a bubble). Therefore, bubbles which give the same fringe modulation (M), and are at the same Θ_h (fig. 2), will be equally well recorded on the film and be equally bright in the replayed hologram.

We define the Beam Branching Ratio (BBR) as the intensity, on the holographic film, of the laser light scattered from a single bubble, divided by the reference beam intensity. The BBR in this application is given by the formula

$$BBR = \frac{F(\Theta_i) \bullet r^2 \bullet G(\alpha) \bullet \cos(\Theta_h)}{I_r \bullet d_l^2 \bullet d_f^2}$$

with (fig. 2)

- r : bubble radius,
- d_l : distance between the bubble and the dispersing lens,
- d_f : distance between the bubble and the holographic film,
- Θ_i : illumination angle,
- α : scattering angle,
- Θ_h : angle between the reference beam and the scattered beam from the bubble at the film,
- I_r : reference beam intensity,
- $F(\Theta_i)$: illumination intensity distribution per solid angle,
- $G(\alpha)$: scattering function (fig. 3, [19]).

In the geometry described above, once the light output distribution from the dispersing lens is fixed by the shape of the lens and the spatial distribution of the input laser beam, the BBR is determined (for 100 µm bubbles) at every point in the illuminated volume of the Chamber, and this ratio can be taken over any area on the film. The output energy of the laser is then adjusted to give the proper exposure of the film. We define:

$I_r = E_r^2$ = intensity on the film plane of the reference beam (from the dispersing lens),

$I_b = E_b^2$ = intensity on the film plane of the light scattered from a bubble,

$BBR = I_b / I_r$

$r = \sqrt{BBR} = |E_b| / |E_r|$

I_x = Maximum intensity on film plane (where E_r & E_b constructively interfere)

I_m = Minimum intensity on film plane (where E_r & E_b destructively interfere)

$M = (I_x - I_m) / (I_x + I_m)$ = Fringe modulation on film plane

Assuming that $E_r \gg E_b$, then

$I_x = (E_r + E_b)^2 = E_r^2 + 2 E_r \bullet E_b$

$I_m = (E_r - E_b)^2 = E_r^2 - 2 E_r \bullet E_b$

$M = 4 E_r \bullet E_b / 2 E_r^2 = 2 r$

If there are other sources of light hitting the film, this calculation must be modified. In our setup, background laser light (noise from, for example, multiple reflections off the Chamber walls) hitting the film will be proportional to the overall laser intensity and hence proportional to the reference beam intensity, $I_n = k \bullet I_r$. The intensity of the light on the film is now $I_r + I_n = I_r (1 + k)$, and we must reduce the overall laser beam intensity to avoid overexposing the film. A new laser intensity of $1 / (1 + k)$ times the original will give the same exposure on film:

$I_{n'} = I_n / (1 + k)$

$I_{r'} = I_r / (1 + k)$

then

$I_{r'} + I_{n'} = (I_r + I_n) / (1 + k) = (1 + k) \bullet I_r / (1 + k) = I_r$

Proceeding as above, but including the noise intensity: using

$I_{x'} = (E_{r'} + E_{b'})^2 + I_{n'}$, , etc. results in

$M' = 2\,r / (1 + k)$

and we see that the net effect of the noise is to reduce the fringe modulation. If the noise were equal to the reference beam (k = 1), the laser output must be lowered to one half the original energy and the fringe modulation has been reduced to one half the original value.

Defining BBR' ($= r'^2$) as the Beam Branching Ratio needed, with noise, to get the same fringe modulation as was obtained without noise:

$M' = M$

$2\,r' / (1 + k) = 2\,r$

$r' = r \bullet (1 + k)$, or

$BBR' = BBR \bullet (1 + k)^2$

thus, the presence of noise requires a higher BBR to obtain the same fringe modulation; in case of noise equal to reference beam intensity, a factor of four times higher BBR is needed.

We then assume that all bubbles whose fringe modulation (M) is higher than a certain limiting value will be visible in the replayed hologram. The dispersing lens shape was optimized to give the largest volume with a BBR of $0.33 \bullet 10^{-7}$ or greater for the lowest light input. Assuming that this corresponds to the M for which a bubble is just visible, adding noise light equal to the reference beam (k = 1) would then require at least a BBR of $1.33 \bullet 10^{-7}$ for a bubble to be visible. Referring to fig. 4, one sees that such noise would drastically reduce the volume visible in the hologram.

One source of such noise could be multiple reflections of the laser light inside the Bubble Chamber. The magnitude of this effect can be estimated with a simple calculation: if 10 Joules of laser light is sent into the Bubble Chamber, the average light intensity on the Chamber walls is 20 $\mu J/cm^2$. The holographic film is part of the wall and requires ~ 0.9 $\mu J/cm^2$ laser light to give the desired density. The average noise light is ~ 20 times the intended point source reference beam, indicating a potential problem. During the first physics run, hologram quality was degraded if more than ~ 0.6 Joule of laser light was sent into the Bubble Chamber. To solve this problem, baffles were designed and installed on the Chamber walls for the second physics run. These baffles trapped and absorbed the laser light after it had crossed the Chamber once (sect. 4.1).

Another potential source of noise laser light hitting the film is the multiple reflections inside the dispersing lens. Of the ≦ 10 J going through this lens, only 36 μJ is intended to hit the film (area = 40 cm^2) as the reference beam. Any of this intense laser light multiple reflected in the dispersing lens and hitting the film would add to the exposure and must be counted as noise, because it is not part of the point source beam used to construct the hologram. To prevent this, the dispersing lens was designed to function also as the Bubble Chamber pressure window, eliminating two potentially reflecting surfaces; the shape of all the dispersing lens surfaces were carefully adjusted, with the aid of a ray tracing program, to make serious multiple reflections miss the film; light absorbing baffles were placed between the lens elements and finally the surfaces in the laser beam were "Vee" anti-reflection coated (sect. 3.6).

When the Bubble Chamber was sensitive, the intense laser beam near the dispersing lens could induce bubble formation. Later in the laser pulse, these bubbles had grown large enough to scatter significant illumination light directly onto the film, becoming another source of noise laser light. Since this "microboiling" depends on the amount of microscopic particles (N_2, H_2O) suspended in the Bubble Chamber liquid, this source of noise laser light proved very hard to control, and is thought to be responsible for much of the variation in hologram quality throughout the run. The amount of microboiling noise laser light could be measured directly for each pulse by comparing the temporal shape of the output of a fast photodiode next to the holographic film with one at the laser output (sect. 4.4). In order to reduce the laser beam intensity where it entered the Bubble Chamber liquid, the dispersing lens was designed so the output beam almost filled the 20-cm diameter of the lens (sect. 3.6).

2.2 Effects of Bubble Growth and Movement, and Vibrations During the Laser Pulse

As will be discussed in sect. 3.2, the need to prevent boiling of the Bubble Chamber liquid by the incident laser energy (≦ 10 J) necessitates the use of a "stretched" laser pulse (≧ 1 μs), rather than the more normally used Q-switched pulse (~ 30 ns), in order to minimize the instantaneous power flux in the pulse. This meant that, in principle, the effects of bubble growth and movement and of mechanical vibrations could cause a significant path length difference change between the reference and object beams during the laser pulse. The resulting changing phase between the two amplitudes reduces I_x and increases I_m giving a lower fringe modulation. We assume the phase changes linearly with time during the laser pulse, and we consider the desired "square wave" (i.e. intensity constant with time) laser pulse. Rewriting I_x (from the previous section) to include a phase angle β between E_r and E_b (where β varies during the duration of the laser pulse)

$\Delta P / \lambda$ = Instantaneous path length difference / wavelength

$\beta = 2\pi \bullet \Delta P / \lambda$

$I_x = E_r^2 + 2E_r \bullet E_b \bullet \cos \beta$

I_x is then integrated over β from $-\delta$ to δ, choosing a central value of $\beta = 0$ to give the maximum intensity:

$$I_x = E_r^2 + 2E_r \bullet E_b \bullet (\sin \delta) / \delta$$

with a total path length difference change ($\Delta P / \lambda$) equal to δ / π from the beginning to the end of the laser pulse.

After I_m has been calculated in a similar manner, we find the fringe modulation

$$M' = 2r \bullet (\sin \delta) / \delta$$

has been multiplied by a factor $(\sin \delta) / \delta$, which is less than or equal to 1.0. Defining BBR' ($= r'^2$) as the Beam Branching Ratio needed, with path difference change, to get the same fringe modulation as was obtained without this change:

$M' = M$

$2r' \bullet (\sin \delta) / \delta = 2r$

$r' = r / (\sin \delta / \delta)$, or

$BBR' = BBR / (\sin \delta / \delta)^2$

For a path length difference change of 1/4 λ ($\delta = \pi/4$), we require 1.23 times the BBR to get the same fringe modulation as we had without the change; this is a barely acceptable upper limit. If the change is limited to 1/8 λ, the factor is only 1.05 times the BBR.

Bubble diameters (D) grow according to $D = 2A \bullet \sqrt{t}$, where t is the time since growth started and A is a constant depending on the operating conditions (see sect. 4.2 for details). Assuming the Chamber is operated to grow our desired 100-μm bubbles in 1 ms, the bubble diameter is then growing at a rate of 0.1 μm/μs.

The optical path difference change for light scattered at an angle α off a bubble which has grown in diameter by ΔD is shown in fig. 5. For light which reflects off the bubble:

$$\Delta P = \Delta D \bullet n_l \bullet \sin(\alpha/2),$$

where $n_l = 1.088$ = refractive index of liquid Ne/H_2.

The expression for light refracting through the bubble is more complicated and will not be given here, but its value is shown in fig. 6 and agrees with the above expression within 5% for $\alpha > 23°$.

For a bubble with its diameter growing at 0.1 μm/μs, at an α of 30° (45°), the path difference change will be 1/4 λ for a laser pulse length of 12.3 (8.3) μs. Laser pulse lengths of 1/2 these values would be required to limit the change in path length difference to the more desirable 1/8 λ.

During the first physics run, before this calculation had been made, most of the holograms were taken with 40-μs laser pulses and with higher bubble growth rates. This unfortunate choice clearly extracted a heavy penalty, both in the quality and in the volume of the Chamber that could be recorded in those holograms [11]. Laser pulse lengths of 7.5 μs or less were used during the second physics run.

Motion of the bubbles during the laser pulse has an effect similar to bubble growth.

Track and bubble movement can be subdivided into two main categories: in their displacement together with the liquid due to its compressibility during expansion and recompression, and relative to the surrounding liquid, mainly due to buoyancy forces.

- The isentropic compressibility of our neon/hydrogen mixture is $1 \bullet 10^{-3}$ cm^2 kg^{-1} [20]. The expansion ratio is $\Delta V/V \simeq 0.6\%$, V being the total liquid volume. The bubble movement together with the liquid is a function of the distance from the piston: it is more pronounced near the bottom of the Chamber than near the top (no displacement near the top, maximum displacement near the piston). Furthermore, it depends upon the time when the tracks are produced: before the piston reaches its lowest position during expansion this displacement will be downwards, and during the recompression upwards. However, since the beam is injected during the pressure minimum, when the piston is at its lowest position and almost at rest, we can neglect the bubble movement together with the liquid.

- Theoretical predictions of the lift velocity of a bubble show only a slight dependence on temperature in the limited operating range of bubble chambers, but a strong dependence on the actual bubble diameter. A change of speed occurs when a diameter of D ~ 0.2 mm is reached during the growth (or recompression) process, i.e. when laminar flow turns into turbulent flow (or vice versa). Measurements had been made in liquid hydrogen in the condition of turbulent flow and gave a constant value of $\leqq$ 20 cm/s, in good agreement with theory [21]. For our liquid mixture we expect values of the same order. Bubbles to be photographed with holography will have attained, however, only diameters of 0.1 to 0.2 mm. Therefore, we still have laminar flow and the lift velocity of bubbles is expected to be proportional to their diameter squared: 1 to 3 cm/s, respectively.

The change in optical path difference for light scattered at an angle α off a bubble which has moved during the laser pulse is shown in fig. 7. Only the component (d) of bubble motion which is along the bisector of the incoming and the scattered light rays contributes a path difference change; motion in the orthogonal directions contributes no change:

$$\Delta P = 2d \bullet \sin(\alpha/2)$$

For a bubble moving along the bisector with a speed of 0.03 μm/μs, at an angle α of 30° (45°), the path length difference change will be 1/4 λ for a laser pulse length of 11.2 (7.6) μs. Laser pulse lengths of 1/2 these values would be required to limit the change in path length difference to the more desirable 1/8 λ. Most bubbles will have only a fraction of their velocity along this direction; if the motion directions were random, the average of the absolute value of the projection along this axis would be 1/2 of the speed.

If the bubble motion is upward, due to buoyancy, the magnitude of the effect will vary in different regions of the holographic volume. In our experiment, the laser axis (i.e. the direction of the reference beam through the Chamber), was inclined at an angle β = 56.2° with the horizontal. We define an azimuthal angle γ about this axis with γ = 0 in the horizontal direction. In the holographic midplane, $d = z \bullet \cos\beta \bullet \sin\gamma$, where $\cos\beta$ = 0.56 and z is the upward bubble displacement. Bubbles exactly to the left or right will not be affected, those above or below the axis will have the largest effect. Nearer the film than the midplane, the effect becomes even larger for bubbles above the axis and less for those below; the reverse is true for bubbles on the dispersing lens side of the midplane.

Vibrations of the dispersing lens and holographic film are induced when the Bubble Chamber is expanded to drop the pressure in order to make the fluid track sensitive. No actual measurements of the vibrations of these components were made during these physics runs, but previous experience indicates that accelerations were less than 5 g and displacements less than 0.1 cm. With these limits, the maximum velocity would be 22 cm/s at a frequency of 35 Hz. Even though this velocity was reached at some time during the expansion cycle, the velocity at the instant the hologram was taken would likely be only a small fraction of the maximum.

If the dispersing lens moves a distance ε perpendicular to the laser axis, the reference beam path length does not change. The object beam path length to a bubble at an angle Θ with the laser axis, as viewed from the lens, will change by $\varepsilon \bullet \sin \Theta$. If the motion is along the axis, the reference beam path length changes by ε. The object beam path length will change by $\varepsilon \bullet \cos \Theta$, giving a net change in path difference of $\varepsilon \bullet (1 - \cos \Theta)$. Similar expressions hold for motions of the holographic film, except the angle is now φ, the angle of the bubble with the axis as viewed from the film. Since these angles are limited to 30° or less in our application, the perpendicular displacements produce larger path difference changes.

For motion of the dispersing lens perpendicular to the laser axis with a speed of 0.22 μm/μs, at an angle Θ of 15° (30°), the path difference change will be 1/4 λ for a laser pulse length of 3.0 (1.6) μs. However, these pulse lengths are unduly restrictive, both because the maximum velocity is unlikely to occur at the instant of taking the hologram and because the actual vibrations are probably less than the maximum estimate made above.

All three of these effects (bubble growth, bubble motion, and vibration) generally increase in magnitude as the scattering angle α increases. For the first two effects and for the effect of vibrations on bubbles in the holographic midplane the variation is as $\sin(\alpha/2)$, vibrations on bubbles out of the midplane show an approximate $\sin(\alpha/2)$ dependence. Since the light scattered from a bubble decreases rapidly as α increases, the BBR and fringe modulation are already low for bubbles at large α. Usually a good hologram can still be made of bubbles at smaller α, because these effects are smaller and these bubbles started with a higher BBR and more "reserve" fringe modulation. A measurement of the holographic volume is needed to judge the magnitude of these optical path length change effects; some conclusions are drawn from the preliminary measurement of this volume (1.5 m^3) in sect. 4.

The main parameter available to reduce these effects is to shorten the laser pulse length. This must be balanced against the occurence of laser-induced boiling (sect. 4.2), which is reduced by increasing the laser pulse length. Since none of these effects (especially vibrations), nor laser-induced microboiling are well understood, the best compromise laser pulse length must be determined experimentally. Also, the temporal shape of the laser pulse should be as close to "square wave" as possible, in order to reduce the instantaneous power of the beam.

2.3 Laser Light Distribution in the Bubble Chamber

Our goal was to view the interaction point of high energy neutrinos in the Bubble Chamber with high resolution in order to study particles with short lifetimes which decay within a few millimeters. While the geometric cross section of the neutrino beam is larger than the diameter of the Chamber, and while events could occur anywhere within the 28-m^3 visible volume, the events are more concentrated near the center of the Chamber. To properly analyze these events in the conventional pictures, we only accept interactions with their vertex inside a restricted "fiducial volume" of $\sim$ 12 m^3. The main reason for restricting this volume is to allow sufficient track length for the interaction products in the visible volume to accurately measure angles and momenta.

While we would like to record as much of this fiducial volume in the hologram as possible, there are practical limits. The amount of light scattered by a bubble drops steeply as the scattering angle α increases (ref. [19] and fig. 3), requiring more and more laser light to record bubbles with large α's. Laser-induced boiling gives the first limit on how much light can be sent to the Chamber, but the limit of total light available from a pulse-stretched holographic ruby laser with present technology is not far behind. More sensitive high resolution fine grain holographic film would be a solution, but the Agfa-Gevaert 10E75, pushed by developing with phenidone, is already the most sensitive available on today's market. Sending more light into the Chamber also places a heavier burden on the light absorbing baffles and reflection prevention design of the dispersing lens, as discussed in sect. 2.1.

We decided to limit the illumination half-angle Θ to 30° from the laser axis, with a reference beam of 0.9 $\mu J/cm^2$ (needed to expose adequately our film). To find the optimum light distribution from the lens, a computer program was used which divided the field into 1/2° Θ bins, and then added energy to the bin where the least amount of energy would make the next small volume element (0.25 ℓ) of the fiducial volume visible. A BBR of $0.33 \cdot 10^{-7}$ was used to define when the volume element would become visible in the hologram (sect. 3.6 and 4.11).

Preliminary designs, for a limited laser energy, had given light distributions which rose continuously to a maximum value at a high Θ, and then dropped off. Laser-induced boiling from such a distribution in the Chamber is a hollow cone [6], with the whole outline of the cone obscured in the conventional photographs, even though there is little boiling in the central part of the cone. We then investigated distributions with a constant limit on the light intensity. Such distributions would give a solid, but shorter, cone of boiling, thus reducing the obscured area in the conventional photographs. The results for limited and unlimited illumination are as follows (Θ_{max} = 30°):

Laser Energy [J]	Maximum Intensity [J / sterad]	Visible Volume [ℓ]
10.0	13.0 (limited)	4694
10.0	16.3 (unlimited)	4719
20.0	67.1 (unlimited)	5020

We selected the first design (fig. 8) to limit the boiling cone and because very little visible volume was gained by increasing the energy above 10 J, which was also the expected upper limit for a good holographic beam from our pulse-stretched ruby laser.

At the time this light distribution was designed, the effect of boiling within the duration of the laser pulse (the microboiling effect, sect. 4.4) had not been proven, and so was not considered in the optimization. In the selected design, the light distribution with illumination angle $5° < \Theta < 15°$ is most effective at producing microboiling. Any future design using an optimization process should consider limiting light in this region, to reduce microboiling.

Microboiling affects mainly the reference beam, and thereby the quality of the hologram. To circumvent this effect, a two-beam technique could be envisaged. In such a setup both the light passing through the central part of the dispersing lens and noise light from microboiling must be prevented from reaching the film and the reference beam is derived directly from the laser. Depending on the energy needed, the latter would be taken out by a beam splitter after one of the amplifiers and then directed onto the film. Some technical aspects of such a system have been studied [17, 18], but such development is arrested at present.

3. THE EXPERIMENTAL ARRANGEMENT

The layout for the laser beam is shown in fig. 9 (top view). The safety requirements for the operation of non-explosion-proofed electrical equipment near a hydrogen area, the stray field from the Bubble Chamber magnet and the demand for a dust-free environment made it necessary to install the laser far away (~ 29 m) from the volume to be holographed. The laser was placed in a separate, air-conditioned clean room. The beam was guided through an evacuated underground pipe to the bottom of the Chamber, where it was made to diverge by the dispersing lens. This beam transport system required adjustable mirrors. The aspheric lens was positioned in the Bubble Chamber vessel, its flat side facing the cryogenic liquid (Ne/H_2 @ ~ 30 K). It also acted as a pressure window. A ruby laser was used because its wavelength does not overlap too much with the spectrum of the flash lamp of the conventional cameras, and also because of the availability of a high quality ruby laser specifically designed for holographic purposes. Nevertheless, care had to be taken to prevent light from the flash tubes of the conventional optics from reaching the holographic film.

A description of the various elements follows.

3.1 The Laser

Originally a KORAD laser [22, 23] had been used (available during our tests for no charge), but was replaced for the physics runs by a commercial holographic ruby laser system (JK Laser System 2000) (fig. 10). Its oscillator has high mechanical stability and is equipped with two tilted intracavity etalons, which are thermally locked into the cooling system of the ruby rod to ensure maximum longitudinal mode stability (long coherence length). Nominal values of the JK 2000 System are a 30-J Q-switched pulse of 30-ns duration, which is obtained by the oscillator, followed by three amplifiers. The oscillator and the amplifiers are mounted on a compact support plate. Due to the mode-selecting aperture (1.7 mm in diameter) in the oscillator, its output has a Gaussian (TEM_{oo}) distribution. The purpose of the spatial filter is to clean up the light output from the oscillator, i.e. to remove large angle rays. After the focus the beam diverges to fill the increasing diameter of the successive ruby rods to make optimal use of their amplification potential. Behind the last amplifier (rod diameter of 2.5 cm) a beam expanding telescope was set up to give a parallel output beam. An apparently uniform spatial energy distribution after the last amplifier in the near field is observed, as is customary for holographic lasers, when observing the profile from the pattern of non-linear burn paper. To maintain the good quality in the far field an optical relay system had to be used (sect. 3.3). The diameter of the laser beam at the dispersing lens was adjusted by changing the position of the first diverging lens of the optical relay system (this relay system was not yet used during the first physics run and the beam size had to be adapted by the telescope). The repetition rate (under conditions described in sect. 4) was one pulse with an energy of $\leqq 8$ J every 10 seconds. Some modifications, including the addition of some optical elements, were made to the JK Laser to adapt it to our requirements.

3.2 The Pulse Stretching

As has been shown in a previous experiment [6], the standard Q-switched or free-lasing pulses at the necessary energy of a few Joules are unsuitable for our application for the following reasons:

(a) a very short pulse may produce excellent holograms, but gives rise to considerable boiling of the Bubble Chamber liquid, thereby affecting the visibility of tracks in the conventional photographs, which are taken some ten milliseconds later,

(b) a millisecond (free-lasing) pulse still produces some boiling due to its "spiky" structure, but gives only a coherence length of ~ 0.5 m and is so long that mechanical vibrations, bubble movement and growth wash out the holographic fringe pattern completely, as has been described in sect. 2.2.

Therefore we had to look for an intermediate solution, giving us initially enough flexibility during the tests to adjust the pulse duration between hundreds of nanoseconds and ~ 100 μs. A coherence length greater than one meter is required. The range of useful pulse durations is, in addition to the given lower and upper limits (a) and (b), determined by all the considerations described in sect. 2.1 and 2.2, namely the need to avoid degradation of the holographic fringe quality recorded on film, and the need to minimize the microboiling effect referred to in sect. 2.3 and described more fully in sect. 4.4.

Initial developments of pulse stretching circuits for the KORAD Laser followed proven techniques, but were too limited in flexibility [22]. Therefore, we developed new circuits for the JK Laser, each optimized for specific conditions. These are described in detail in refs [23-25]; a block diagram is shown in fig. 11. The characteristics of the pulses obtained with the circuit described in [25] and used during the physics runs were:

- Pulse duration adjustable from ~ 2 μs to 100 μs, but studied in more detail in the range from 3 μs to 16 μs,
- fairly flat pulses with little overswing at the beginning (figs 12(a), (b)),
- coherence length in excess of 11 m for ~ 2 μs pulses,
- maximum energy varying with these conditions, but < 8 J with a stability of ± 10 % (figs 13(a), (b) for two run periods),
- repetition rate for the above conditions: ~1 pulse every 10 s with reproducible pulse shapes.

This circuit has the ability to respond quickly to changes in the energy content in the oscillator, given by the ~ 200-MHz bandwidth of the feedback circuit.

3.3 The Beam Transport

The output beam of the laser was sent down by a mirror, and it traveled underground in a 30-cm diameter beam pipe with three bends and a total length of ~ 27 m. The pipe was closed at both ends by flat windows. Three mirrors inside the pipe directed the beam towards the Bubble Chamber. The system was kept under vacuum, both to avoid back reflections from focusing the laser beam in a medium, and for safety and cleanliness.

Special mounts were designed to allow for the adjustment of the mirrors while the system was under vacuum. Front surface dielectric-coated high-reflectivity mirrors were used in all four locations. Once inside the Bubble Chamber building, the laser beam pipe was reduced to 15 cm in diameter, which was adequate for the 5-cm laser beam and dispersing lens diameter. The laser beam was increased to ~ 8 cm in diameter during the second physics run.

In order to obtain a spatial distribution of laser light on the dispersing lens of good quality, we designed and installed an optical relay in the beam pipe.

An optical relay is intended to transfer a beam of light from one plane to another, maintaining both the position, angles and phases of all rays (e.g. [26]). The basic relay is two positive lenses of focal length f, separated by a distance 2f. Light from a plane on one side of these lenses will be relayed to a plane on the other side, provided the two planes are a distance 4f apart. We generalized this to include a magnification change between the planes, both to expand our laser beam (~ 2 cm output at the amplifier) to the 5 cm diameter needed and to help remove the need for any relay lenses within the virtually inaccesible 19-m underground section of our existing laser beam pipe.

A two-stage relay was used. The first stage used the existing JK Laser lenses, modified only by reversing the two telescope lenses so that the positive lens was now closer to the laser, and relayed a plane at the output of the oscillator, through the amplifiers, to a plane at the output of the telescope. The focus (required in each relay stage) was at the spatial filter. This could be done in air, because only the low power laser beam from the oscillator was present at this point. The second stage relayed this plane to the input of the dispersing lens.

The focus of this second stage was in the underground beam pipe and has the full laser power because the beam has gone through the amplifiers. At this focus, it is essential to have vacuum (< 0.1 Torr), since high beam intensity in air results in plasma formation with a harmful back reflection of the beam. We experienced such damage during initial tests with the beam-expanding telescope.

The lenses for the second stage relay were telephoto combinations, where a strong positive and a strong negative lens act together to produce the same effect as a weaker positive lens some distance away. The telephoto combination (f_n = -0.35 m, f_p = +0.6 m) mounted just outside the laser end of the underground section of beam pipe functioned optically as if it were a weaker positive lens (f = +3 m) mounted 3 m further into the pipe. These BK7 lenses were available commercially and then "Vee" coated for the ruby wavelength. Finally, the distance between the lenses in the combination was adjusted to correct for the actual focal length of the lenses.

The first lens in this combination was mounted outside the evacuated beam pipe and could be adjusted to vary the size of the laser beam at the dispersing lens, while still maintaining an acceptable approximation to the relay condition. The other second stage relay lenses were mounted inside the vacuum pipe, near the ends of the underground section.

The detailed design and final optimization of the two-stage relay system was done using Code V(*). This program was also used to trace reflections from each lens surface backward through the relay to learn if any were focused near optical elements or the laser. One such potentially damaging back reflection was found; it was steered to miss the mirror at risk by a small tilt off-axis of the second lens in the first combination.

This two-stage relay greatly improved the spatial distribution of the laser beam on the dispersing lens; see the next section for examples.

(*) Optical design ray tracing program leased from Optical Research Associates, Pasadena, Calif.

Modifications for holography had to be made on the bottom part of the 15-Foot Bubble Chamber, as shown in fig. 1. The laser beam entered its vacuum tank through a warm window to reach the Chamber window and the dispersing lens assembly. Since the main vacuum tank is pumped by oil diffusion pumps, a pipe had to isolate the optic elements to prevent oil contamination and contain the Chamber liquid in case of the unlikely breakage of two pressure windows. The spaces between the dispersing lens, which served as Chamber window, the safety window, and the vacuum tank window were pumped by the same high quality, clean (ion getter) pumps that serviced the 6 sets of hemisperical fisheye windows at the top of the Bubble Chamber.

For protection against the remote possibility of breaking or leaking of all three pressure windows, which would allow the escape of the Bubble Chamber liquid, this pipe was equipped with an automatic valve just outside the vacuum tank. The pipe contained a bellows to allow for movement of the Bubble Chamber vessel relative to the vacuum tank during cooldown and during the expansion cycle.

All transparent elements in the laser beam path to the Bubble Chamber (i.e. four windows, the dispersing lens plus a small negative lens) were made from fused silica of optical grade Homosil. This material has an extremely small coefficient of thermal contraction, excellent homogeneity, and a very high threshold for damage from the high power laser beam ($\geq$ 1.3 GW/cm^2). In our experiment the beam was spread over a surface area of $\sim$ 20 cm^2 on most of the lenses, and, with the laser operated in the pulse-stretched mode decribed in 3.2 above, an ample safety margin against laser damage was maintained.

3.4 Laser Beam Monitoring

Preliminary alignment was done by directing a He-Ne laser down the ruby laser beam path and using ground glass. Initially the alignment, position, and spatial structure of the ruby laser beam were studied by temporarily redirecting the beam out the side of the pipe with a movable mirror just before it entered the dispersing lens and using burn paper. This was later replaced by a more sophisticated system, which monitored the beam profile and its position, angle of incidence on the diverging lens and energy on a pulse-by-pulse basis, using an on-line computer in the Bubble Chamber control room. This system is described in refs [27, 28].

3.5 Back Reflections of the Laser Beam

Optical elements downstream of the laser oscillator could affect the temporal output characteristics of the amplified laser beam in two ways:

- When the total gain of the three amplifiers was sufficiently high, they would start to self-oscillate for fractions of a microsecond. The self-oscillation occured between one of the two lenses of the beam telescope and the output coupler of the laser oscillator. Both lenses of the beam telescope had hard dielectric antireflection "Vee" coatings on both surfaces. The output coupler had one surface antireflection coated and the other surface was 20% reflective (transition air-film-glass). This self-oscillation did not significantly change the shape of the main pulse, but created pre- and/or postlasing (i.e. some light output before or after the main laser pulse). These extra pulses shorten the coherence length and extend the pulse duration, with detremental effects on the hologram quality. Pre- or postlasing could come 50 to 150 μs before or after the main pulse, causing more microboiling near the lens - liquid interface.

  The prelasing could be eliminated by installing a dye-cell filled with 0.6 cm^3 dye in a solution of 2.3 cm^3 acetonitrile between the first and second amplifier.

  The self-oscillation effect could be minimized by aligning the laser beam to a small angle with respect to the optical axis but, at high gains (energy after the last amplifier $\geq$ 10 J), we were never able to eliminate it completely.

- Specular and diffuse reflections can come from almost all of the optical elements in the beam pipe (lenses of the relay system, mirrors), as well as from the windows further downstream. This back-reflected light can gain energy by passing through the amplifiers, traverse the oscillator and arrive at the photodiode of the pulse stretcher. The pulse-stretching circuitry is then too late to correct for the sudden increase of energy in the oscillator. A spike in the oscillator pulse results.

These problems could be solved by placing an optical isolator between the amplifiers and the oscillator. The light from the oscillator has a linear vertical polarization and the amplifier rods were aligned for this polarization. This isolator must not alter the polarization of light going from the oscillator to the amplifiers. But the plane of polarization of light travelling in the opposite direction should be rotated by 90° in order to discriminate between the back reflected light and the light coming from the oscillator. Such a system was built using a polarizer, a Faraday rotator (aperture 5 mm, optimum spectrum between 500 and 800 nm, forward transmission of ~ 85%, and minimum reverse isolation of 1000 : 1, Manufacturer: Optics for Research, Inc.) and a half-wave plate.

An additional option to suppress back reflections from downstream optical elements would be an optical isolator after the last amplifier. However, the above modifications solved the problem without the need to resort to such a larger device.

3.6 The Dispersing Lens

During the initial part of the experiment a single element dispersing lens was used. It had been tested earlier in BEBC [6, 29] and was designed for a parallel, 5 cm in diameter, Gaussian-distributed beam from a ruby laser. It dispersed the light over a cone with a half angle of ~28° within the Bubble Chamber's visible volume. It was mounted in the vacuum space between the flat Chamber and vacuum tank windows, and could even be moved along the optical axis to allow for the study of laser-induced boiling as a function of the peak power density at the entry of the beam into the liquid.

For the second physics run we used a new, two-element lens (quartz: optical grade Homosil), which served also as Bubble Chamber window.

The lens was designed so as to minimize boiling on the quartz-liquid interface: (a) The laser beam intensity was spread over a larger surface as compared to the one-element lens (315 cm^2 and 125 cm^2, respectively), (b) the flat output surface was inclined by 34° from horizontal (as was the Chamber window for the one-element lens), which reduced the possibility of accumulation of "dirt" on this surface, and (c) the mounting flange was now underneath the lens surface to avoid trapping of parasitic bubbles (fig. 14).

The combined dispersing lens/Bubble Chamber window system was designed under several constraints. It was required to disperse a parallel incident beam of diameter 5 cm to fill a cone of half angle 30° in the Bubble Chamber liquid. The incident intensity distribution, assumed to be uniform after propagation of the beam from the laser 29 m away, was to be transformed into the calculated optimum angular intensity distribution in the Chamber. The surface energy density as the beam entered the liquid was required to be $< 0.1\ J/cm^2$ to prevent boiling. There should be no significant peaks in the light intensity due to reflections of the beam from the lens surfaces. Finally, the center of the lens system was required to have a focal length determined by the requirement that the reference beam exposes the film correctly.

In order to achieve the large beam diameter at the quartz-liquid interface a system of two lenses with intervening drift space was utilized. For ease of manufacture, the first lens was plano-concave with a standard radius for the concave surface. A first design of the second lens/window resulted in a surface contacting the liquid that was not quite plano. Since this design would have required grinding and polishing two optical surfaces with accurate control of their concentricity, it was decided to constrain the second surface of this lens to be plano also.

The actual design of the aspheric first surface of the lens/window was performed numerically. Starting from the center, rays of increasing input beam radius were traced through the plano-concave lens. The integrated laser energy inside each ray was calculated using the assumed flat input beam distribution. The required outgoing energy distribution in the Bubble Chamber liquid was also integrated to produce a table of total energy contained within various angles. This table was entered with the integrated incident beam energy and the desired outgoing angle was determined. Using Snell's law, this angle was propagated back through the quartz-liquid surface to determine the angle of the ray within the quartz.

Using the angles of the upcoming ray from the plano-concave lens and the outgoing ray within the quartz as determined by back propagation, Snell's law determined the slope of the aspheric surface. The series of slopes thus determined by tracing rays of increasing radius was integrated to yield the shape of the aspheric surface. Finally, the inner 0.7 mm of the calculated surface was modified to be spherical with a radius of 5.283 mm determined by the requirement that the central portion of the beam covers an output half angle to 1.6° and a circle at the film (4.1 m away) of radius 11 cm. This was chosen to be 3 times larger than the film size to allow for misalignment. It produces the required beam intensity for correct exposure.

Fig. 14 shows the lens combination and the baffles between the two components. The latter are intended to catch the light from the antireflection-coated surfaces of the first lens and the inner surface of the aspheric lens, as well as reflections from any other parts of the assembly, which would otherwise spoil the reference beam.

As pointed out earlier, multiple reflections inside the dispersing lens are a potential source of noise light which would increase the minimum detected BBR and greatly reduce the holograph volume. A computer program was written to trace all reflected rays through the optical system shown in fig. 14. The program kept track of the energy in both S and P polarization for the ray and divided these energies into the reflected and transmitted rays at each optical surface, according to the coating assumed. Laser energy leaving the system from the various surfaces was histogramed and individual ray paths could be printed. Detailed information for rays hitting the film was output. For these calculations, the holographic film was taken to be a 3 cm radius circle on the lens axis, 400 cm above the lower edge of the lens. The energy of the design reference beam in this circle is 26 μJ.

Consider the reflected rays shown in fig. 15(a) for an early design of the dispersing lens with uncoated surfaces. (To save figure space, two rays are shown, one on each side of the figure; in fact, both rays are cylindrically symmetric.) If this design had been used 11.3 μJ from these two reflections alone would have produced an average noise to total light intensity ratio of $11.3 / 37.3 = 0.3$, which would have doubled the minimum detectable BBR (fig. 21), and drastically reduced the volume of the Chamber visible in the holograms (fig. 4). This noise light can be reduced by either applying a high quality anti-reflective coating to the optical surfaces or redesigning the lens to prevent the reflected rays from reaching the film. We elected to do both.

Similar rays (actually the new worst case rays were selected) are shown in fig. 15(b) for the final lens design. Tapering the lower sidewall of the lens has reduced reflections from the ray starting on the left to an insignificant level, even with uncoated surfaces, and caused reflections from the ray starting on the right to miss the film completely. The other shape changes to the lens sides similarly reduced reflections from rays starting from different radial positions. After making all design shape changes, an exhaustive ray tracing check was made with the computer program to be sure that solving known reflection problems had not created new ones.

The effect of anti-reflective coating on the principle (aspheric and top flat) surfaces of the dispersing lens was also investigated with the ray tracing program. (The cylindrical side surfaces of the 20-cm diameter lens would have been too difficult to coat.) Using a single layer magnesium fluoride coating would have reduced the 11.3 μJ of fig. 15(a) to 6.2 μJ hitting the film. This rather small effect is because of the rather low optical index of fused silica (1.455) compared to MnF_2 (1.38). The 3-layer V coating for the ruby laser wavelength actually used was calculated to reduce the energy of fig. 15(a) to 0.19 μJ.

A good anti-reflective coating is also very important in reducing diffuse reflections. With uncoated surfaces, almost 0.3 J reflected light goes out the dispersing lens sides and bottom flat. Most of this light encountered the black (carbon filled) teflon lining of the lens mount, but some fraction is diffusely reflected back through the lens into the Chamber, contributing to the level of the noise light. The 3-layer V coating reduces this by a factor of ~ 50.

3.7 The 15-Foot Bubble Chamber

The 15-Foot Bubble Chamber is an almost spherical vessel (fig. 1), 12.5 feet in diameter [30](*). The Chamber was operated with cryogenic liquids, such as hydrogen, deuterium or neon/hydrogen mixtures. Its total volume is about 33 m^3, the visible volume is limited by the optics to some 28 m^3. It can be photographed simultaneously by 6 cameras arranged on the top. These cameras have wide-angle lenses, each of which sees through three concentric hemispherical windows, so-called fisheye lenses, into the liquid. Conventional photography is made in bright-field illumination, using an annular flashtube around each wide-angle lens. The inside of the Chamber is wall-papered with a retrodirective material (Scotchlite), which has the property of returning incoming light parallel (with a small opening angle of only ~0.5°) to the lens, almost independent of the angle of incidence up to 60°. Optionally, the camera ports can be equipped with a lens about 2.5 times the resolution of the standard lenses, but, with a considerably smaller volume (~ 1 m^3) in focus. For our experiment such a lens was put into one optic port. Another port was used for the holographic camera.

(*) The beam entrance cone had been removed, which originally extended the chamber's length in the beam direction to 15 feet.

The Chamber has on its bottom a large expansion piston (1.8 m in diameter) to sensitize the liquid during the arrival of the pulsed particle beam. For optical reasons this piston is covered by a floating disc (2 m in diameter) covered with Scotchlite. During our runs the expansion sequence was three pulses at 10-second intervals, followed by a 40-second pause. It was determined mainly by the possible three fast ejections of protons from the Tevatron during the flat top of one acceleration cycle of ~ 60 s.

For thermal insulation the Chamber vessel is surrounded by a vacuum tank, which also contains the two superconducting coils with their cryostat, producing a magnetic field of 3 Tesla.

The Bubble Chamber is surrounded by electronic detectors (fig. 16), one being installed inside the vacuum tank between the liquid vessel and the magnet, covering almost 360° (Internal Picket Fence, IPF [31]), and counter planes downstream, outside the vacuum tank (External Muon Identifier, EMI [32, 33]).

3.8 The Holographic Camera

The new laser window on the bottom of the Bubble Chamber aimed directly at one of the optic ports. An existing camera was modified such that the holographic film was transported down to the center of the fisheye lenses, 4.1 meters away from the dispersing lens. The film was positioned in the fisheye such that its plane contained the center of curvature of the fisheye and was perpendicular to the reference beam direction to within about 1°. The film drive was modified to handle the stiffer (thicker) holographic film used during part of the run. The new platen was lapped flat to $\lambda/4$ and a new vacuum system was added to securely clamp the film. Three platen-based fiducials were exposed on the holographic film to permit accurate placement of the film on a replay machine. A red colour filter (RG 665) was installed in front of the holographic film as well as filters with a complementary colour (BG 39) in front of the flashtubes of the conventional cameras in the other ports. These filters prevented light from the conventional cameras from exposing the holographic film. Exposure of the conventional film by laser light was not a problem at the present energy level, due to the high f-number of the conventional lenses (f/12), the presence of a Wratten 58 colour filter in each lens, and the low sensitivity of the KODAK 2482 film to the deep red ruby laser light. Four fast photodiodes were mounted on the platen next to the holographic film to monitor the reference beam intensity.

3.9 Timing

The exact timing for the firing of the laser with respect to the occurence of the neutrino interaction is crucial for the successful application of the holographic technique. The beam spill from the accelerator has a width of ~ 3 ms, and an interaction can occur during this entire interval. However, we needed to determine the interaction time with a precision better than ~ 0.1 ms to be able to record the bubbles from such an event after a growth time of ~ 1 ms, when they obtained the desired diameter of ~ 100 μm (see results in sect. 4.10). Therefore, we had to rely on the real time information from the coincidence of hits in the electronic counters (EMI, IPF) outside the active Bubble Chamber volume. These counters had to discriminate between background, such as through-going muons and cosmic rays, and the interesting (charged current) neutrino events.

A lower limit on the time delay (≧ 0.9 ms) for the laser is given by the inherent features of the laser power supply and the rise time of the flash lamp voltage. The ruby rod contains the maximum energy at ~ 1.1 ms after power is applied to the flash tubes, and at a time less than 1.0 ms the laser output energy is too low to produce good holograms. It was thus necessary to construct a trigger logic to generate a signal immediately after the event occurs. The injection time of the neutrino beam relative to the expansion of the Bubble Chamber, the expansion ratio and the liquid temperature are parameters which allow the adjustment of the growth rate of bubbles. We operate such that 100 μm bubbles are produced after ~ 1 ms for the holograms and ~ 400 μm bubbles after ~ 10 ms for the conventional photographs. An increase beyond this delay would be desirable for more flexibility in Chamber operation. However, turbulences in the liquid, causing irregular bubble displacements, become more pronounced and would affect adversely the momentum measurements from the curvature of tracks.

The fast event trigger for holography was derived from information from the Internal Picket Fence IPF A and IPF B and from four layers of the External Muon Identifier EMI B (fig. 16). To get the sufficiently sensitive trigger the IPF was divided into 8 upstream and 8 downstream segments [34-36], helping to discriminate between interactions produced by incoming charged particles and those by neutrinos inside the liquid. Several topologies for a variety of number of hits in the EMI B and the IPF's were selected for the trigger. In case there was no event which matched the chosen topologies a default trigger was initiated and set to a time of 1.3 ms after start of the accelerator beam signal. The time determination of an event had a precision of 1 μs. After generating one trigger type, the trigger logic was disabled and the trigger sent to the laser to fire the light pulse. The efficiency for recording a hologram of a neutrino event in the range 1 ms to 1.5 ms after its occurrence was ~ 64% [37].

3.10 Replay Facility at Fermilab

For the holograms made in the 15-Foot Bubble Chamber there are two types of primary images available, virtual and real. The principle difference in reconstruction of these two types of images is the reconstruction reference beam. For the real image a beam identical to the recording beam but time reversed is needed. The real image then appears on the side of the hologram opposite the lens. In the virtual image case a diverging beam is placed in front of the hologram. The images can then be seen when looking through the hologram. These features are shown in figs 17 and 18.

A virtual image reconstruction machine was built at Fermilab [16] to replay holograms during the run for quality control purposes and after the run for data analysis purposes. The major components of the system are shown in fig. 19. The hologram is illuminated by either a dye laser tuned to the ruby wavelength or a Helium-Neon laser. The Helium-Neon laser produced good quality replay images in spite of the difference between the replay and recording wavelengths and the quality of the replay image is improved by tilting the film platen. The tilting of the hologram is actually a slight rotation of the hologram about two perpendicular axes. The platen provides two more additional degrees of freedom in the form of two translations for positioning. The resolution of the system was further improved by the use of a liquid film gate. This film gate is a device which sandwiches the hologram between two pieces of glass and allows an index matching liquid to be coated on both sides of the film. A liquid used with good results is decalin (decahydronaphthalene). The source of the illumination is a 6-μm single-mode step index optical fiber. The fiber took the place of three components: optical transport, dispersing lens and spatial filter. The use of an optical fiber made it possible to have the source of illumination mounted directly on and move with the stage system.

The stage system consists of two rotating stages; one mounted horizontally and the other mounted vertically. The moving stage allows the hologram and fiber to be rotated simultaneously on a rigid base providing azimuth and dip angles for viewing holographic virtual images. The telescope is used for viewing the holographic virtual images. The telescope is made of a Nikkor 135-mm f/2.0 camera lens, a 50-mm Schneider f/5.6 enlarging lens, and an image plane photosensitive device. By moving the lenses a variety of magnifications are available. Two different photosensitive devices are used. The first device is a high resolution video camera and display. The second device is a 35-mm camera loaded with Kodak Technical Pan film (Kodak 2415) which has high resolution and extended red sensitivity.

When the vertex of an interaction is located in the Bubble Chamber by scanning and measuring the conventional film, a transformation is made which specifies the location of the event in holographic coordinates. The stages of the replay machine are then manually set to this position. The holographic replay then appears on the video display. Small adjustments are needed to optimize the sharpness of the replay and photographs of interesting events are recorded on Kodak 2415 film. This film is used as a source for measurements and for high quality prints of the events for further study.

4. EXPERIMENTAL RESULTS

Apart from pursuing the main physics aim of the experiment, namely to provide a high resolution view of the neutrino interactions, several technical aspects of huge Bubble Chamber holography were studied. These investigations centered around the laser-induced boiling, which affects the usefulness of the conventional photographs and the hologram quality, and the results of these investigations are reported in this section. We studied qualitatively, and partially quantitatively, the effects of the following parameters:

- alignment, size and spatial distribution of the laser beam in front of the dispersing lens upon visible volume and image quality,
- pulse duration (and energy) upon macroscopic boiling,
- laser-induced microscopic (and other parasitic) bubbles upon the minimum detectable Beam Branching Ratio,
- pulse duration upon picture clarity (vibration of optical elements, liquid turbulence, bubble movement and growth),
- filtering the liquid upon boiling,
- back reflections upon shape of the stretched pulse,
- operating conditions of the Bubble Chamber (temperature, expanded pressure) upon bubble density and size and upon the visibility of tracks in holograms.

4.1 Laser Beam Alignment and Reflections in the Chamber

The setup of the holographic system for the 15-Foot Bubble Chamber differs from the earlier one in BEBC [6]. Therefore it was necessary to check the recording technique in an open, warm Chamber, when there was easy access to all elements. The alignment of the system was made with a Helium-Neon laser (7 mW), mounted on the JK Laser support plate, sending its light via two 45° (removable) mirrors through all amplifiers. The position of the laser beam, after small corrections for the difference in wavelengths were taken into account, was checked at the dispersing lens.

Warm Chamber tests indicated the necessity of having ~ 6 J of laser light to get the right exposure on the film and to obtain holograms in a reasonably large volume. At this high intensity a large amount of stray light can be produced and must be prevented from reaching the holographic film by multiple reflections. A calculation of the effect of stray light on the holographic fringe modulation on the film has already been given in sect. 2.1, and the importance of minimizing this effect was treated there.

Baffles were mounted in the Bubble Chamber covering the entire 30-degree half angle laser illumination cone to absorb as much of the light as possible. Any unabsorbed light will undergo multiple reflections inside the Chamber and a fraction will hit the holographic film, reducing the fringe modulation.

The baffles on the main spherical wall were arranged somewhat like venetian blinds. They were constructed of black anodized aluminum. Each baffle blade was L-shaped, with an approximately horizontal part measuring typically 50 cm by 10 cm, and with a vertical part typically 50 cm by 2.5 cm. Blades were separated vertically by 6.4 cm. There were 220 blades, arranged in twelve contiguous columns. Each column was attached to a trapezoidal-shaped sheet of black anodized aluminum that was bent to form part of a cylinder and this assembly constituted a baffle. These baffles were mounted close to the Chamber wall, covering every part of the spherical surface within the cone of laser light. The design was such that any ray of laser light would be reflected at least twice by a black anodised surface before reentering the main volume of the Bubble Chamber. Those upper horizontal surfaces that were visible from the conventional cameras were covered by Scotchlite to minimize the reduction in the Chamber's useful volume.

The baffles in the "beenie", or small hemisphere at the top of the Bubble Chamber were similar to the ones on the main sphere, but differed in several details. Because of the smaller radius of the hemisphere, the need to avoid the cylindrical camera window mounts ("nozzles"), and the need to block the line of sight from any of the six cameras, the 221 beenie baffle blades were mounted in 24 planar segments. The main part of the individual blades varied between 135 x 20 cm (on the single large segment) to as small as 13 x 9 cm or 25 x 6 cm. Because the Chamber pressure relief (safety) valve and the main cooling loop were located above these baffles, they were required to be open to free vertical circulation of the Bubble Chamber liquid. Therefore no flat aluminum sheet was placed behind the beenie baffles, but they were arranged so that all laser light rays underwent two reflections on black anodized aluminum surfaces before exiting to the space above the baffle planes.

Because of the restricted space available outside the camera field of view, the ends of the 6 camera window nozzles were covered by baffles of a completely different design. These were constructed from 2.5 cm thick flat aluminum plates, typically 60 x 70 cm, with a 35-cm diameter hole in the center for the camera window. Except for supporting ribs around the window hole and on the outside edge, closely spaced holes were drilled to the remaining area leaving only a thin (0.15 cm minimum) web between holes. These drilled holes were designed so that the laser light rays would be reflected twice on the hole wall before exiting above the plate. They were 1.75 to 2.06 cm in diameter and at an angle of 28.5 degrees with the plate normal; a typical plate had 360 such holes. After machining, the plate was black anodized and mounted 0.6 cm from the nozzle end.

Fig. 20(a) is a photograph of the baffles (not yet all of them installed in the beenie), taken when the Chamber was open, from the region of the expansion piston. Fig. 20(b) shows part of the baffles, as seen during the operation of the track-sensitive Chamber with camera #4. It shows that parasitic boiling on the borders of the baffles was at a very low and acceptable level. The efforts to reduce stray light from the laser to a minimum were successful, as can be seen from fig. 21.

4.2 General Remarks on Parasitic (Laser-Induced) Boiling

The study of the pulse stretching upon laser-induced boiling was a main concern. Bubble sizes are "microscopic" ($\leqq$ 10 μm) during the laser pulse, but can scatter enough light to dilute the reference beam. The diameter of these densely packed bubbles increases in proportion to the square root of their growth time, and they are "macroscopic" ($\sim$ 100 μm) when the conventional photographs are taken. This will be discussed in more detail in the following sections.

Bubble creation has not been described analytically in a completely satisfactory manner, neither for the so-called parasitic bubbles formed on uneven surfaces, nor for production by ionizing particles (e.g. [38, 39] and [39-42], respectively). The main difficulty arises from the insufficient knowledge of the energy deposited within the volume of a critical bubble with a diameter of $\sim 5 \bullet 10^{-6}$ cm (about 200 eV for heavy liquids), which has to take place within less than 10^{-10} s. Also the validity of thermodynamic data for bubbles with subcritical radii can be questioned, when only a small number of molecules is involved. Nevertheless, we will discuss semi-quantitatively a few hypotheses for laser-induced boiling, which we then compare with experimental observations.

Firstly, laser light could ionize hydrogen or neon (ionization energy for liquid hydrogen $\sim$ 20 eV, for neon $\sim$ 130 eV) by a multi-photon process and thus reproduce the usual mechanism for bubble creation; the excitation of the hydrogen molecule could constitute another option. As shown in refs [43, 44], this possibility was ruled out for the production of bubbles with a nitrogen laser (λ = 337 nm, 3.68 eV) in an argon, nitrogen, and a hydrogen bubble chamber. However, since the thermodynamic conditions in the neon-hydrogen mixture, the wavelength of the laser (λ = 694 nm, 1.79 eV), its pulse duration, and the light distribution in space are different for the present experiment, we repeat the calculation.

We estimate the photon density of the beam near the entrance to the liquid (one-element lens close to the flat Chamber window) as follows: $\leqq$ 1 Joule of laser light (a typical value for the first physics run) goes through the lens, the highest density of photons is at an angle of 19° relative to its axis and amounts to $\sim 3.5 \bullet 10^{16}$ photons/cm^2 at the glass-liquid interface. Each photon has an energy of 1.79 eV.

Within a critical volume ($5 \bullet 10^{-18}$ cm^3) at least ~ 200 eV (115 photons) must be absorbed to create a bubble [41, 42]. The total photon flux through the cross section of such a bubble during one laser pulse is $2.75 \bullet 10^6$. The absorption of this flux would allow for the production of a string of ~ 200 successive bubbles: within a distance of 2 mm all available energy would be used up. This disagrees with the presence of bubbles a few meters downstream of the dispersing lens, produced by a Q-switched pulse of ~ 100 ns fwhm duration. Further evidence against this process of laser-induced boiling is presented in sect. 4.3.

The excellent transparency of these cryogenic liquids for light in the visible spectrum does not support the idea of rapid absorption either. In addition, the formation of a critical bubble requires that this energy is deposited within the typical dissipation time for the heat of ≤ 0.1 ns. Given the energy and duration of our pulse, we find that the number of photons is too small for bubble creation by several orders of magnitudes.

Secondly, it does not seem probable that fluctuations in the liquid composition of neon-hydrogen (inhomogeneities, small vortices) are responsible for the laser-induced boiling, since the refractive indices of neon and hydrogen are very similar ($n_{H_2} = 1.083$, $n_{Ne} = 1.088$, @ 29.6 K and $\lambda = 546$ nm). Even if we allow for a ± 1-K change in the operating temperature the difference between the refractive indices does not increase. Therefore, scattering or focusing effects should not have any influence on the light path and on bubble creation.

We can, however, plausibly explain the mechanism of laser-induced boiling by the absorption and accumulation of energy on particulate matter with high heat capacity and low conductivity. Its size could be in the range between a few micrometers to a fraction of a micrometer, so that it can remain suspended in the liquid, which has a density of ~ 0.55 g/cm^3. Due to its small size, the particulate matter remains invisible in our conventional optics. The piston movement provides enough turbulence so that it is homogenously distributed in the liquid. It can be heated by the photons to such a degree that it can serve as a nucleus for bubble creation [43]. Its heat accumulation and dissipation is a multi-parameter problem. Any reliable calculation would require the knowledge of (a) the exact volume of this matter, (b) its geometrical shape, (c) its quantity, and, most important, (d) its composition. We suspect, in particular, solidified water (ice), which had settled in larger quantities during a part of the run on the Scotchlite, destroying its reflective properties, and which disappeared during an intermediate warmup of the Chamber. Other candidates are solidified air (nitrogen,

oxygen), metal and teflon dust from the piston seals, epoxy from the piston skirt, glass beads and mylar from the Scotchlite, as well as other unknown material originating from transfer lines, dewars, etc. Even if we were able to pin down the aforementioned parameters and the relative composition of the particulate matter, we would still need to know the absorption, transmission, and reflection of light by these tiny objects, as well as their specific heat and heat conductivity. Their surface structure (spikes, holes) might also be of importance to the bubble formation process [38]. Heat from laser light can be accumulated in the particulate matter over the whole laser pulse duration. This is in contrast to the (few) nanoseconds relaxation time, during which relativistic particles must deposit energy in the liquid by ionization.

The number (and size) of bubbles which can be produced by laser light depends not only on the laser power, but also upon the temperature of the liquid and the expanded pressure (degree of superheating), and the duration of expansion cycle.

A fairly precise description for the growth of bubbles can be given, provided they are not too close to each other, i.e. that their volume density is small. The duration of the cosinusoidal expansion cycle of the 15-Foot Bubble Chamber is ~ 100 ms. Since the flash delay used during the experiment is only ~ 10 ms, we can assume a constant expanded pressure during the growth time. Then the bubble diameter D [cm] is proportional to the square root of time t [s]:

$$D = 2A \bullet \sqrt{t}$$

The proportionality factor A [$cm/s^{1/2}$] depends upon

k	= thermal conductivity of the liquid,
T_ℓ	= temperature of the liquid at large distance from the bubble,
T_V	= temperature of the vapour inside the bubble,
L	= latent heat of vaporization,
ρ_V	= density of the vapour inside the bubble,
c	= specific heat of the liquid,
ρ_ℓ	= density of the liquid,
$k/c \bullet \rho_\ell$	= constant of thermal diffusion,

according to the formula

$$A = 2 \bullet (3/\pi)^{1/2} \bullet (k \bullet c \bullet \rho_\ell)^{1/2} \bullet (T_\ell - T_V) / (L \bullet \rho_V).$$

This factor has been previously measured for track bubbles under similar experimental conditions: $A \simeq 0.1 - 0.2\ cm/s^{1/2}$ [40]. Theoretical calculations suffer somewhat from the insufficient knowledge of thermodynamic parameters and give values of A which are a factor 1.7 too small as compared to the experimental results determined in pure hydrogen and deuterium [41]).

The bubble growth along the particles' tracks was in reasonable agreement with previous results [40]. The different growth rate of laser-induced bubbles is discussed in sect. 4.4.

4.3 Pulse Stretching and Macroscopic Boiling

Most of the tests on macroscopic boiling were made with the one-element dispersing lens during the technical and the first physics run. We investigated the effects of laser intensity, pulse duration, beam profile, injection time relative to the pressure minimum, flash delay of the conventional cameras, liquid temperature and expanded pressure upon macroscopic boiling. The aim was to find conditions which reduce the "density" of laser-induced bubbles (number of bubbles per unit volume) to an acceptable level.

During all tests with short pulses, when we produced bubbles abundantly, we found that they did not grow anywhere to sizes comparable to bubbles along particle tracks, irrespective of the injection time of the laser relative to the expansion curve. A plausible explanation is that they are too densely packed: there is not enough heat available in their vicinity to supply the energy for "normal" growth. It was not possible to determine accurately the diameter of these bubbles: (a) identification of individual bubbles in stereo-views is not possible, and therefore we do not know the spatial coordinates (magnification), and (b) the diameter of the laser-induced bubbles is considerably smaller than the resolution limit of the standard optics ($\sim$ 500 μm) [6, 11]. An attempt to do this was made by projecting these bubble images on a conventional scanning table with high magnification. The bubble image sizes along the upward edge of the hollow boiling cone were measured as fwhm-value of their intensity profile using an array of photodiodes and an oscilloscope. The Bubble Chamber coordinates of the measured points were obtained using two-view reconstruction from which the demagnification of the fisheye windows and camera lenses were calculated. The proportionality constant A in the bubble growth law was determined, with a fairly large uncertainty, and found to be a factor of $\sim$ 3 smaller than the constant determined for track bubbles (fig. 22, taken from [10]).

Ideally, one would like to determine, as a function of laser energy and pulse duration, the volume in which laser-induced bubbles appear, as well as its shape. Due to the energy distribution of the laser light given by the design of the dispersing lens used in the first physics run, this cone was hollow (see also the stereo-photographs from the BEBC test in [6]). Since the contours of this volume fade out, only estimates could be made, using two slightly different procedures:

For the tests in the technical run the height of the boiling cone, measured from the dispersing lens, was assessed. The laser was operated in free-lasing, Q-switched, and stretched pulse modes. These laser pulses, at various energies, were injected into the track-sensitive Bubble Chamber during its pressure minimum (75/25 mole percent Ne/H_2 at 30 K (P_{vapour} = 7.8 bar), $P_{chamber}$ = 8.6 bar, $P_{expanded}$ = 5.6 bar). Conventional photographs were taken ~ 10 ms after the laser pulse. Figs 23(a), (b), and (c) show photographs for the three kinds of pulses at about the same energy. The height of the boiling cone was found to have a roughly linear increase when plotted against the square root of the incoming laser energy. Fig. 24 shows measurements of the height of the boiling cone versus the incoming laser energy for Q-switched and stretched (~ 2.2 μs) pulses. The energy was measured with a cone calorimeter directly behind the last amplifier. The actual energy reaching the dispersing lens was somewhat smaller due to beam divergence. This plot shows that the height of the boiling cone is proportional to the square root of the total light input energy. This result is consistent with theoretical calculations if one assumes a threshold light flux for bubble creation. Within large errors, both measurements (i.e. the pulse stretched and the Q-switched data) are in agreement with a threshold light flux of the order of 100 W/cm^2. This is however two orders of magnitude below the threshold light flux one would expect on the ground of thermodynamic considerations. These data thus seem to show as well that another mechanism is involved in laser-induced bubble creation as discussed in sect. 4.2.

For the same amount of boiling one can increase the laser energy by a factor of ~ 7 by stretching the pulse from 120 ns to 2.2 μs. The boiling is reduced to negligible amount when stretching the pulse to the range of tens of μs. Early terminated free-lasing pulses were tried, but are not useful for us due to their spiky character and small coherence length.

When using the two-element dispersing lens we could send up to 6-J laser pulses with durations as short as 4 μs into the Chamber without producing significant macroscopic boiling. This improved behaviour, as compared to the use of the one-element lens, was partially due to the decreased energy density of the beam when entering the Chamber liquid, and partially due to the enhanced flatness of the laser pulse.

4.4 Pulse Stretching and Microscopic Boiling

The laser-induced bubble formation and growth during the laser pulse, affects the hologram by scattering additional light into the reference beam, thus reducing the fringe modulation (sect. 2.1), but it is expected to have very little influence upon the object beam.

There might be a time threshold for the absorption of sufficient energy on particulate matter, before the first bubbles can be created, reach the critical size and continue to grow. After this initial delay more bubbles are created on these hot spots during the remainder of (and even beyond) the laser pulse. Their growth rate will follow the $t^{1/2}$-law. With our operating conditions and taking the proportionality factor A for track bubble growth, this would result in diameters of 4, 12, and 40 μm for pulse durations of 1, 10 and 100 μs, respectively. These calculated diameters constitute an upper limit, and the actual diameters are probably smaller by a factor of ~ 3 (sect. 4.3, fig. 22).

Convincing evidence for the presence of microscopic bubbles near the dispersing lens came from the simultaneous measurement of the laser beam intensity behind the last amplifier and at the film platen, and is shown in fig. 25. The quality of the holograms was in general good when the time-dependence of the intensity at the two monitors was similar and flat with time. However, the hologram quality degraded and tracks became fuzzy when, for an incoming flat pulse, the intensity at the film platen showed a substantial increase with time. We explain this behaviour by the production of micro-bubbles, which scatter useless light into the reference beam. Then the lens no longer acts as a point source. The reconstructed holograms of the laser entrance window also indicate the presence of the boiling.

Fig. 26 shows the increasing slope of the light intensity vs. time curve, which was used as an on-line monitor for the amount of microboiling, measured at the film platen with increasing laser input energies at a pulse duration of 7.7 μs.

4.5 Filtering of the Liquid and Boiling

The 15-Foot Bubble Chamber is equipped with a special pump loop cooling circuit. Chamber fluid is withdrawn from the space underneath the piston, cooled, and sent to an external liquid pump through transfer lines. The pump is in an external dewar to remove it from the high magnetic field of the Bubble Chamber. The fluid is then returned to the Chamber in one of two ways. The primary path is through a cooling loop around the piston seal area, to remove the heat generated by the sliding piston seals, and then back into the space underneath the piston. An alternate path is to the top of the Bubble Chamber; this mode is frequently used to help mix the part neon, part hydrogen fluid. The necessary piping, valves, and two filter holders were installed at the output of the pump to hold commercially available 5, 2, 0.5, or 0.2-μm sintered metal cryogenic filters. The flow was directed through one filter at a time; the other filter element could be inspected or replaced without stopping pump loop flow. In the mixing mode, a volume equal to the Chamber volume passed through the pump loop and filters about every 10 hours. This filtering was done whenever the Chamber was not pulsing.

The attempt to remove small particles could be monitored by measuring the pressure drop across the filter. We started with a 5-μm filter and switched then for several days to a 2-μm filter. Since we did not observe any drastic increase in the pressure drop we replaced the 5-μm filter by a 0.5-μm filter, and eventually by a 0.2-μm filter, the smallest commercially available filter for cryogenic liquids. Inspection during intermediate warm-up of the filters did not show any accumulation of macroscopic solid matter.

From the limited experience gained during the runs it is impossible to make a definite statement if filtering removed particulate matter from the Chamber liquid and reduced the laser-induced boiling. However, since we are almost certain that this boiling is due to absorption on particulate matter, the above observation leaves us with various hypotheses: (a) particulate matter is so small, that it can even pass through a 0.2 μm filter, (b) that due to the low viscosity of the liquid these particles were not moved towards the filter, (c) and/or that adhesive (electrostatic) forces attached most of it to the Scotchlite of the Chamber wall and to the dispersing lens.

4.6 The Laser Beam Profile

Typical intensity profiles after the oscillator stage of the laser and near the entrance into the vacuum tank of the Bubble Chamber, measured with a CCD camera and displayed by the computer, are shown in figs. 27(a) and 27(b), respectively. Behind the oscillator the expected Gaussian (TEM_{oo}-mode) beam distribution is seen, whereas an almost flat, but more spotty structure at the end of the relay system is visible. This change may be explained by a combination of various effects:

- Speckle on optical elements due to either dust or coating damage.

- Pumping of the amplifier rods produces a lower population inversion in the center of the rods than in the outer regions.

- There is a 250 μm diameter aperture after the oscillator; the calculated TEM_{oo} beam size at the aperture is 35 μm (produced by the 1.7 mm output aperture of the oscillator and a microscope lens), which could give rise to a diffraction pattern when not properly aligned.

- After leaving the last amplifier the light passes through ~ 3 m of air prior to its entrance into the vacuum pipe; although thermal blooming [45, 46] might just be possible, no experimental evidence of the effect is present .

Information about the distribution of the beam after passage through the dispersing lens can be obtained either indirectly from the holograms, or from Q-switched pulses, which produce significant boiling. Deviations from the expected distribution inside the liquid could come from heating of the dispersing lens during the laser pulse causing a non-permanent minute deformation of its critical central radius, thus changing the Beam Branching Ratio. Some minor imperfections of the lens itself cannot be ruled out.

4.7 Bubble Chamber Operating Conditions

Once the mixture ratio of neon to hydrogen is chosen for physics reasons (density, absorption, collision and radiation lengths), the only adjustable parameters are the liquid temperature and the expansion ratio. They must be chosen such as to give optimum bubble size and density (≧ 50/cm), both for holography and conventional photographs.

A way to satisfy these requirements simultaneously is to raise the liquid temperature above values generally used in big bubble chambers (figs 7 and 8 in ref [42]). However, one then has to accept the (minor) disadvantage that tracks become fairly solid in the conventional photographs due to bubble coalescence. Any ionization measurements for particle identification suffer from this operation mode.

The conditions (temperature of the liquid, pressures, delays for triggering the laser and the flash lamps) used for most of the second physics run were:

62/38 mole percent neon/hydrogen

T_{ℓ} (mixture) = 7.47 bar = 108.4 psia = 29.6 K

P_{vapour} (H_2-bulb) = 7.82 bar = 112 psia

$P_{chamber}$ = 8.41 bar = 122 psia

$P_{expanded}$ = 5.31 bar = 77 psia

Δt_{laser} = 1 ms

Δt_{conv} = 8 ms

Our single-beam technique was particularily sensitive to microboiling near the entrance of the laser beam into the liquid. Heat convection inside the Chamber is slow. Once the liquid near the dispersing lens is heated, the following laser pulse(s) will tend to escalate the boiling process due to the now higher sensitivity of the liquid. Therefore, efforts were undertaken to keep the liquid in the lower part of the Chamber cooler by a few hundredth of a degree than on its top. In addition, the pressure drop during expansion could be reduced slightly, so that the desired bubble growth rate and density could be maintained, but the sensitivity of the liquid near the laser entrance was lowered.

It is probable that particulate matter settled on the surface of the dispersing lens and acted as bubble nuclei when hit by the laser beam. Attempts were made with some success to remove this matter by sending a few Q-switched laser pulses of high energy into the Chamber, thereby producing violent boiling and large convection to wash the dirt away.

4.8 Holographic Film Material and Processing

The holographic film used for recording was an Agfa-Gevaert, Holotest 10E75 emulsion, 70 mm wide with sprocket holes (Kodak type II perforations) in 600 feet rolls, coated on a polyester base. The laser-induced boiling and stray light limited the peak power density that could be used for the exposure of the film. Therefore, a special processing technique was required which increased the sensitivity of the film and, in particular, reduced the influence of the high intensity reciprocity failure(*). The developer utilized the superadditive effect of phenidone (1-phenyl-3-pyrazolidone) combined with hydroquinone. A standard Kodak D-19b developer was used to which 1.5 g/ℓ phenidone was added [47].

Amplitude transmission holograms were produced, which required only development and fixing. The holographic film produced during the run was developed in a modified Kodak Versamat processing machine by a commercial holographic company. Latent image fading slows down when the emulsion is kept cold and therefore exposed rolls were kept in a refrigerator until they were processed. The variation in obtained optical density at the processing stage due to variations in exposure and fading [48], could be compensated for to a certain degree by adjusting the development time or temperature.

A H&D density-exposure plot for holograms is shown in fig. 28(a), together with the amplitude transmittance curve in fig. 28(b), for our exposure and development of the AGFA-Gevaert 10E75 emulsion.

(*) According to the reciprocity law the same photographic density is obtained as long as the product of light intensity with time of illumination is constant. This law fails when either the exposure time is extremely short or the intensity extremely high.

4.9 Quality of Holograms

The hologram quality was monitored during the physics run by immediately developing the last 20 frames of each roll removed from the camera. The optical density of these holograms was measured at 5 spots per frame using a standard densitometer. A delicate balance had to be maintained between sending enough laser light into the Chamber to give a useful hologram density and not sending too much, which would generate excessive microboiling resulting in additional noise light reaching the film and reducing hologram quality. Typical base fog density of the film was 0.2 and we obtained the best results when the hologram had a total density of 0.6; total densities of 1.0 or more resulted in useless holograms. A subset of holograms used for monitoring was looked at using a diverging Helium-Neon laser beam (virtual image system) and the overall quality of each of them was recorded. A good indicator of the hologram quality was the image visibility and sharpness of various beam reflections (fisheye reflections, dispersing-lens mount reflection), as well as of the tracks visible in the hologram. Furthermore, about 10% of all the holograms were scanned and every event seen was recorded and classified according to its visible quality. The number and quality of these events also reflected the overall quality of the holographic roll.

This information was then correlated with the data provided by the laser beam monitoring system [27]. This would indicate whenever a change in the operating conditions of the Bubble Chamber or the laser was necessary.

The corresponding strips of conventional film were looked at in order to control qualitatively the amount of laser-induced macroscopic boiling.

Beside these "on-line" checking procedures, the quality of every exposed roll was checked after development; this, in particular, was necessary since significant fading occurs before development. For a detailed study of this phenomenon see [48].

As mentioned in the Introduction to this paper, out of ~ 218,000 holograms about 110,000 (based on the preliminary checks described above) have sufficient track quality to be useful for a physics analysis. Only after all the holograms, together with the conventional photographs and the timing information from the electronic counters have been studied in detail, it will be possible to give a definite breakdown of the variety of reasons contributing to the efficiency factor of ~ 50%. However, we can already name some adverse effects, leading to bad holograms: (a) instabilities of the illumination system (b) thermodynamics of Bubble Chamber operation and purity of its liquid, and (c) timing problems (event trigger).

All important information about the operation of the laser for each firing is stored on EMI tapes [27] and will be compared on a pulse by pulse basis with the corresponding hologram. During the run we tried to adapt the laser performance to the Chamber conditions.

Some loss of good holograms was due to delays involved changing the operating temperature of the almost 20 tons of cryogenic liquid, and to unstable startup conditions of the Chamber after extended scheduled standby periods.

"Wrong" timing from the electronic counters could lead either to the recording of barely visible tracks when the laser pulse came too early, or to too extremely wide tracks when it came too late.

4.10 Track Properties in Holograms

During warm tests in the open Chamber objects were photographed holographically inside the vessel at various positions. We chose glass beads of 100-μm diameter glued on to 20-μm wires, as well as a U.S.A.F. resolution test target. Satisfactory results were obtained irrespective of the pulse duration, to be expected since their are no vibrations from the expansion system. The one-track (one-line) resolution was 125 μm, or in the usual optical definition, two tracks (two lines) whose centers were separated by 250 μm could be distinguished according to the Rayleigh criterion.

Preliminary measurements of bubble diameters and track resolution [49, 50] were made on the Fermilab Virtual Image Replay Machine [16], sect. 3.10. The system magnification was measured by placing the U.S.A.F. target in the virtual image volume and photographing it. The photograph was then digitized giving the system magnification in respect to the pixel elements of the linear CCD array. The linear array used has 1024 pixel elements with 25-μm center to center spacing and was used in conjunction with the Fermilab MOMM film measuring machines.

The spatial coordinates of events in the Bubble Chamber were measured in the conventional stereo views, and this provides the holographic magnification for an event. Photographs of events in the hologram were made with various illumination intensities and exposure times, and were analyzed with the linear array. The bubble diameter is defined as the full width at half maximum of the image above background noise, usually measured on the film with a microdensitometer or a similar device. The average speckle size agrees well with the theoretical value of ≤ 100 μm, calculated for coherent light for the diffraction limit of a point source [51], not taking into account the fisheye lenses. The calculated diffraction limited resolution at the center of the Chamber, i.e. at a distance 2 m away from the film, for a circular hologram area 50 mm in diameter is ~ 43 μm (without fisheye lenses). Bubbles as small as ~ 100 μm were recorded and replayed with good contrast [50], corresponding to a resolution of ~ 113 μm (according to the Rayleigh criterion), in very reasonable agreement with the bubble size expected from the theory of bubble growth and measured time delay when the hologram was taken. However, the average bubble size during the run was ~ 120 μm, corresponding to a resolution of ~ 135 μm. The track separation was found to have about the same value. The result is in agreement with roughly measured bubble sizes on two real image replay facilities [13, 14].

The comparison of an interesting neutrino interaction, photographed with three conventional cameras (figs 29(a), (b), (c)), with its recorded hologram (fig. 29(d)) shows the significant difference in resolution. Whereas in all conventional views nothing spectacular near the neutrino interaction is visible, we see in the hologram a secondary vertex close (0.7 cm) to the primary. This secondary vertex is consistent with the decay of a D^+ charmed meson into 3 charged mesons plus neutral mesons (schematic drawing fig. 29(e)). The neutral mesons decay; the resulting photons then convert into electron-positron pairs which are measured in the conventional Bubble Chamber photographs.

4.11 Beam Branching Ratio

An important quantity in the design of the dispersing lens, and ultimately for the quality of the holograms and the size of the visible volume, is the **Minimum Beam Branching Ratio**, which was assumed to be $0.33 \cdot 10^{-7}$ [52] (sect. 2.1).

A sample of 1650 holograms has been scanned at the Fermilab replay machine for neutrino interactions. The following cuts have been made on the event sample. It was required that the events are in the fiducial volume of the Bubble Chamber and satisfy the cut $\Theta_i \leq 30°$. The position of the event vertices was measured from the conventional film, which allowed calculation of the geometrical quantities. The bubble growth time of the event was determined from the difference in Pockels cell trigger time and event trigger time, which was determined using the hit patterns in two electronic detectors installed outside the active volume of the Bubble Chamber (IPF, EMI). If there was some ambiguity in assigning the event with the hit pattern, it was removed from the sample. This is mainly the case for events with low track multiplicity, events with none of the particles leaving the liquid volume, or events located in a frame where another event was found. After these cuts the sample contained 51 events.

An estimate of the bubble diameter was obtained using the formula $D = 2 \bullet A \bullet \sqrt{t}$ and assuming $A = 0.2\ cm/s^{1/2}$ (120-µm bubble diameter after a growth time of 1 ms). The theoretical estimates for $F(\Theta_i)$, $G(\alpha)$ and I_r were used. The input profile of the laser beam was assumed to be flat over the diameter of the lens.

The BBR distribution is shown in fig. 30. One event has a BBR which is less than $0.33 \bullet 10^{-7}$, the maximum BBR is $0.2 \bullet 10^{-5}$. In fig. 31 the holographic z-coordinate is plotted vs. the illumination angle and contains seen and unseen events. Most of the events, which were predicted from the analysis of the conventional film, but were not found on holograms, were on the borderline of the illumination cone. This could indicate that a higher laser intensity in this region would have resulted in the visibilty of the missing events. The volume visible in the holograms was determined from this preliminary study to be $\sim 1.5\ m^3$.

The fact that an event with BBR $\simeq 0.33 \bullet 10^{-7}$ has been found indicates, that the assumption of the minimum visible BBR for the design of the dispersing lens was correct.

CONCLUSIONS

Holographic recording of neutrino interactions in a large Bubble Chamber was successfully done for the first time on a production scale. At least 1.5 m^3 of the Fermilab 15-Foot Bubble Chamber's volume was photographed with a resolution which approached 100 μm, being better than four times the resolution of its standard optics in the middle plane of the Chamber. This allowed the study of close-in interactions and decays in a substantial part of the Chamber with greatly improved precision, leaving enough track lengths outside this volume for measurement of the momentum and identification of particles. The evaluation of these photographs and holograms is in progress.

Several new techniques were developed and successfully implemented. They comprise the design of (a) an innovative pulse-stretching circuitry with adjustable pulse length for a powerful holographic laser, (b) an optical relay system to transport the beam with undiminished quality over a large distance, and (c) an on-line monitoring system of the spatial and temporal features of the laser beam pulse-by-pulse. Furthermore, (d) the holographic film sensitivity was improved by special development techniques, (e) real- and virtual-image replay machines for the holograms were constructed and operated reliably according to design. The heat absorption of intense laser light in a cryogenic liquid was studied in some detail and may help to understand better the bubble creation mechanism. Many of these developments may find further interesting applications in the design of a holographic bubble chamber for a 3-TeV accelerator under construction (UNK) and also outside the field of elementary particle physics.

ACKNOWLEDGEMENTS

We would like to thank C. Baltay, M. Bregman, M. Hibbs, R.D. Schaffer, T. Woch (Columbia University), T. Hart (Stevens), R. Michaels (Rutgers), E. Clayton (IC London), and S. Lomatch (IIT) for their help during the initial tests and preparations for the experiment. The advice of J. Hunt (Nova project, Lawrence Livermore Laboratory) on optical relay design is greatly appreciated. H. Haggerty is thanked for the development of an image digitizer system for the laser, F. Cook for the precise manufacturing of dispersing lenses. In Fermilab we are indebted to Prof. L. Lederman and to several groups who greatly aided us. The patience and dedicated work of the 15-Foot crew and of the operators of the EMI/IPF system is greatly appreciated.

REFERENCES

[1] M. Dykes, P. Lecoq, D. Güsewell, A. Hervé, H. Wenninger, R. Royer, B. Hahn, E. Hugentobler, E. Ramseyer and M. Boratov
Nucl. Instr.& Methods 179 (1981) 487-493

[2] A. Hervé, K.E. Johansson, P. Lecoq, P. Olivier, J. Pothier, L. Veillet, G. Waurick and S. Tavernier
Nucl. Instr.& Methods 202 (1982) 417-426

[3] Holography in Large Bubble Chambers, Fermilab 15' B.C. and CERN BEBC
C. Baltay, M. Bregman, M. Hibbs, A. Schaffer, G. Harigel, F. Eisler, R. Cence, E.B. Brucker and T. Hart
Talk at BEBC Users Meeting, CERN (November 1982)

[4] T. Kitagaki, K. Abe, T. Akagi, Y. Chiba, K. Furuno, M. Gunji, H. Hanada, K. Hasegawa, H. Hayano, T. Hayashino, H. Kaga, J. Katayama, H. Kurino, H. Masuda, Y. Morita, S. Nakai, T. Nakajima, K. Numano, H. Sagawa, M. Sasaki, H. Suzuki, T. Takayama, K. Tamai, S. Tanaka, A. Yamaguchi, T. Yamamura and H. Yuta
Nucl. Instr.& Methods A281 (1989) 81-92

[5] E-632 Holography Development
R. Cence
University of Hawaii, Internal Report JR-85-82 (1982)

[6] H. Bjelkhagen, G. Harigel, F. Pouyat, W. Seidl, C. Baltay, M. Bregman, F. Eisler, M. Hibbs, A. Schaffer, R. Cence, E.B. Brucker and T.J. Hart
Nucl. Instr. & Methods 227 (1984) 437-451

[7] Holographic Recording of Cosmic Ray Tracks in BEBC
G. Harigel, H. Bjelkhagen, F. Pouyat, W. Seidl, C. Baltay, M. Bregman, F. Eisler, M. Hibbs, A. Schaffer, R. Cence, E.B. Brucker and T.J. Hart
in Photonics Applied to Nuclear Physics: 2, Nucleophot, Strasbourg (1984), pg.69-71

[8] H. Akbari, and H.I. Bjelkhagen
SPIE 615 (1986) 7-12

[9] G.G. Harigel (E-632 Collaboration)
Nucl. Instr. & Methods in Phys. Res. A257 (1987) 614-617

[10] G.G. Harigel (E-632 Collaboration)
Nucl. Instr. & Methods in Phys. Res. A279 (1989) 249-252

[11] High Resolution Imaging of Particle Interactions in a Large Bubble Chamber using Holographic Techniques
H. Akbari
Thesis, Tufts University (1987) (unpublished)

[12] HOLRED, A Machine to Reproduce and Photograph Real Images from Holograms Taken in the 15-Foot Bubble Chamber at Fermilab,
P. Nailor
in Photonics Applied to Nuclear Physics: 2, Nucleophot, Strasbourg (1984), pg.83-94

[13] Design, Construction and Testing of a Holographic Measuring Machine,
M.W. Peters and R.J. Cence
ibid. pg.95-98

[14] M. Aderholz, P.P. Allport, J.-P. Baton, M. Bourdinaud, G. Corrigan, H. Drevermann, K.K. Geissler, J.V. Gibb, L. Gosset, G. Gros, G. Harigel, R. Krawiec, J. Lloyd, D.B. Miller, J. Moreels, D.R.O. Morrison, P.R. Nailor, M. Neveu, J. Quidort, P. Sawallisch, R.L. Sekulin, S. Sewell, G. Smith, K. Varvell, L. Verluyten, L. Walton and M. Waters
Nucl. Instr. & Methods in Phys. Res. A284 (1989) 311-322

[15] The Rutgers Holographic Analysis Machine (HAM)
E.B. Brucker, D. DeProspo, Doroshenko, P. Jacques, M. Kalelkar, E.L. Koller, M. Lauko, R. Plano and P. Stamer
Rutgers University, Internal Report, March (1988) (unpublished)

[16] R. Naon, H. Bjelkhagen, R. Burnstein, L. Voyvodic
Nucl. Instr. & Methods in Phys. Res. A283 (1989) 24-36

[17] Preliminary Tests on Holography in BEBC
F. Pouyat
in Proc. Workshop on Holographic Techniques and Applications, (1981), Strasbourg, and CERN/EF 82-6

[18] H. Bjelkhagen, F. Pouyat, P. Kasper, E.E. Miranda, R.L. Sekulin, W. Venus and L. Walton
Nucl. Instr. & Methods 220 (1984) 300-308

[19] R.J. Withrington
Applied Optics 7(1) (1968) 175-181

[20] On the Thermodynamics of Bubble Chamber Expansions,
G. Horlitz, S. Wolff and G. Harigel
DESY 68/43, September (1968)

[21] On the Movement of Bubbles in a Medium-Sized Bubble Chamber
G. Harigel, G. Horlitz and S. Wolff
DESY 72/16, March (1972)

[22] Pulse Stretching in a Q-switched Ruby Laser for Bubble Chamber Holography
G. Harigel, C. Baltay, M. Bregman, M. Hibbs, A. Schaffer, H. Akbari, H. Bjelkhagen, W.M. Smart, P. Dingus, R. Michaels, P. Nailor and R. Sekulin
in Photonics Applied to Nuclear Physics: 2, Nucleophot, Strasbourg (1984), pg.72-82

[23] G. Harigel, C. Baltay, M. Bregman, M. Hibbs, A. Schaffer, H. Bjelkhagen, J. Hawkins, W. Williams, P. Nailor, R. Michaels and H. Akbari
Applied Optics, 25 (1986) 4102-4110

[24] J.K. Hawkins and W.A. Williams
Proc. Intern. Conf. on Lasers-86, STS Press McLean, VA. (1987) 553-560

[25] Laser Pulse Stretching via Enhanced Closed Loop Control With Slow Q-Switching
L. Verluyten, S. Willocq, G.G. Harigel, J.K. Hawkins, W.M. Smart, W.A. Williams, M.W. Peters and H. Akbari
Submitted to Nucl. Instr.& Methods in Phys. Research

[26] A.L. Gordon, B.A. Tozer and J.M. Webster
Opt. & Laser Eng. vol.6 (1985) 191-201

[27] Online Monitoring of Laser Pulses using the GPIB-Interface of a Tektronix 2430 Digital Storage Oscilloscope
L. Verluyten and M.W. Peters
Fermilab, TM-1484, October (1987) (unpublished)

[28] Monitoring of a High Power Pulsed Ruby Laser
L. Verluyten, S. Willocq, W.M. Smart and M.W. Peters
submitted to Nucl. Instr.& Methods

[29] Laser Dispersing Lenses for Holography in Large Bubble Chambers
M. Hibbs
Internal Report, Columbia University (1984), (unpublished)

[30] 15-Foot Bubble Chamber Safety Report,
National Accelerator Laboratory, Batavia, Illinois, July (1972)

[31] H. Foeth
Nucl. Instr. & Methods in Phys. Res. 176 (1980) 203-206

[32] Dimuon Production by 0-600 GeV Neutrinos in the Fermilab 15 ft. Bubble Chamber
V. Jain
Dissertation, Univ. Hawaii, (1988) (unpublished)

[33] Dimuon Production by Neutrinos in the Fermilab 15 ft. Bubble Chamber at the Tevatron

V. Jain, F.A. Harris, M. Aderholz, M.M. Aggarwal, H. Akbari, P.P. Allport, P.V.K.S. Baba, S.K. Badyal, M. Barth, J.P. Baton, H.H. Bingham, E.B. Brucker, R.A. Burnstein, J.R. Campbell, R.J. Cence, T.K. Chatterjee, E.F. Clayton, G. Corrigan, C. Coutures, D. Deprospo, Devanand, E. De Wolf, P.J.W. Faulkner, W.B. Fretter, V.K. Gupta, J. Guy, J. Hanlon, G.G. Harigel, M.A.Jabiol, P. Jacques, G.T. Jones, M.D. Jones, T. Kafka, M. Kalelkar, P. Kasper, G.J. Kaul, M. Kaur, J.M. Kohli, E.L. Koller, R.J. Krawiec, M. Lauko, J. Lys, P. Marage, R.H. Milburn, D.B. Miller, I.S. Mittra, M.M. Mobayyen, J. Moreels, D.R.O. Morrison, G. Myatt, P. Nailor, R. Naon, A. Napier, M. Neveu, D. Passmore, M.W. Peters, V.Z. Peterson, R. Plano, N.K. Rao, H.A. Rubin, J. Sacton, B. Saitta, P. Schmid, N. Schmitz, J. Schneps, R. Sekulin, S. Sewell, J.B. Singh, P.M. Sood, W. Smart, P. Stamer, K.E. Varvell, W. Venus, L. Verluyten, L. Voyvodic, H. Wachsmuth, S. Wainstein, S. Willocq and G.P. Yost et al.

to be published in Phys. Rev.D

[34] Fast Event Trigger for Holography or High Resolution Camera HRC

P.P. Allport and E. De Wolf

Internal report E632 collaboration, February (1985)

[35] High Energy Neutrino Scattering at Low Q^2

P.P. Allport

RAL-T-045 (1987) (Thesis)

[36] E632 Online System for the EMI/IPF/15' Hybrid Bubble Chamber

F.A. Harris, R. Campbell and V. Jain

Technical Report, University of Hawaii, UH-511-542-84, February (1985)

[37] Private Communication from M.D. Jones (University of Hawaii, (1988))

[38] Chambre à Hydrogène à Haut Taux de Repetition,

J. Badier, Blondet, Briandet, Cornic, Delcros, M. Demoulin, P. Dupont, R. Florent, Guibert, R. Jacob, Maiorana, Maury, Milito, Morize, Abolivier, Goldeberg, Holtz, Ledoux, Lefrere, Lemesle, Metairie, Oostens, Schoen

Rapport CEA-R 3144 (1967), Centre d'Etudes Nucléaires de Saclay

[39] F.H. Poesposoetjipto and E. Hugentobler
Helvetica Physica Acta 43 (1970) 203-222

[40] G. Horlitz, S. Wolff and G. Harigel
Nucl. Instr. & Methods 117 (1974) 115-124

[41] Blasenbildung und Blasenwachstum in einer mit Wasserstoff und Deuterium gefüllten Blasenkammer
S. Wolff
Dissertation, Hamburg (1969) (unpublished)

[42] G. Horlitz, S. Wolff and G. Harigel
Nucl. Instr. & Methods 115 (1974) 365-372

[43] G. Harigel, H.J. Hilke, G. Linser and F. Schenk
Nucl. Instr. & Methods 188 (1981) 517-520

[44] On Bubble Track Formation by a Laser in BEBC Filled with Hydrogen
G. Harigel, H.J. Hilke and G. Linser
CERN/EF 81-8, June (1981), (unpublished)

[45] Laser Beam Propagation in the Atmosphere,
Topics in Applied Physics, Vol.25, Editor J.W. Strohbehn
"Thermal Blooming in the Atmosphere", J.L. Walsh and P.B. Ulrich, pg.223 ff.
Springer-Verlag, Berlin Heidelberg New York (1978)

[46] Thermal Blooming in the JK Ruby Laser
T. Scholz
Fermilab, Internal Report, July 7 (1986) (unpublished)

[47] Holographic Recording materials and the Possibility to Increase their Sensitivity
H. Bjelkhagen
CERN/EF 84-7, March 23 (1984) (unpublished)

[48] Latent-Image Fading
Holographic Group
Fermilab, Internal Note, March 24 (1987) (unpublished)

[49] Search for Short Lived Decays Produced by Tevatron Neutrino Beam using Holographic Optics
R. Naon
Internal Report IIT, Chicago, April (1988), (unpublished)

[50] Investigation of Bubble Diameters and Holographic Resolution
R. Naon
Internal Report IIT, Oct.26 (1987) (unpublished)

[51] M. Young, B. Faulkner and J. Cole
J. Opt. Soc. Am. 60 (1970) 137-139

[52] Use of Holographic Optics to Obtain High Resolution over a Large Volume to Search for Short Lived Particles
L. Verluyten
IIHE-88.01 Report, Brussels, May (1988), (unpublished)

FIGURE CAPTIONS

Fig.1 15-Foot Bubble Chamber, side view. Shown are the laser entrance port with dispersing lens, and the fisheye windows on the top of the chamber; they are equipped with the cameras for conventional and holographic recording.

Fig.2 Simplified representation of the holographic set-up with the holographic parameters.

Fig.3 Geometric scattering function $G(\alpha)$ as function of the scattering angle α.

Fig.4 Visible volume versus minimum detectable BBR in case no noise light is reaching the holographic emulsion.

Fig.5 Optical path difference of growing bubble (schematic).

Fig.6 Change in optical path length per change in diameter for a growing gas bubble in Neon-Hydrogen (liquid optical index 1.088) as a function of scattering angle α, for both refracted and reflected rays.

Fig.7 Optical path difference change of moving bubble.

Fig.8 Design values of the illumination intensity $F(\Theta_i)$ per solid angle as function of the illumination angle Θ_i for the dispersing lens used in the second physics run.

Fig.9 Laser room, beam pipes, and Bubble Chamber (top view). Shown are lines of constant magnetic field near the laser room.

Fig.10 Layout of the JK Laser:

R : ruby rod of oscillator,
RM : rear mirror,
OM : output mirror,
IE : intracavity etalon,
PC : Pockels cell,
PD : photo diode,
L : lens,
SF : spatial filter,
FR : Faraday rotator,
HWP : half-wave plate,
DC : dye cell (location for tests),
BE : beam expander,
A1, A2, A3 : amplifiers.

Fig.11 Block diagram of the pulse stretcher for the JK Laser.

Fig.12 (a) Time structure of a typical stretched pulse, measured downstream of the oscillator (1 ms/div) (lower trace),
Voltage on the Pockels cell (upper trace),

(b) Variations in flatness of 4-μs pulses: Ratio of the average deviation (40 sample points per pulse) from the average amplitude of each individual pulse, plotted for a total of 7500 consecutive laser pulses.

Fig.13 Laser energy used during the physics run (165 entries, 1 entry = 1 shift = 8 h):
(a) Mean energy per shift during the first (peak at 2.6 J) and the second period of the run (peak at 3.9 J)
(b) Spread in energy during a shift divided by the mean energy of the shift for the entire run.

Fig.14 Drawing of the dispersing lens, with the baffles between the two lens elements.

Fig.15 (a) Paths of two light rays (with slightly different initial radial position in the laser beam) through an early design of the dispersing lens. The main rays are shown by solid lines; reflected rays by dashed lines. A "T" indicates a total internal reflection. The total energy reaching the film, from the bundle of reflected rays similar to the one shown, is also given, assuming uncoated lens surfaces.

(b) Paths of two light rays (choosen to be the worst remaining cases, similar to the two rays in (a) above) through the final design of the dispersing lens. As the result of tapering the lower sidewall of the lens, the ray starting on the left undergoes two additional (non-total internal) reflections before reaching the film with greatly reduced energy. Reflections from the ray starting on the right now miss the film entirely. Uncoated surfaces were also assumed here.

Fig.16 Top view of the EMI/IPF with dimensions of various planes. Not to scale.

Fig.17 Holographic Replay - Real Image (schematic).

Fig.18 Holographic Replay - Virtual Image (schematic).

Fig.19 Schematic layout of virtual image reconstruction machine:

1 : single-mode optical fiber
2 : film reels
3 : imaging lens
4 : holographic virtual image
5 : hologram and liquid film gate
6 : illumination laser light.

Fig.20 Baffles inside the Bubble Chamber:

(a) View from the piston region towards the top of the empty Bubble Chamber, showing the six optic ports, the rippled structure of the main heat exchanger (beanie head), some of its baffles, as well as most of the baffles on the side walls,

(b) View from one of the cameras into the track-sensitive Bubble Chamber, showing the baffles on the side walls, which produce almost no parasitic bubbles during expansion of the Chamber.

Fig.21 Factor by which the minimum detectable BBR is multiplied by if noise light is present as a function of the ratio of noise light intensity to total (noise plus reference beam) light intensity on the film. Experimental points show the measured change in this intensity ratio as a result of installing the baffles in the beenie, aligning the laser beam into the Chamber, and removing test targets. The baffles on the main spherical wall were in place throughout this series of measurements.

Fig.22 Growth rate, A ($cm/s^{1/2}$), for track (dashed line) and laser-induced bubbles (solid line).

Fig.23 Pictures of laser-induced boiling inside the Chamber as seen from one conventional camera. Cosmic ray tracks are visible (no magnetic field).

(a) Q-switched pulse, ~120 ns, 1000 mJ

(b) Stretched pulse. 2.2 μs, 1000 mJ

(c) Free-lasing pulse, ~1 ms, 700 mJ

Fig.24 Height of boiling cone inside the liquid as function of laser input power for two pulse durations.

Fig.25 Oscilloscope picture of light intensities (arbitrary units) of a laser pulse (duration 2 μs) vs time. Upper trace: measured downstream of the last laser amplifier; lower trace: measured with photodiodes on the film plane. Horizontal scale: 0.5 μs/div.

Fig.26 Slope of the laser light intensity vs. time curve measured at the film plane, as function of laser input energies into the Chamber for 7.7 μs pulse duration.

Fig.27 Digitized beam profiles as recorded with a CCD camera:

(a) after the oscillator stage of the laser (diameter ~2 mm),

(b) underneath the dispersing lens, measured in the monitoring box, laser beam going into the expanding Bubble Chamber (actual diameter ~50 mm).

Fig.28 (a) Hurter & Driffield curve, measured for $\lambda = 694.3$ nm, pulse duration $\tau = 2.5$ μs and our development conditions of the AGFA-Gevaert 10E75 emulsion

(b) Same results in an amplitude transmittance vs laser energy plot.

Fig.29 Comparison of a conventionally and holographically recorded neutrino interaction:

(a), (b), (c) photos taken with three conventional cameras,

(d) hologram,

(e) interpretation of the event (schematic)

1, 4, 5: charged particles,

3: particle decaying into C1, C2, C3.

Fig.30 Beam Branching Ratios of 51 event vertices found in 1650 holograms (result from the Fermilab replay machine).

Fig.31 Scatter plot of seen and unseen events (one holographic roll): holographic z-axis versus illumination angle.

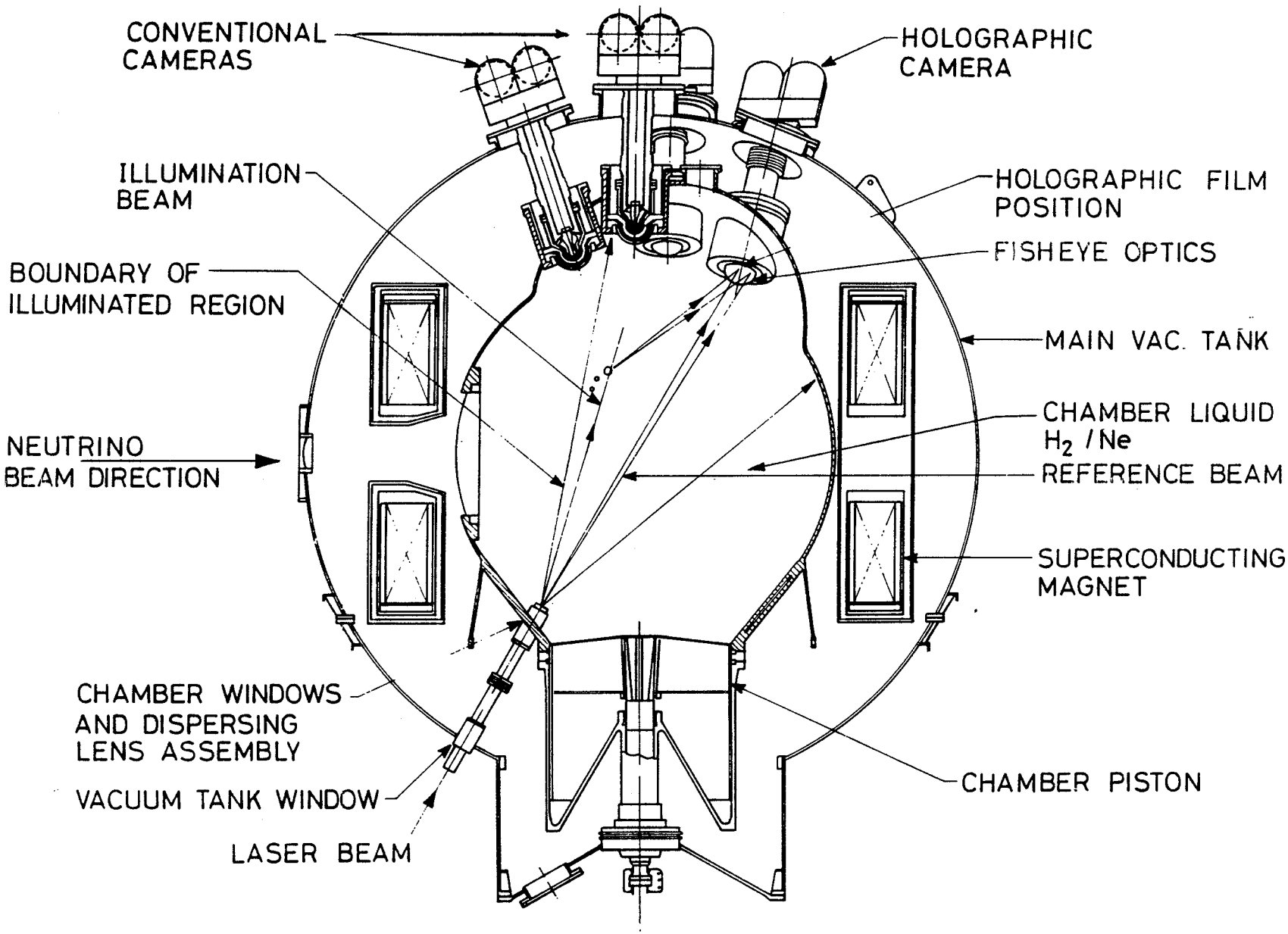
CONVENTIONAL CAMERAS
HOLOGRAPHIC CAMERA
ILLUMINATION BEAM
HOLOGRAPHIC FILM POSITION
FISHEYE OPTICS
BOUNDARY OF ILLUMINATED REGION
MAIN VAC. TANK
CHAMBER LIQUID H_2 / Ne
NEUTRINO BEAM DIRECTION
REFERENCE BEAM
SUPERCONDUCTING MAGNET
CHAMBER WINDOWS AND DISPERSING LENS ASSEMBLY
VACUUM TANK WINDOW
LASER BEAM
CHAMBER PISTON

Fig. 1

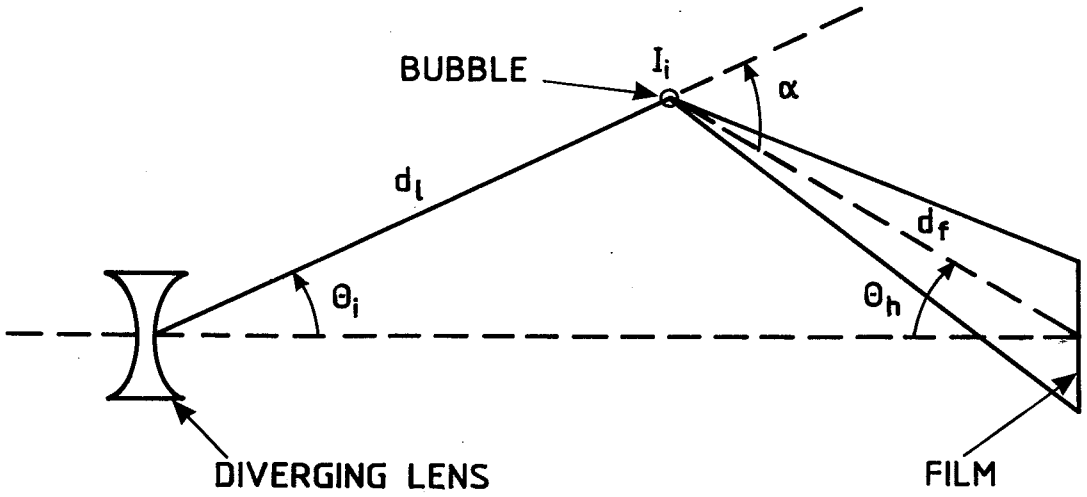

Fig. 2

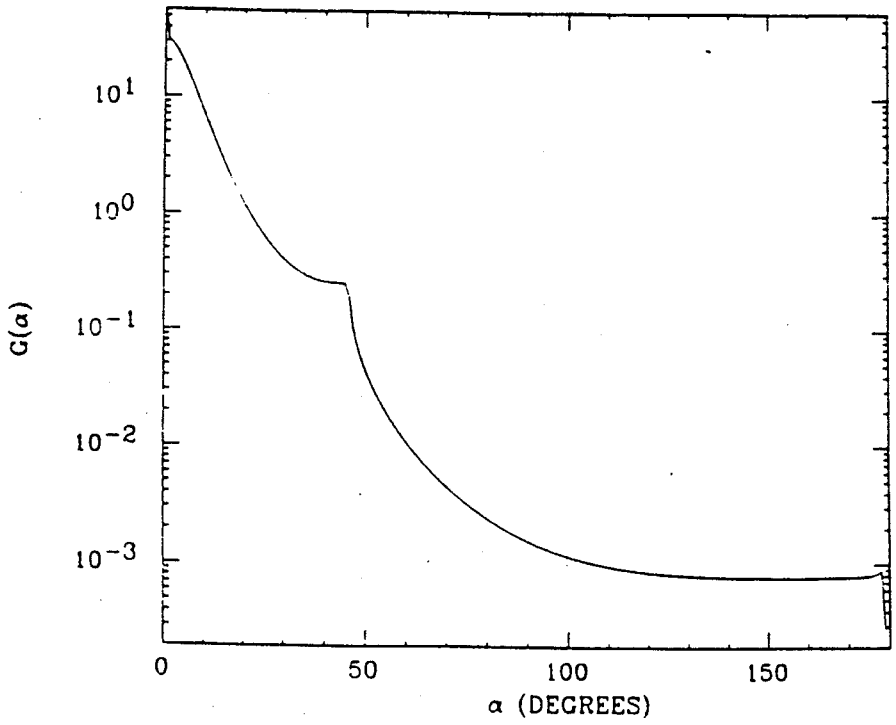
G(α)
10^1
10^0
10^{-1}
10^{-2}
10^{-3}
0
50
100
150
α (DEGREES)

Fig. 3

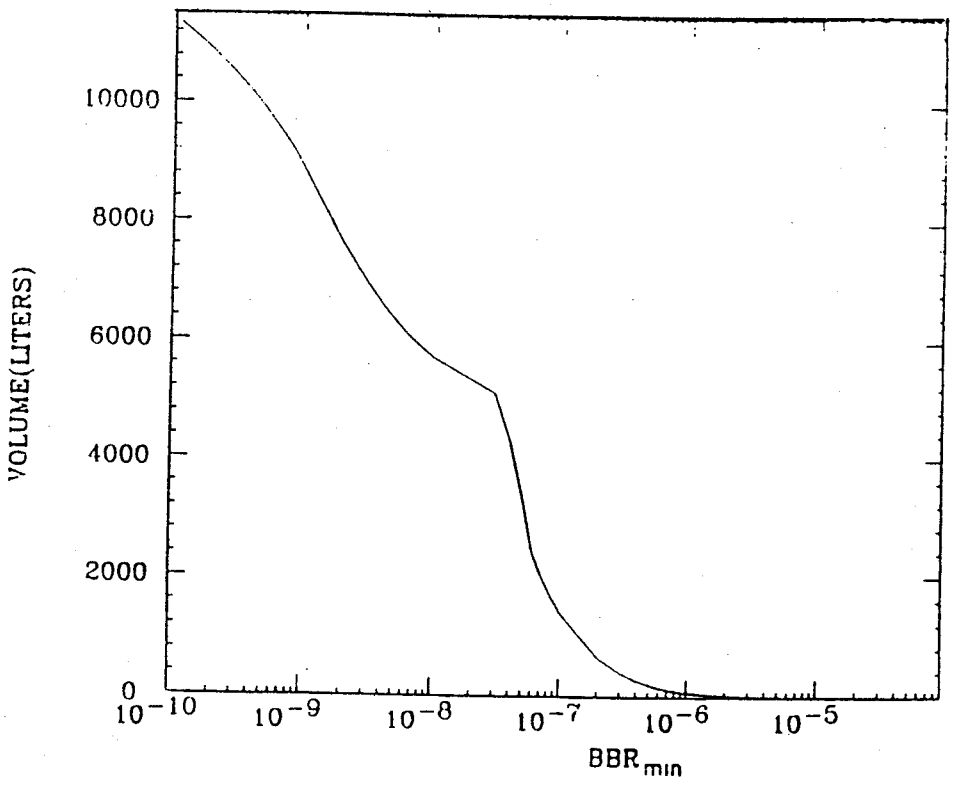
VOLUME(LITERS)
10000
8000
6000
4000
2000
0
10^{-10}
10^{-9}
10^{-8}
10^{-7}
10^{-6}
10^{-5}
BBR_{min}

Fig. 4

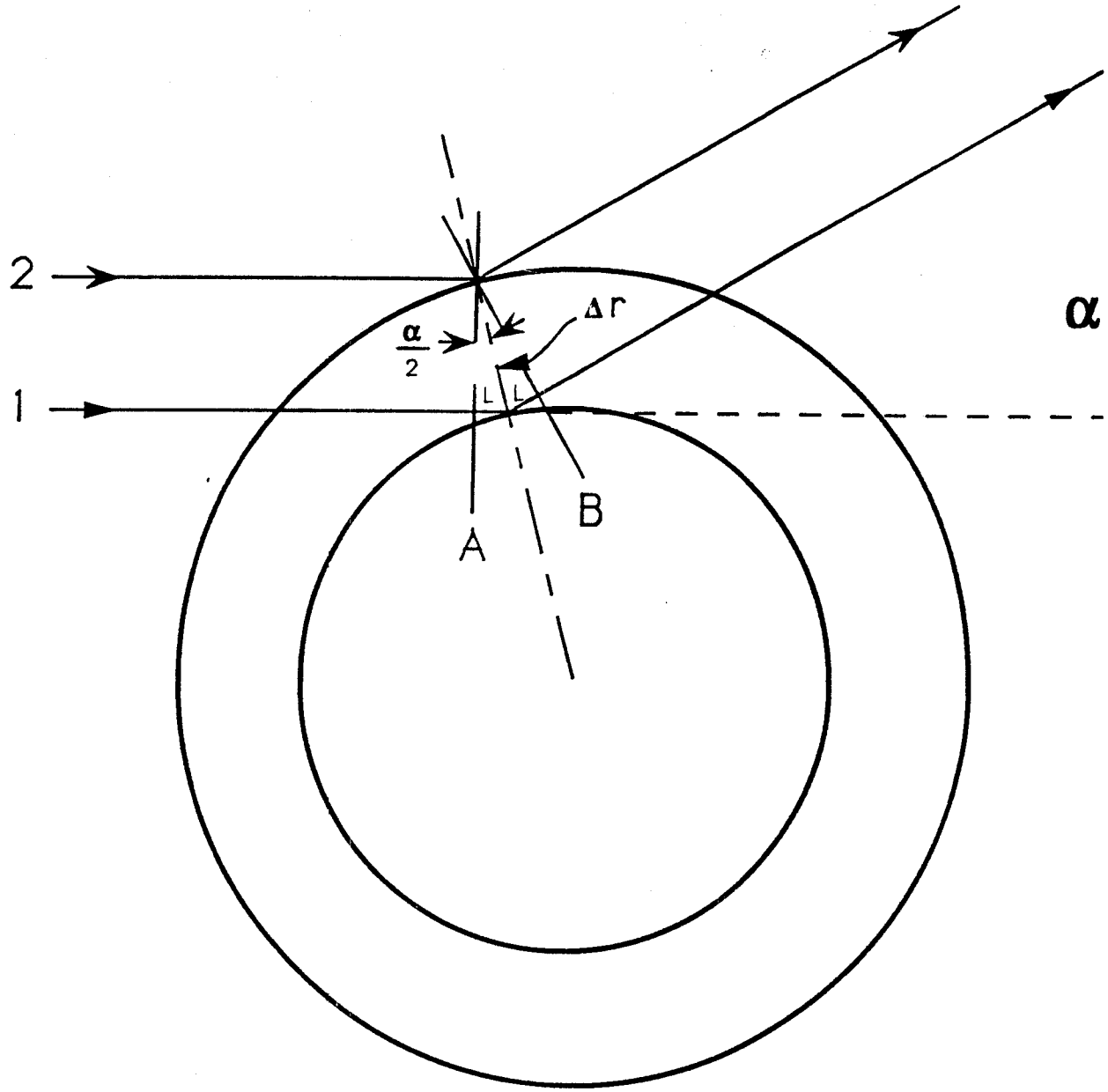

Fig. 5

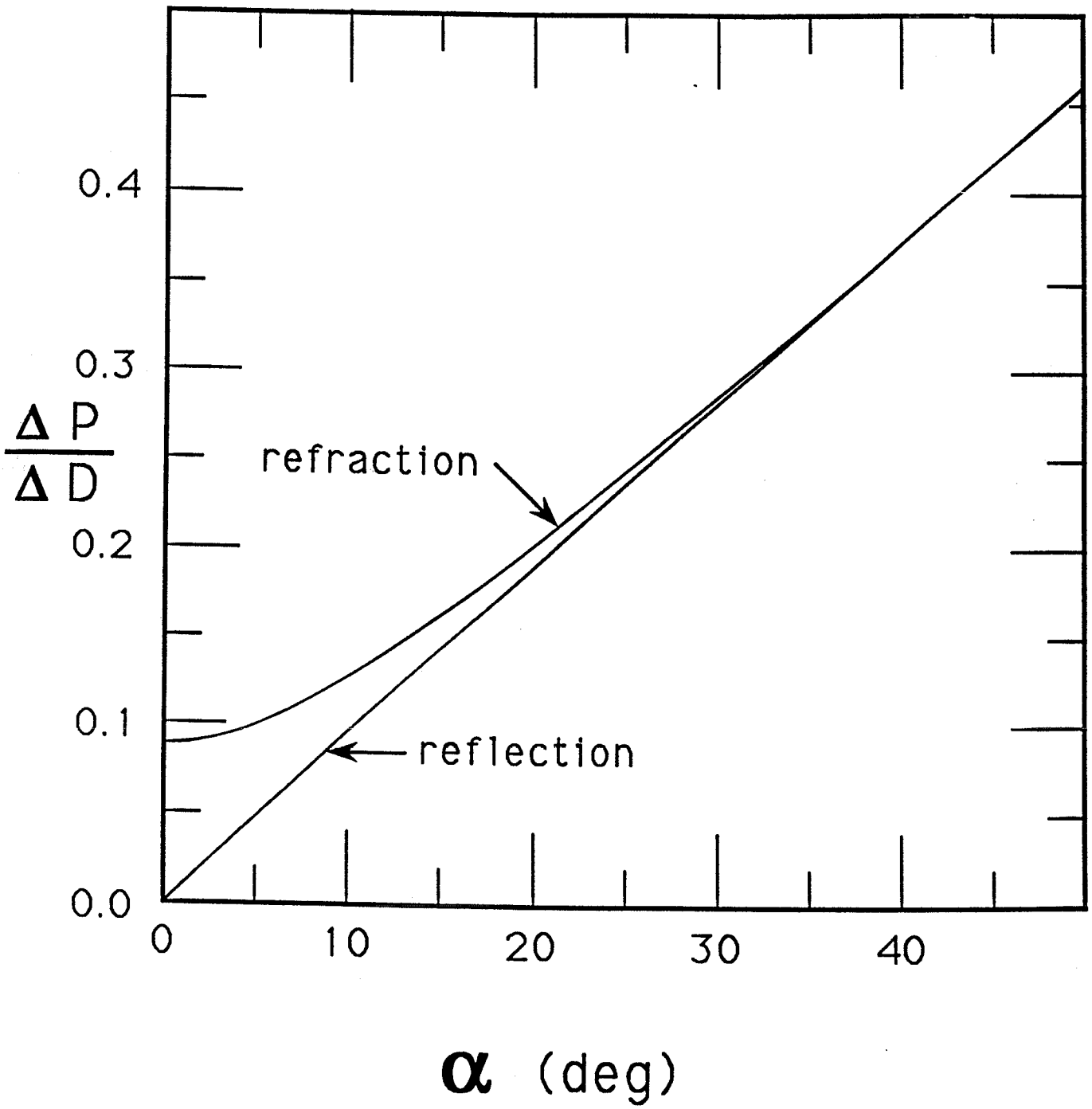

Fig. 6

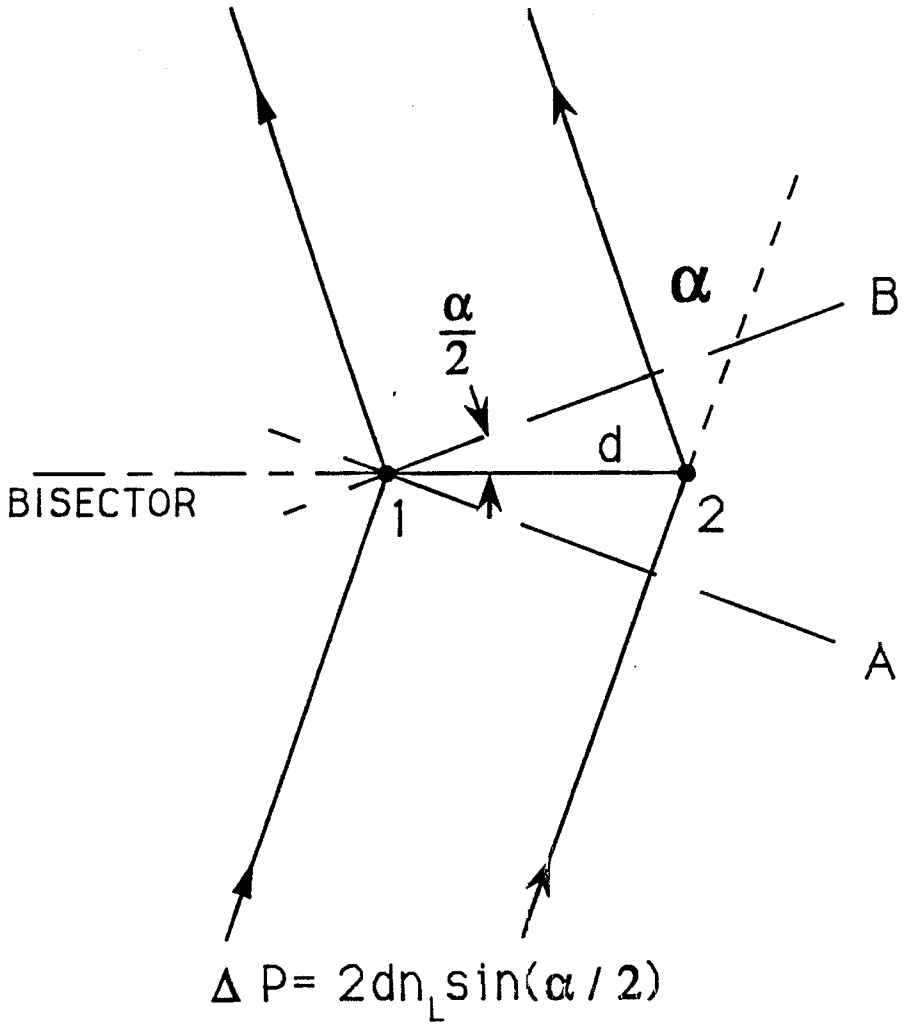

displacement d along bisector

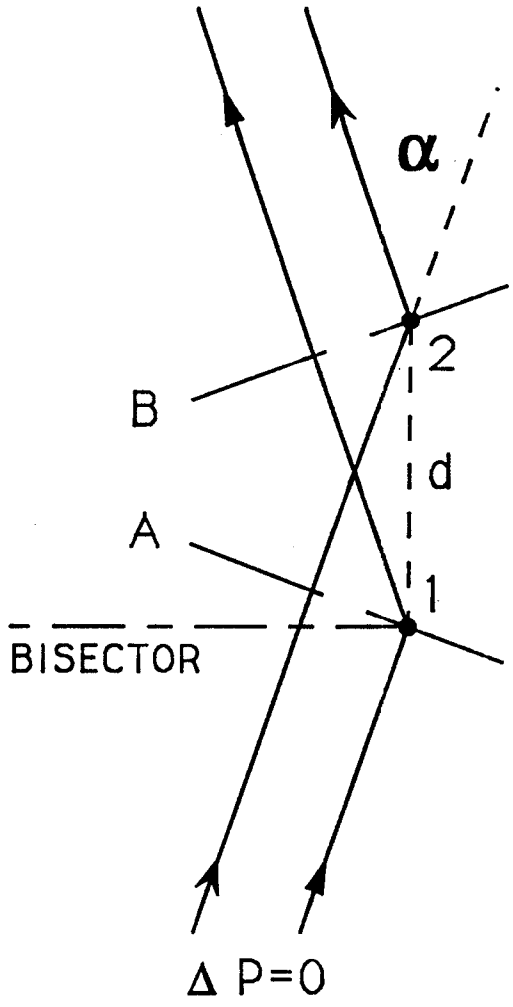

displacement d ⊥ to bisector

Fig. 7

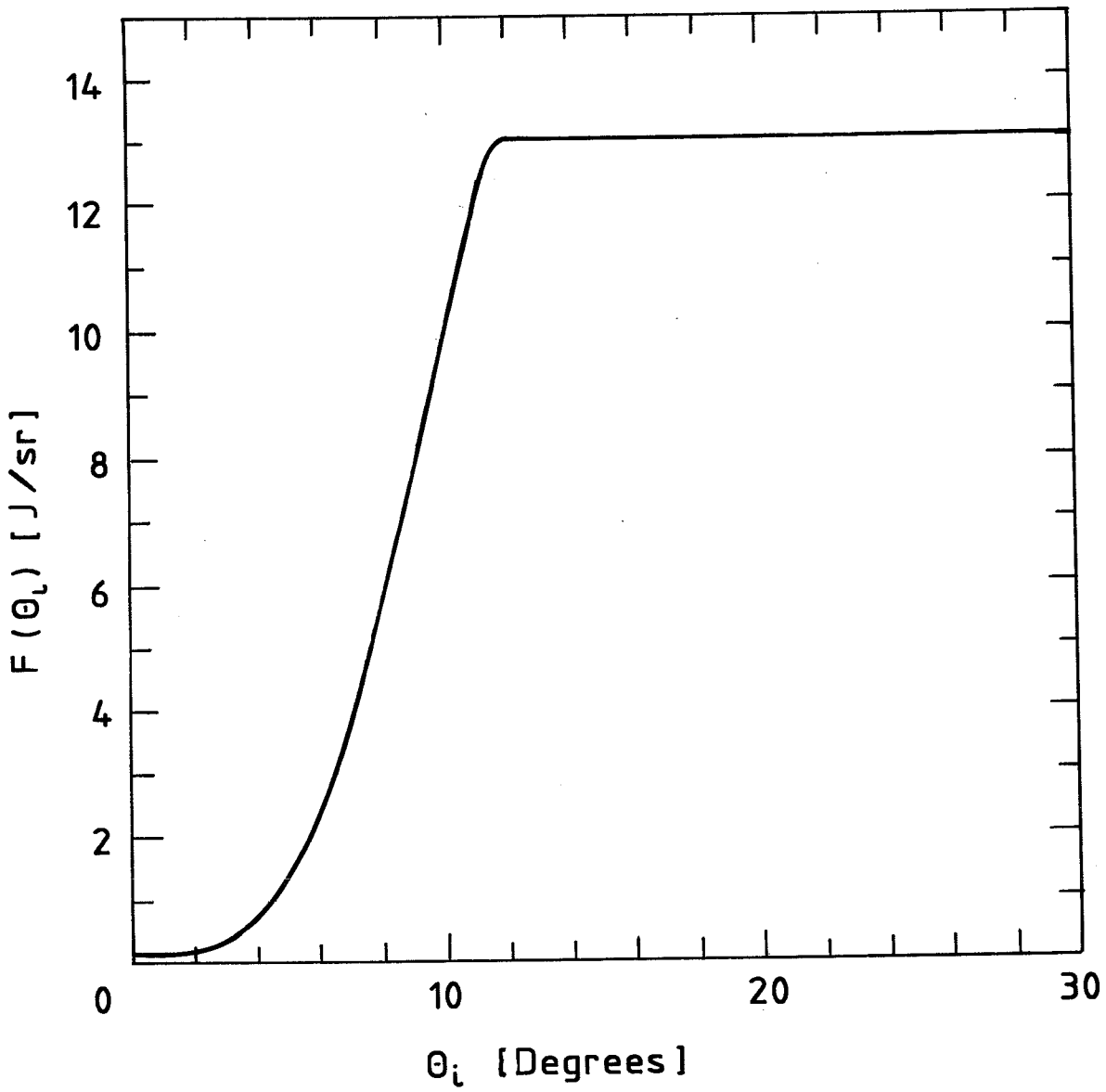

Fig. 8

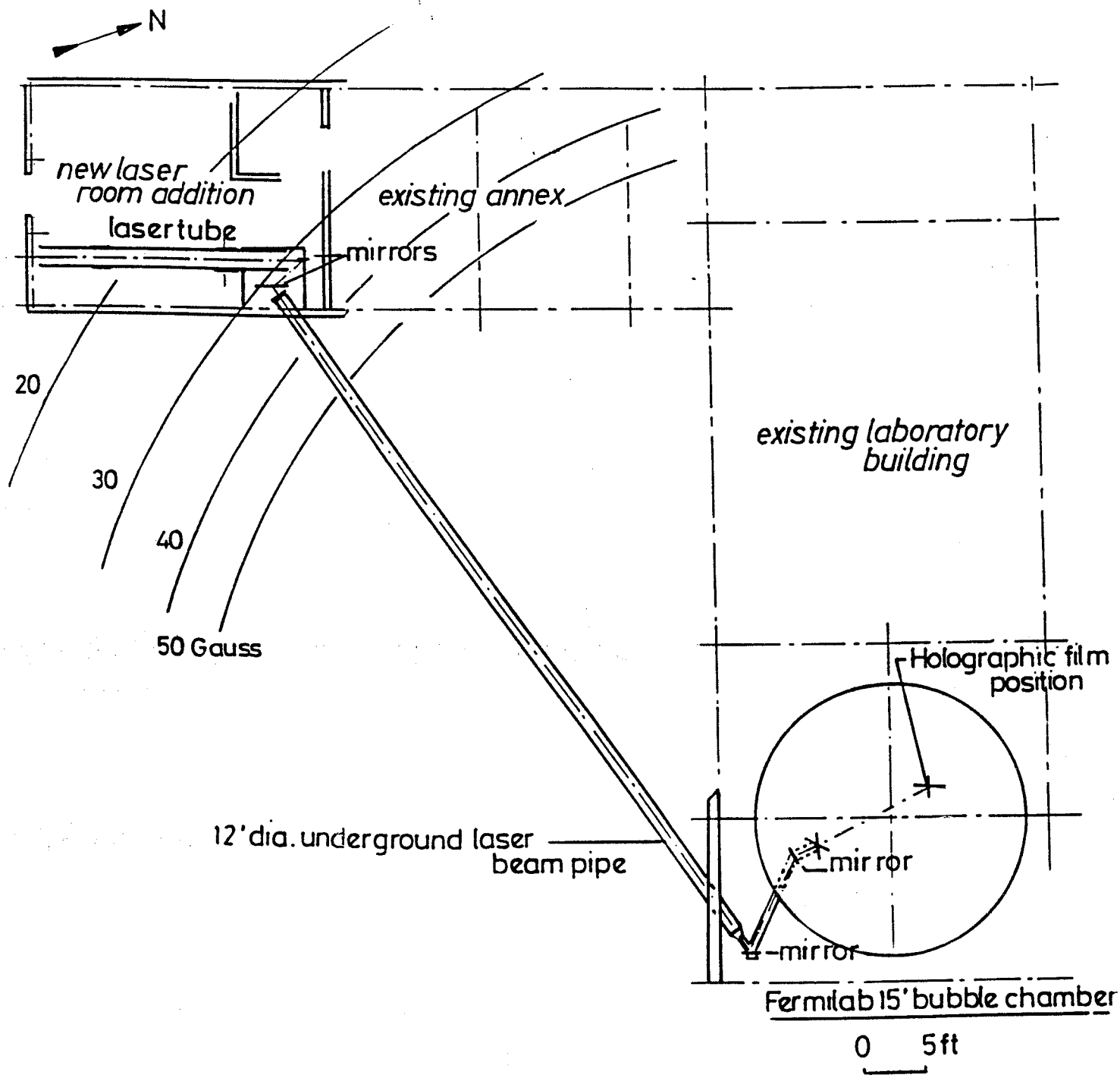
N
new laser
room addition
laser tube
existing annex
mirrors
20
30
40
50 Gauss
existing laboratory
building
Holographic film
position
12' dia. underground laser
beam pipe
mirror
mirror
Fermilab 15' bubble chamber
0 5ft

Fig. 9

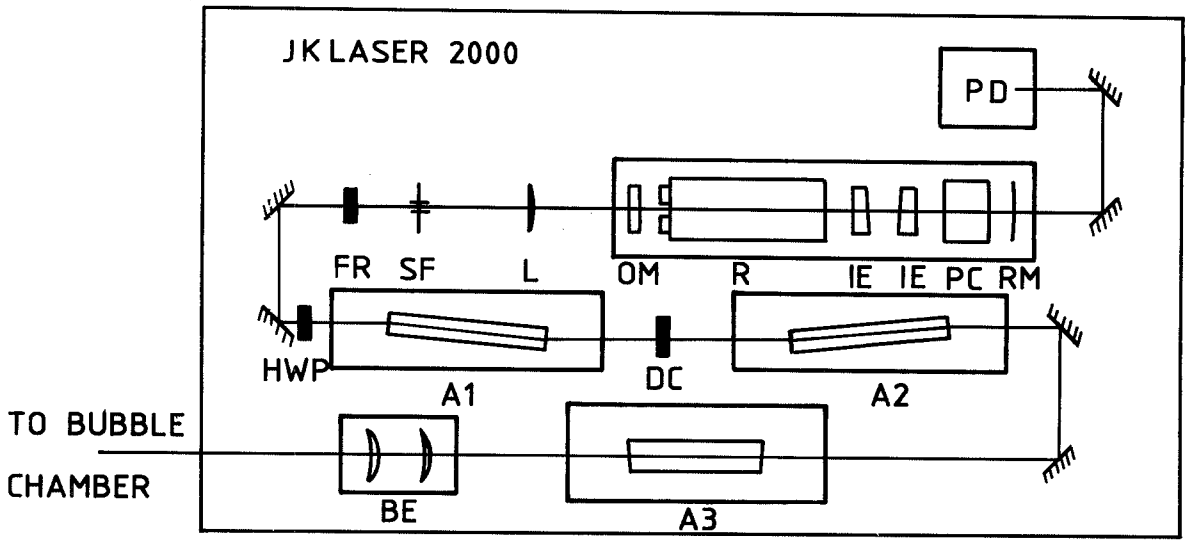
JK LASER 2000
PD
FR
SF
L
OM
R
IE
IE
PC
RM
HWP
A1
DC
A2
TO BUBBLE
CHAMBER
BE
A3

Fig. 10

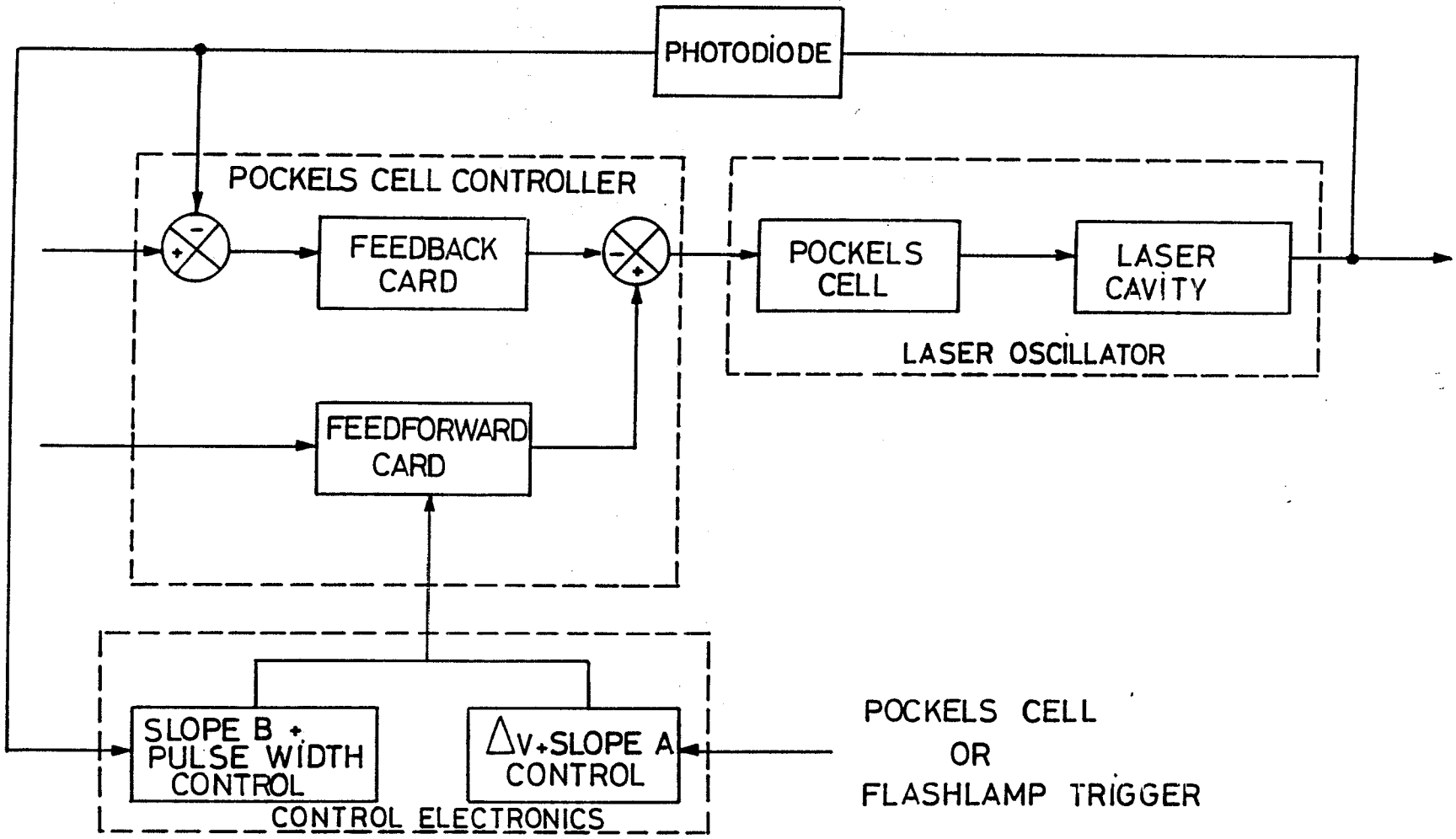

Blockdiagram of the pulse stretcher for the JK Laser.

Fig. 11

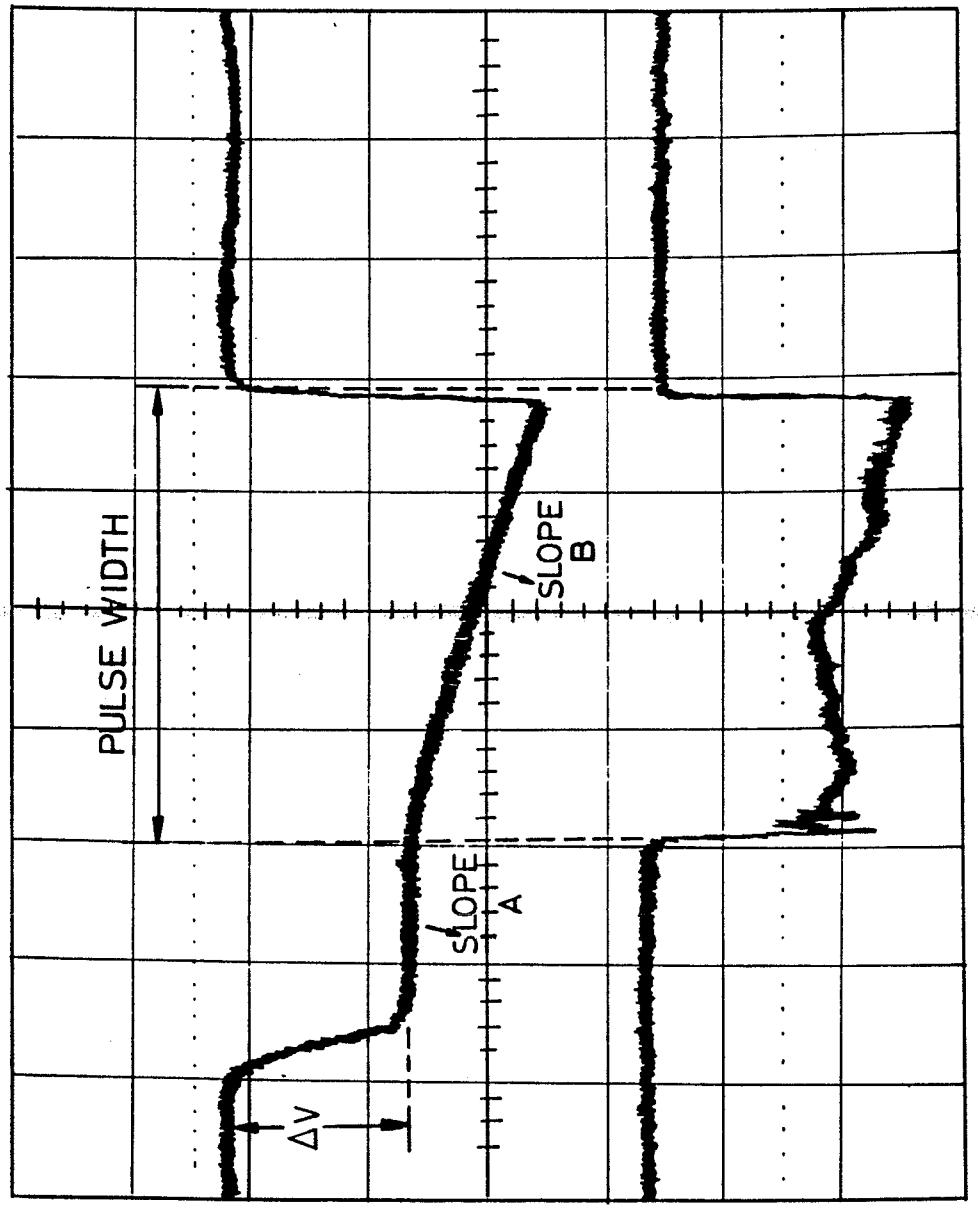

Fig. 12 (a)

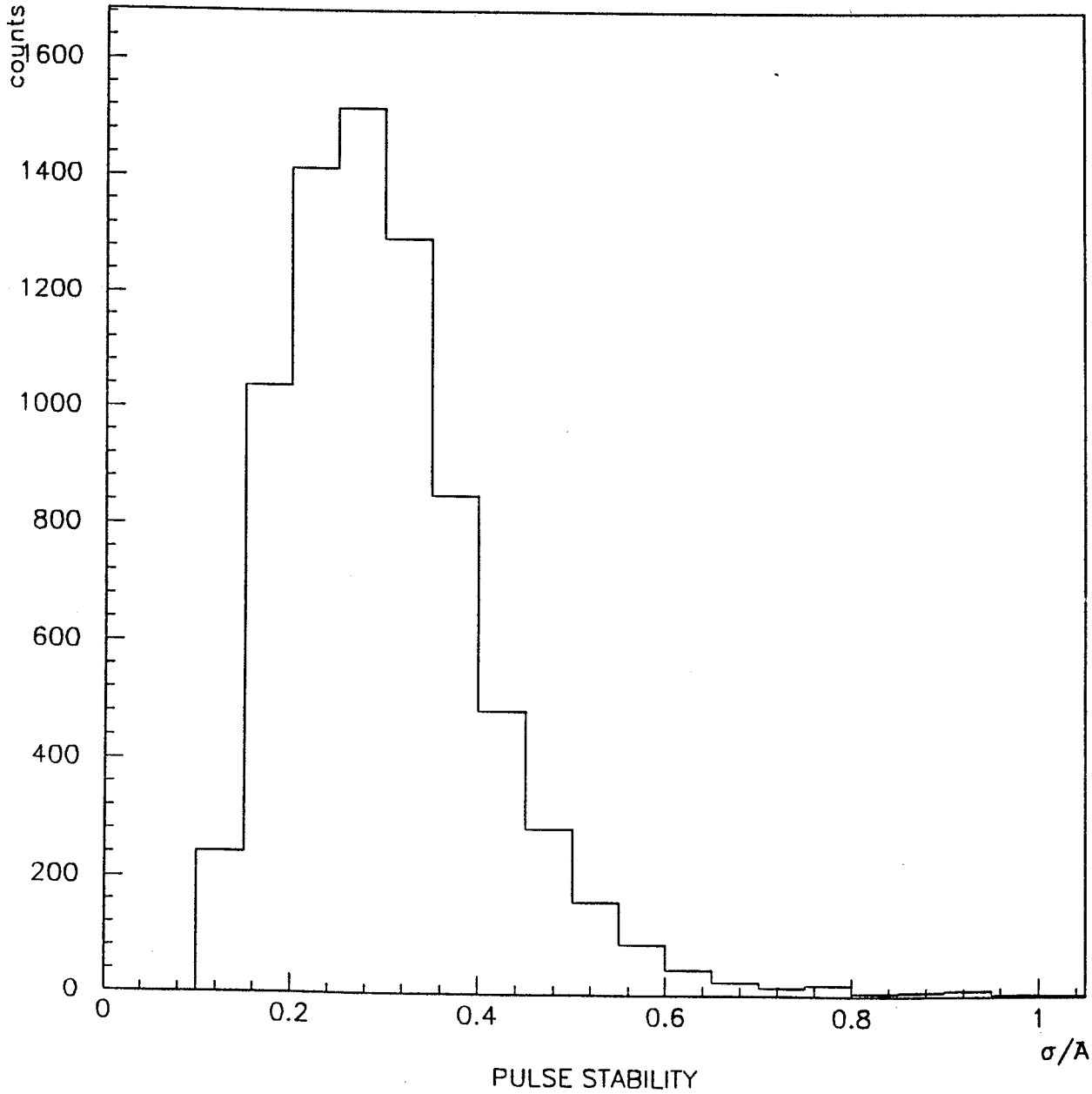
counts
1600
1400
1200
1000
800
600
400
200
0
0
0.2
0.4
0.6
0.8
1
σ/A
PULSE STABILITY

Fig. 12 (b)

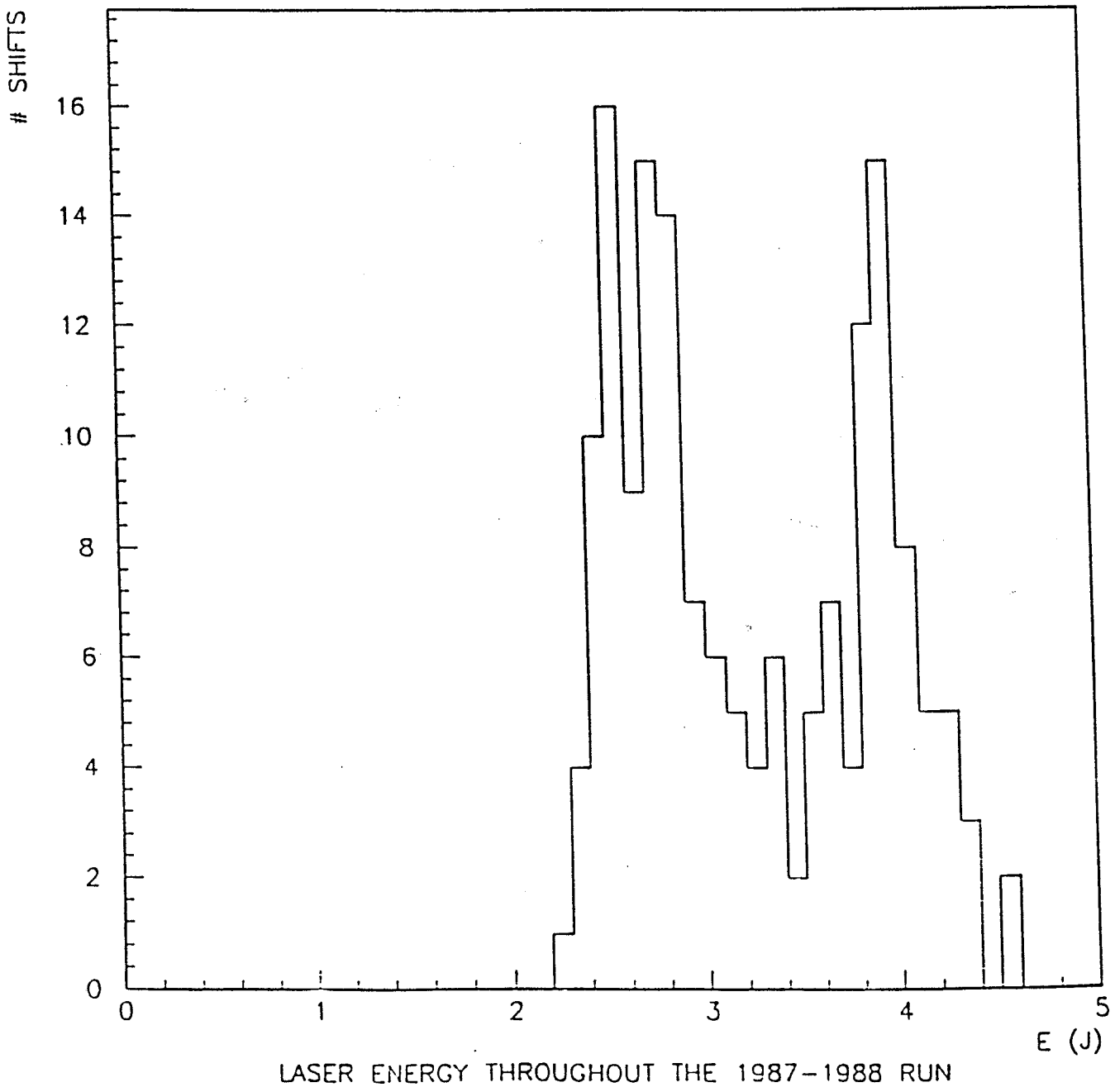
SHIFTS
16
14
12
10
8
6
4
2
0
0
1
2
3
4
5
E (J)
LASER ENERGY THROUGHOUT THE 1987-1988 RUN

Fig. 13 (a)

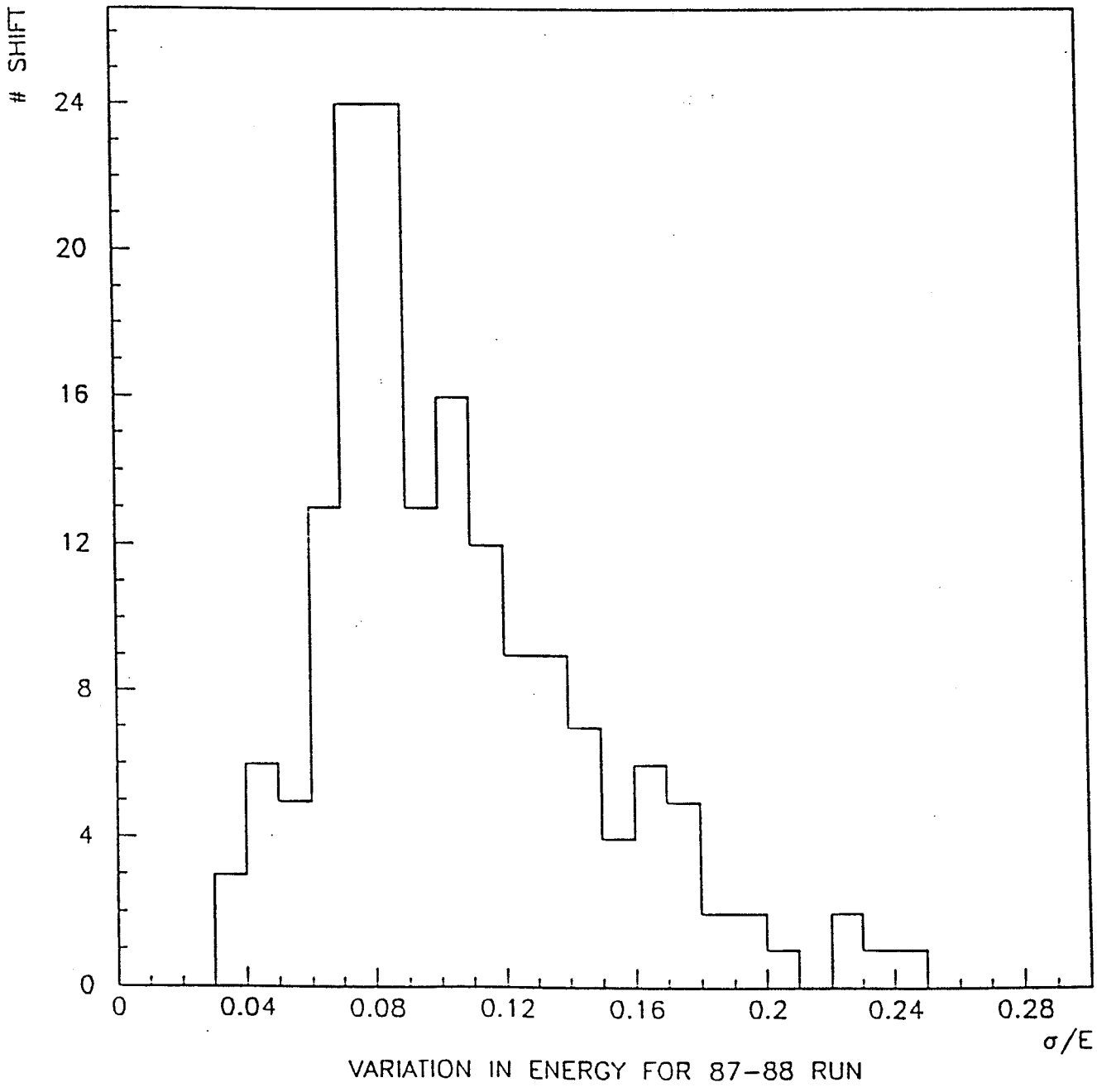
SHIFT
24
20
16
12
8
4
0
0
0.04
0.08
0.12
0.16
0.2
0.24
0.28
σ/E
VARIATION IN ENERGY FOR 87-88 RUN

Fig. 13 (b)

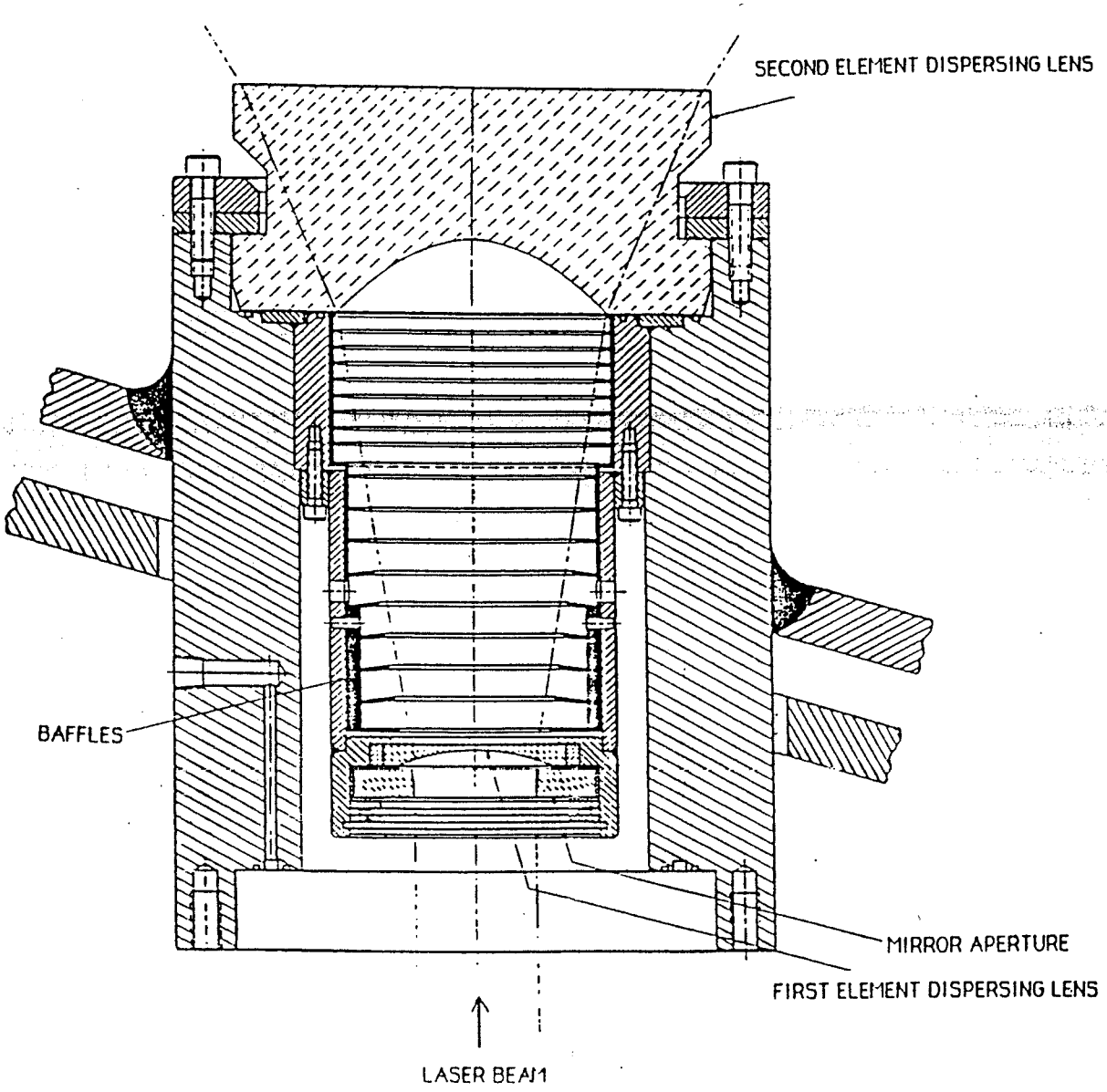
SECOND ELEMENT DISPERSING LENS
BAFFLES
MIRROR APERTURE
FIRST ELEMENT DISPERSING LENS
LASER BEAM

Fig. 14

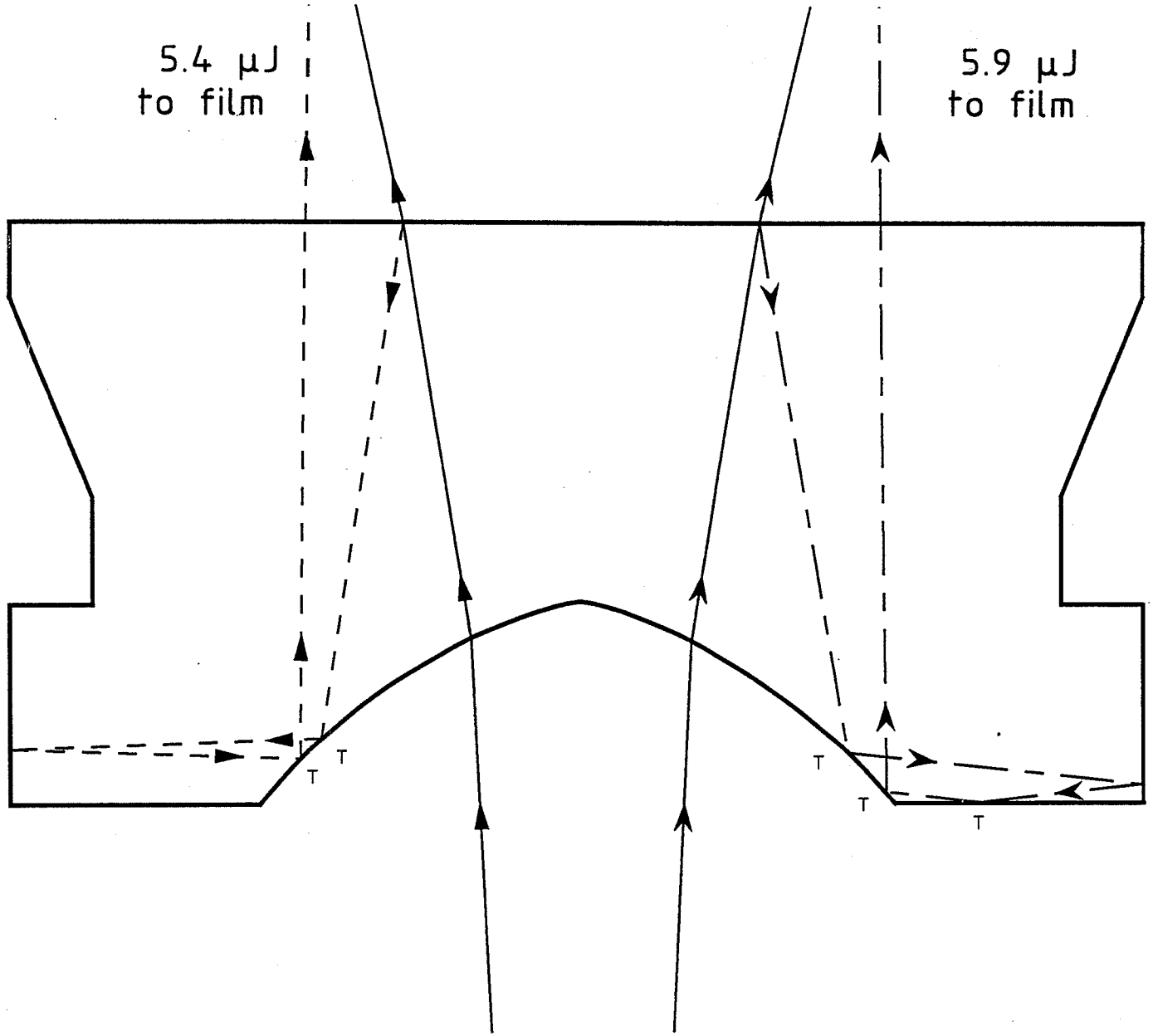

Fig. 15 (a)

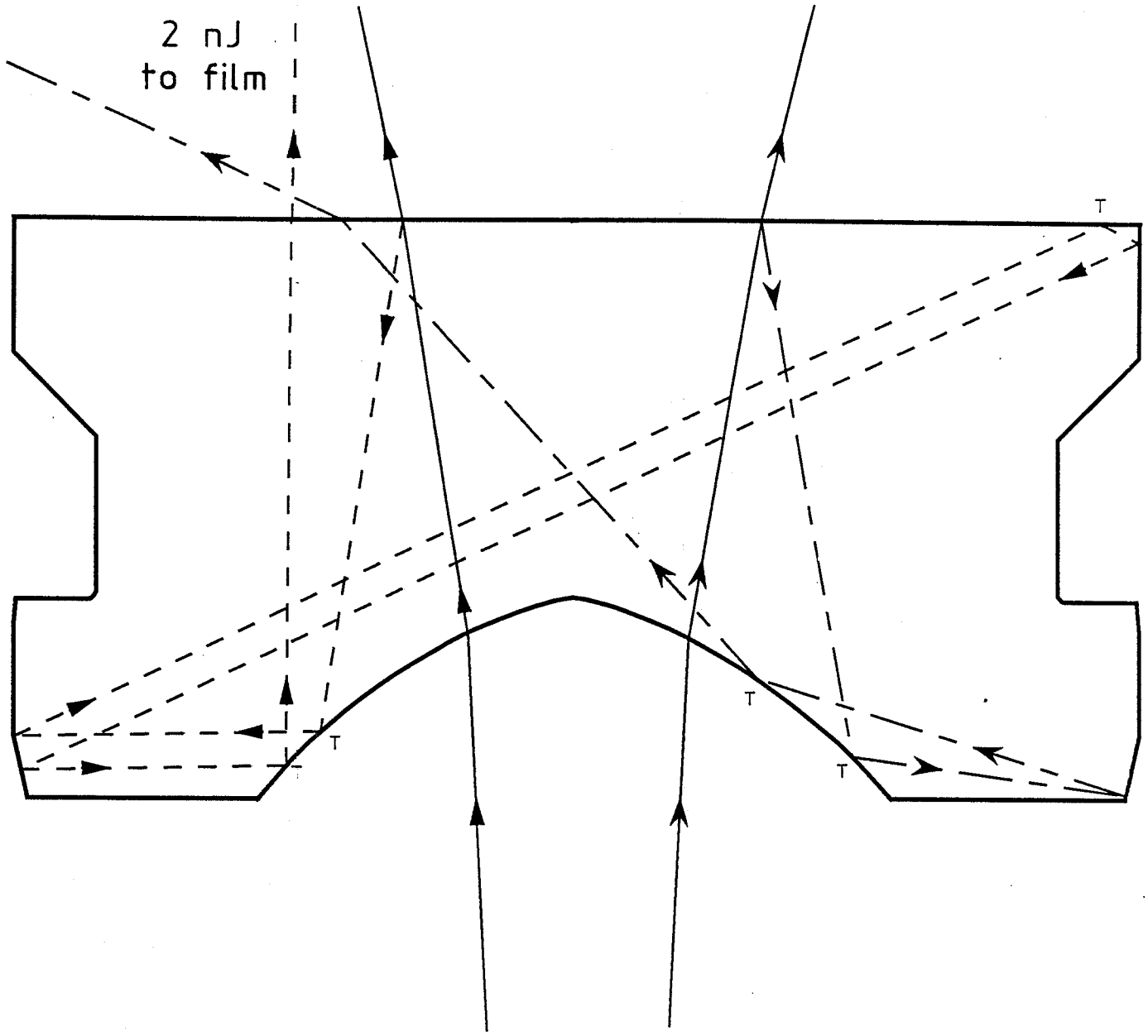

Fig. 15 (b)

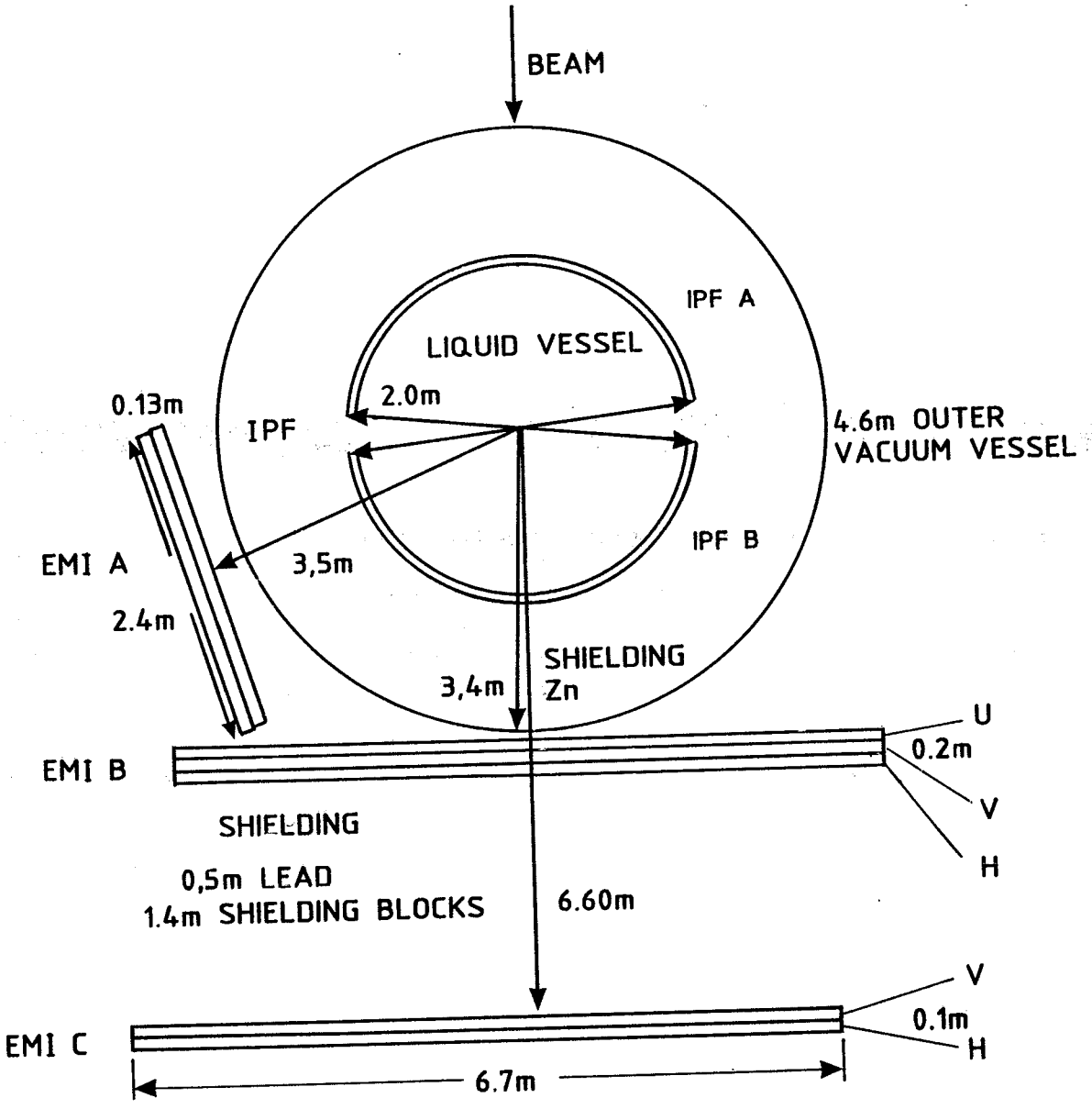
BEAM
IPF A
LIQUID VESSEL
2.0m
0.13m
IPF
4.6m OUTER
VACUUM VESSEL
IPF B
EMI A
3,5m
2.4m
SHIELDING
Zn
3,4m
U
0.2m
EMI B
V
H
SHIELDING
0,5m LEAD
1.4m SHIELDING BLOCKS
6.60m
V
0.1m
EMI C
H
6.7m

Fig. 16

HOLOGRAPHIC REPLAY - REAL IMAGE

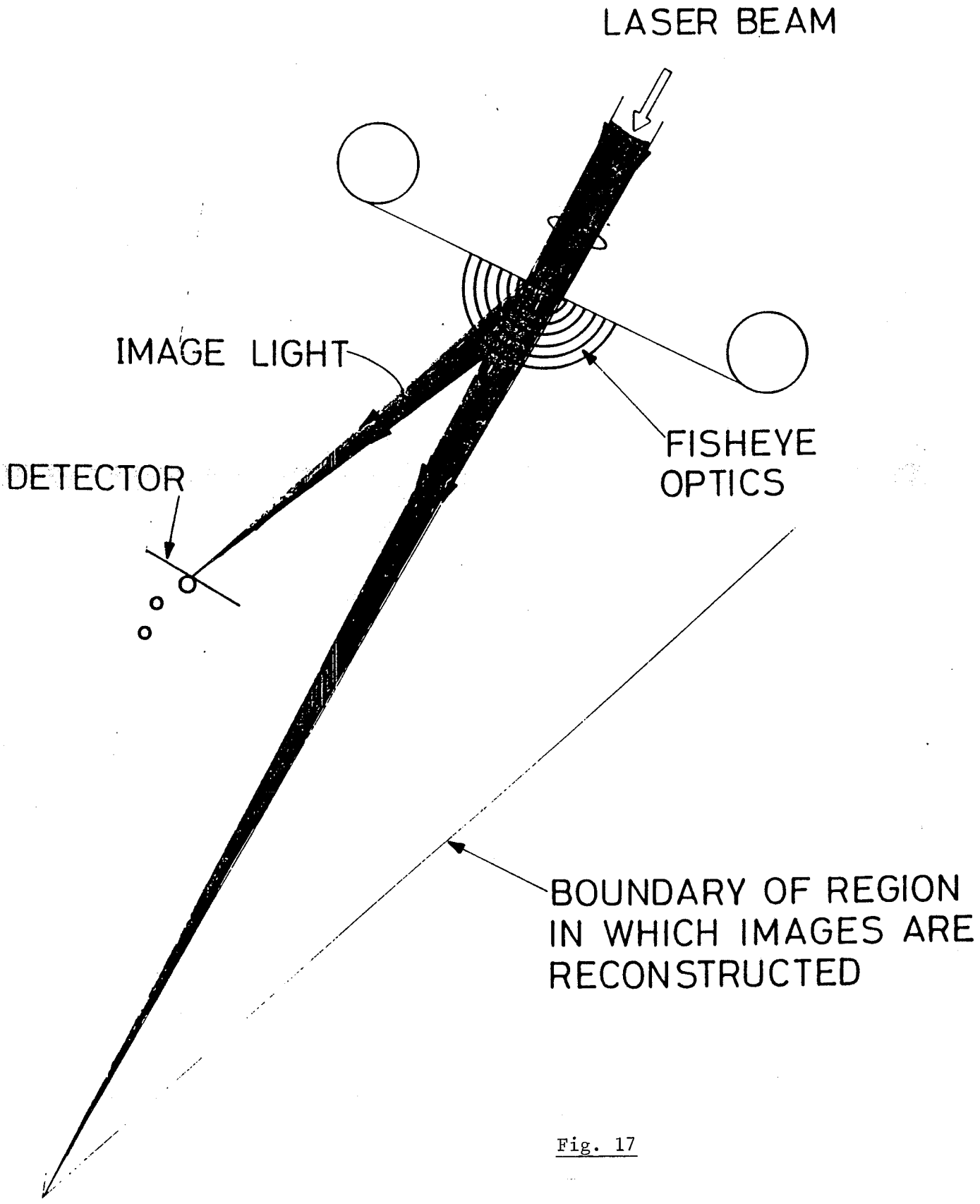

Fig. 17

HOLOGRAPHIC REPLAY - VIRTUAL IMAGE

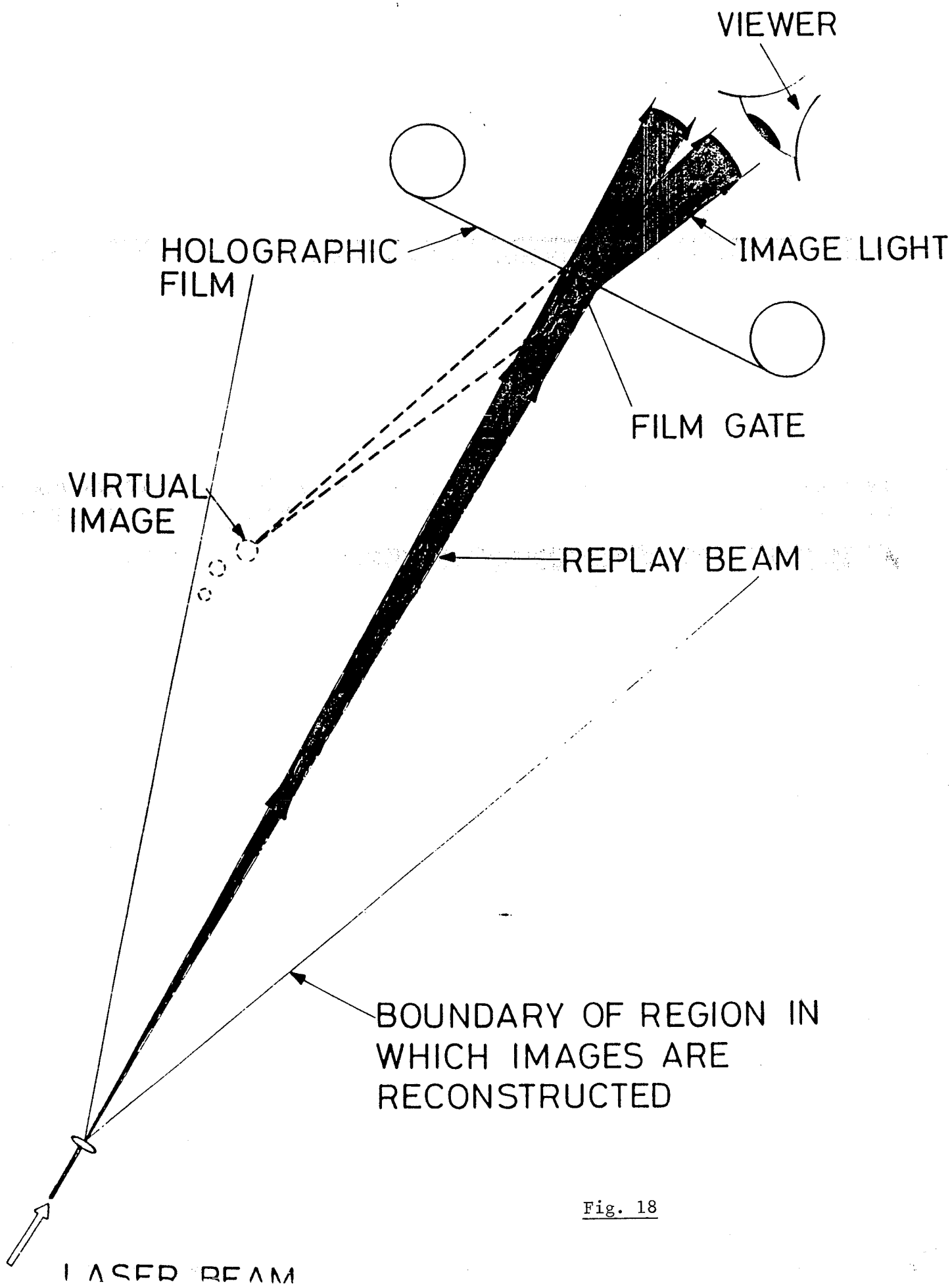

Fig. 18

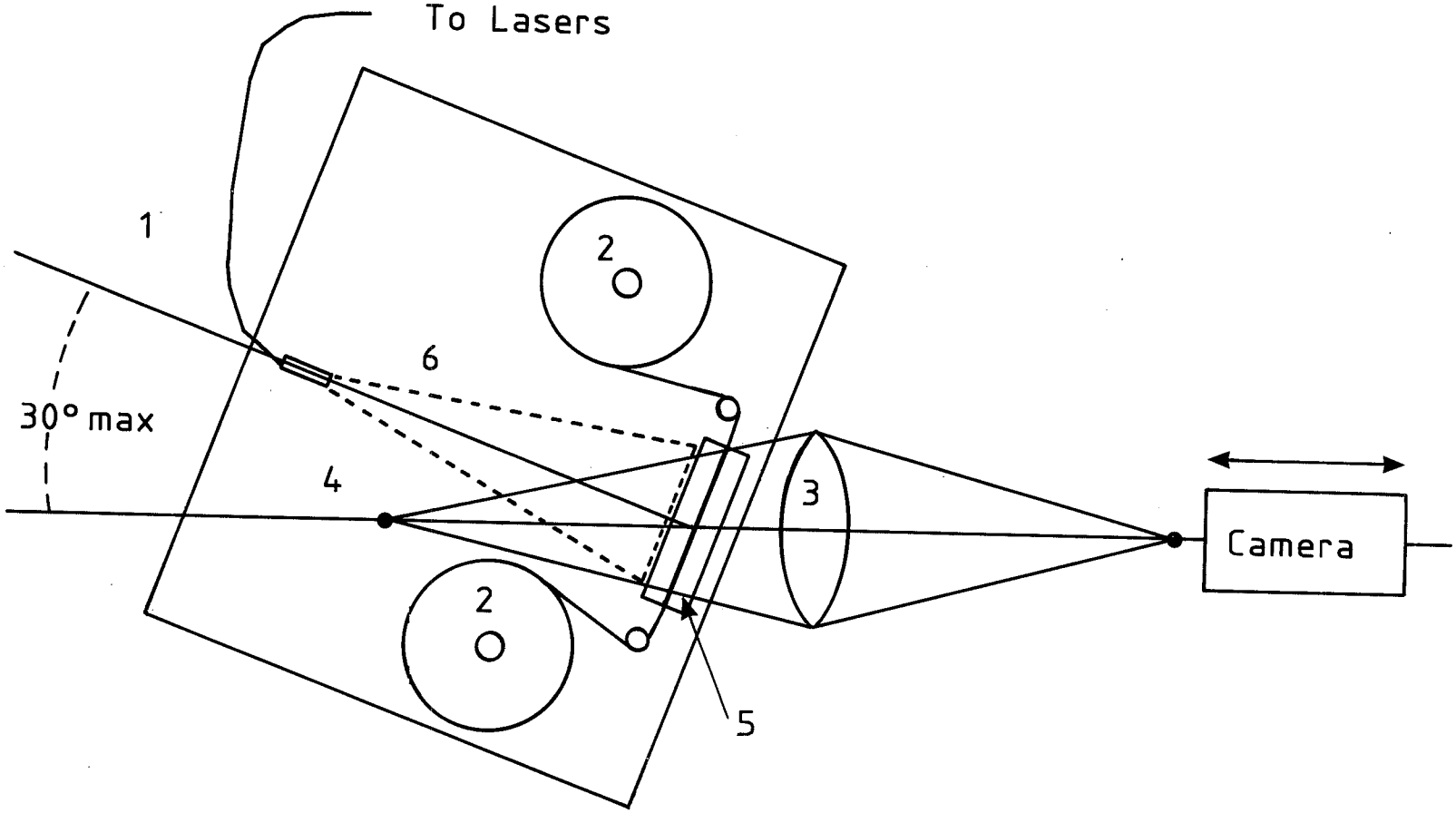

Fig. 19

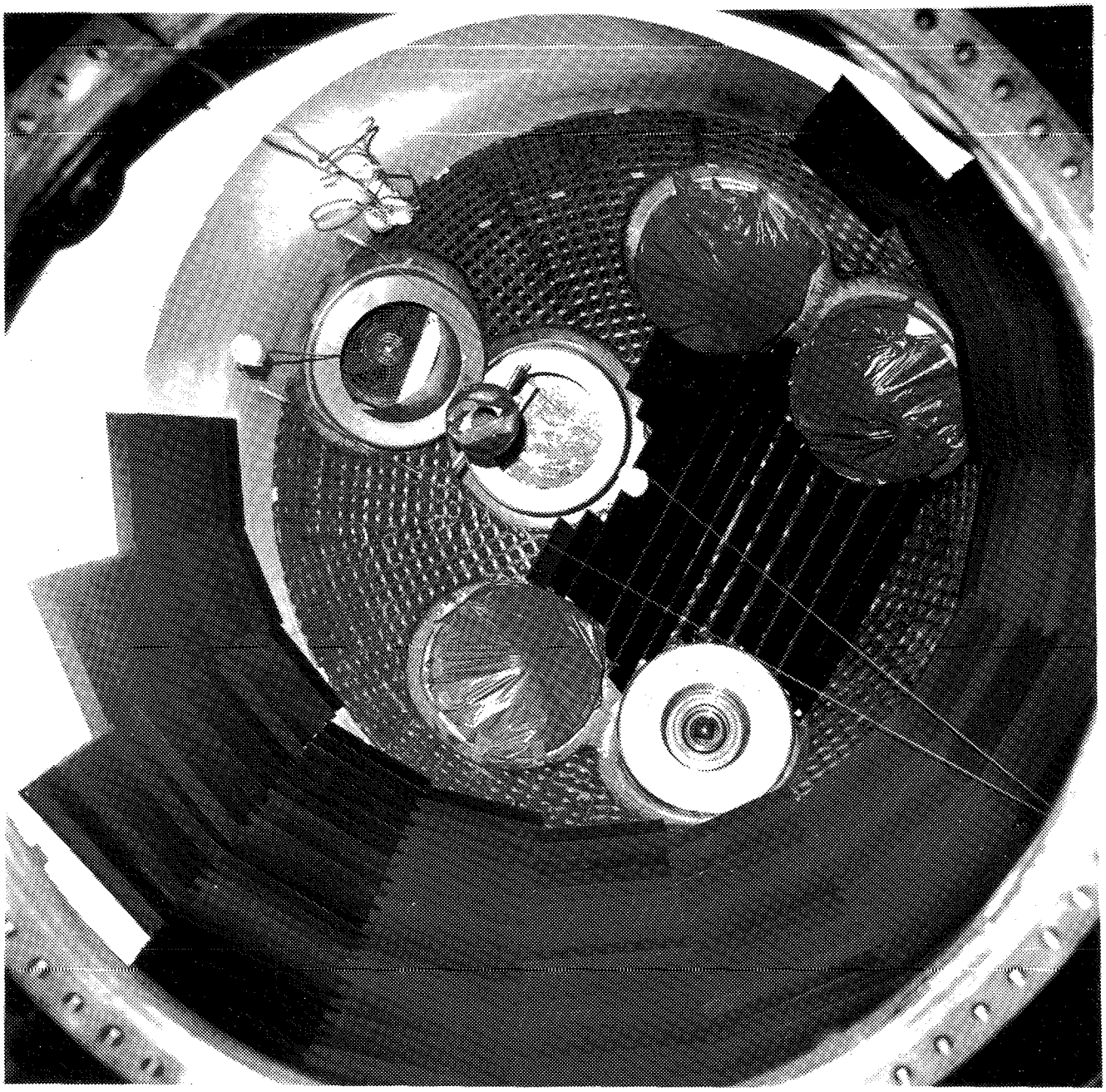

Fig. 20 (a)

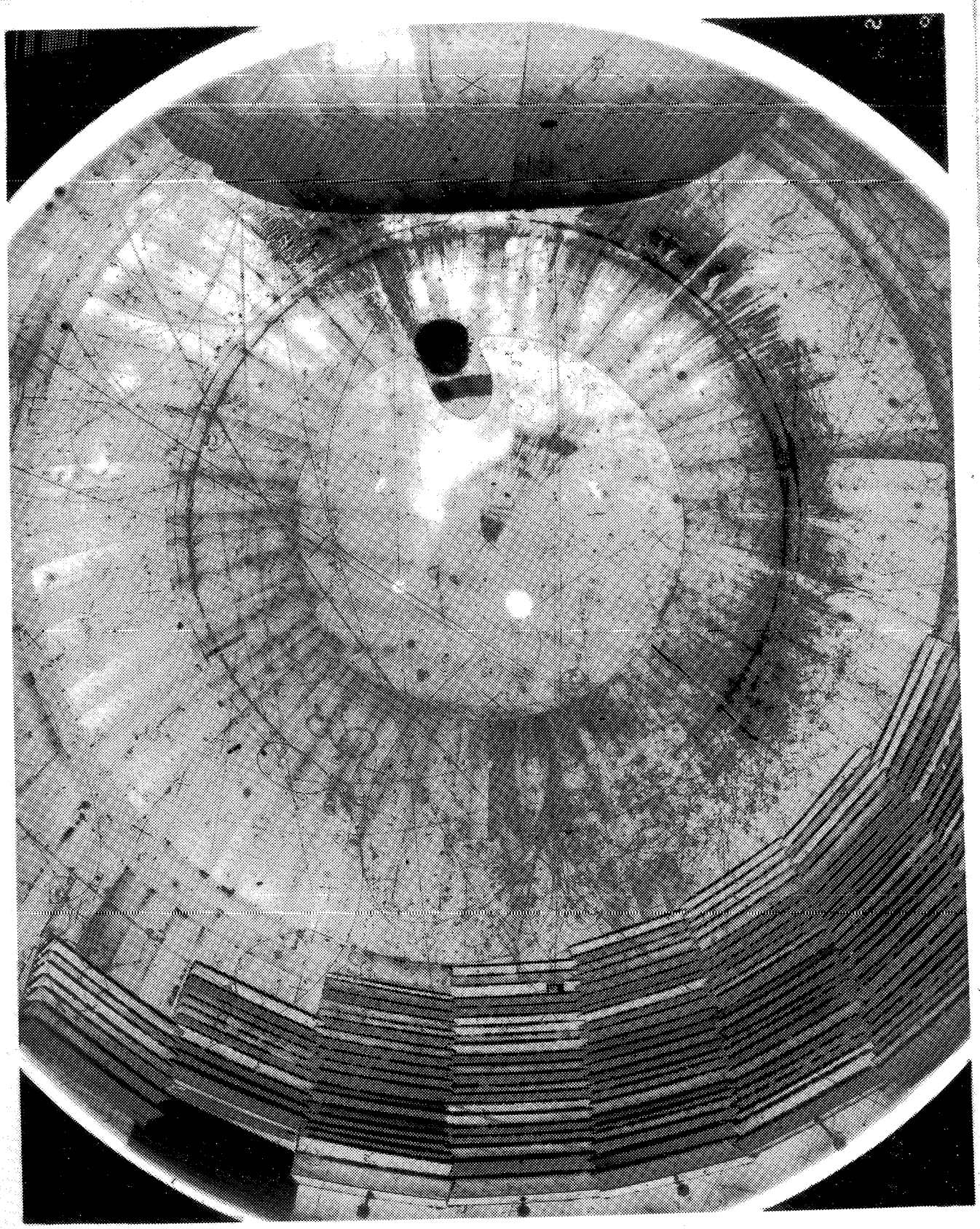

Fig. 20 (b)

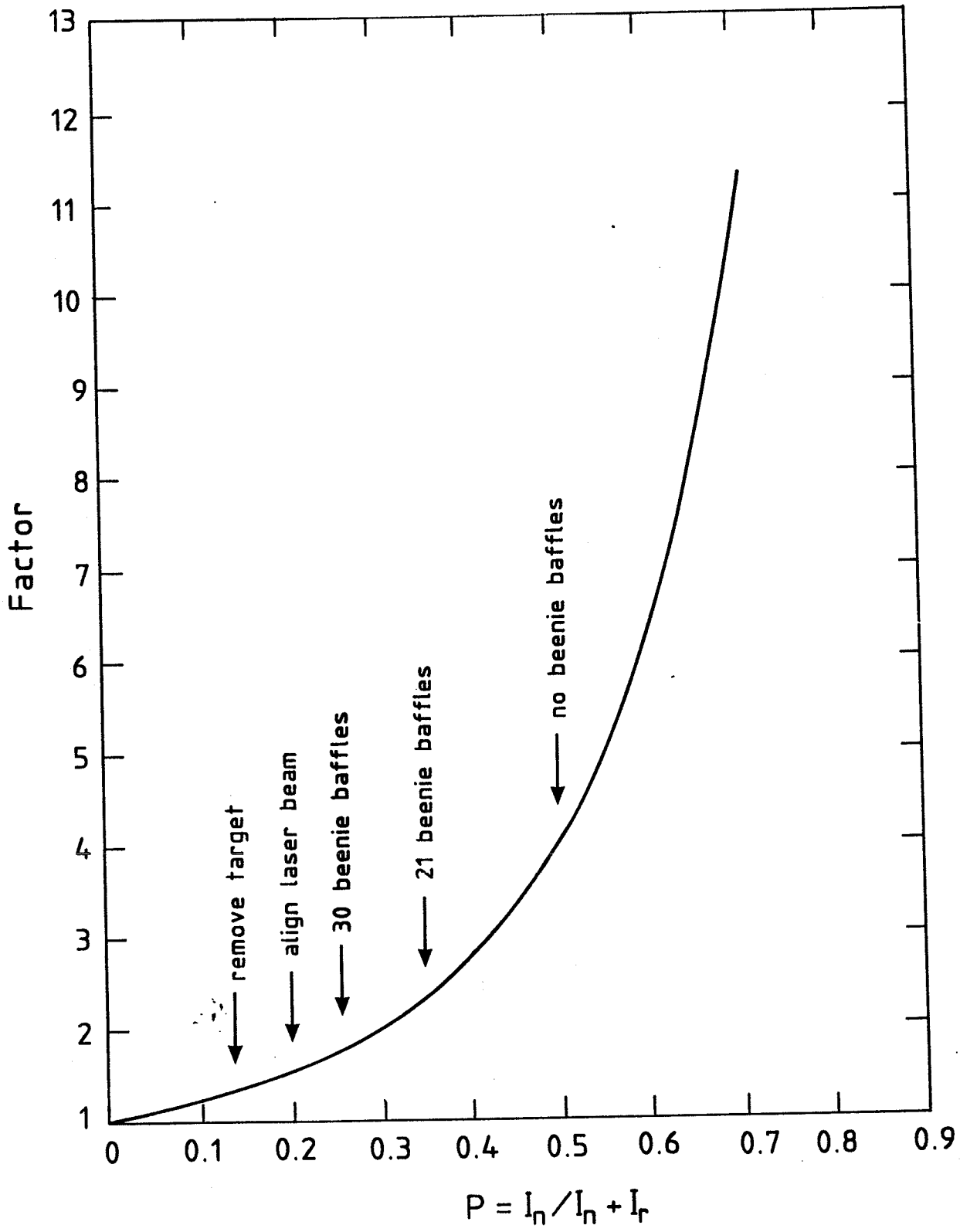
Factor
13
12
11
10
9
8
7
6
5
4
3
2
1
0
0.1
0.2
0.3
0.4
0.5
0.6
0.7
0.8
0.9
remove target
align laser beam
30 beenie baffles
21 beenie baffles
no beenie baffles
P = $I_n / I_n + I_r$

Fig. 21

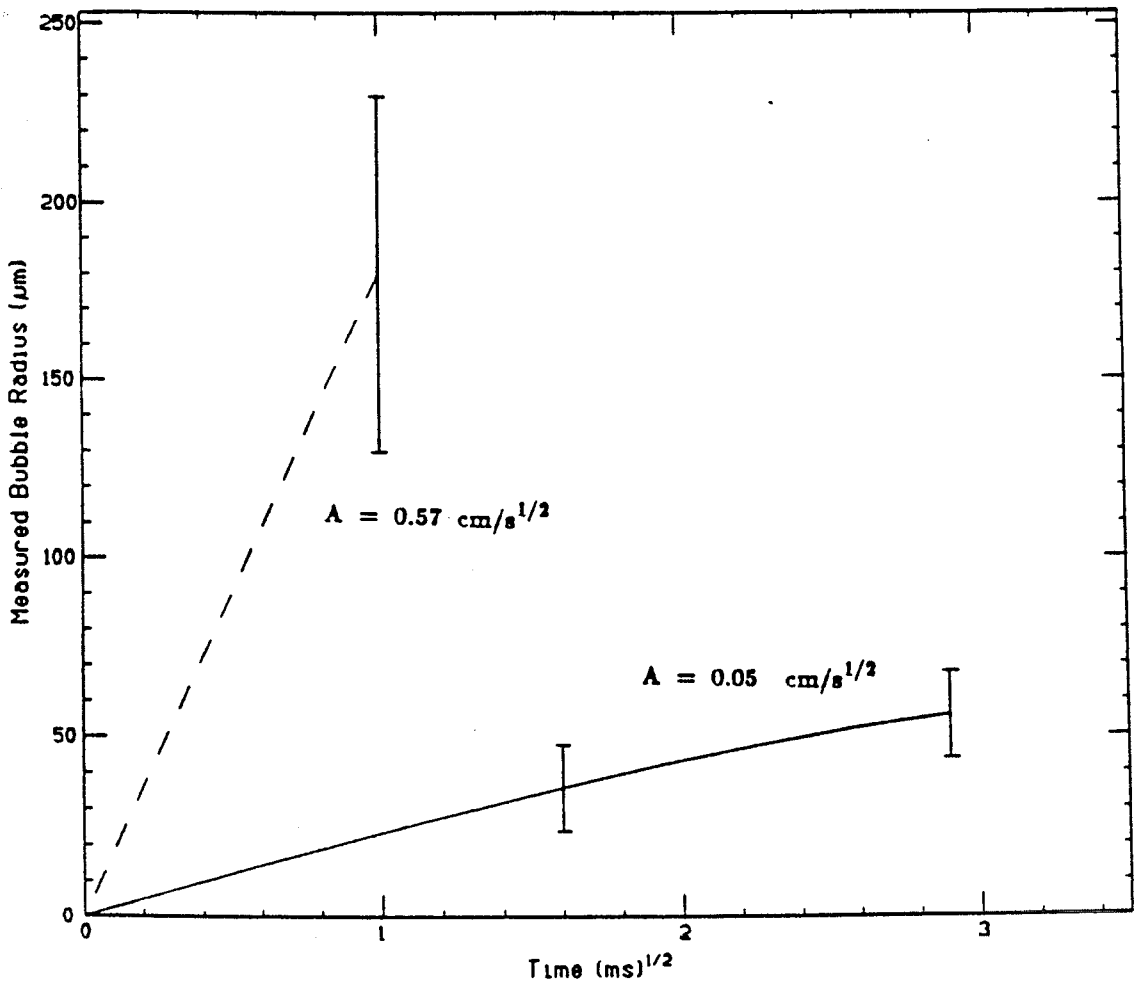
250
200
150
100
50
0
Measured Bubble Radius (μm)
A = 0.57 cm/s^1/2
A = 0.05 cm/s^1/2
0
1
2
3
Time (ms)^1/2

Fig. 22

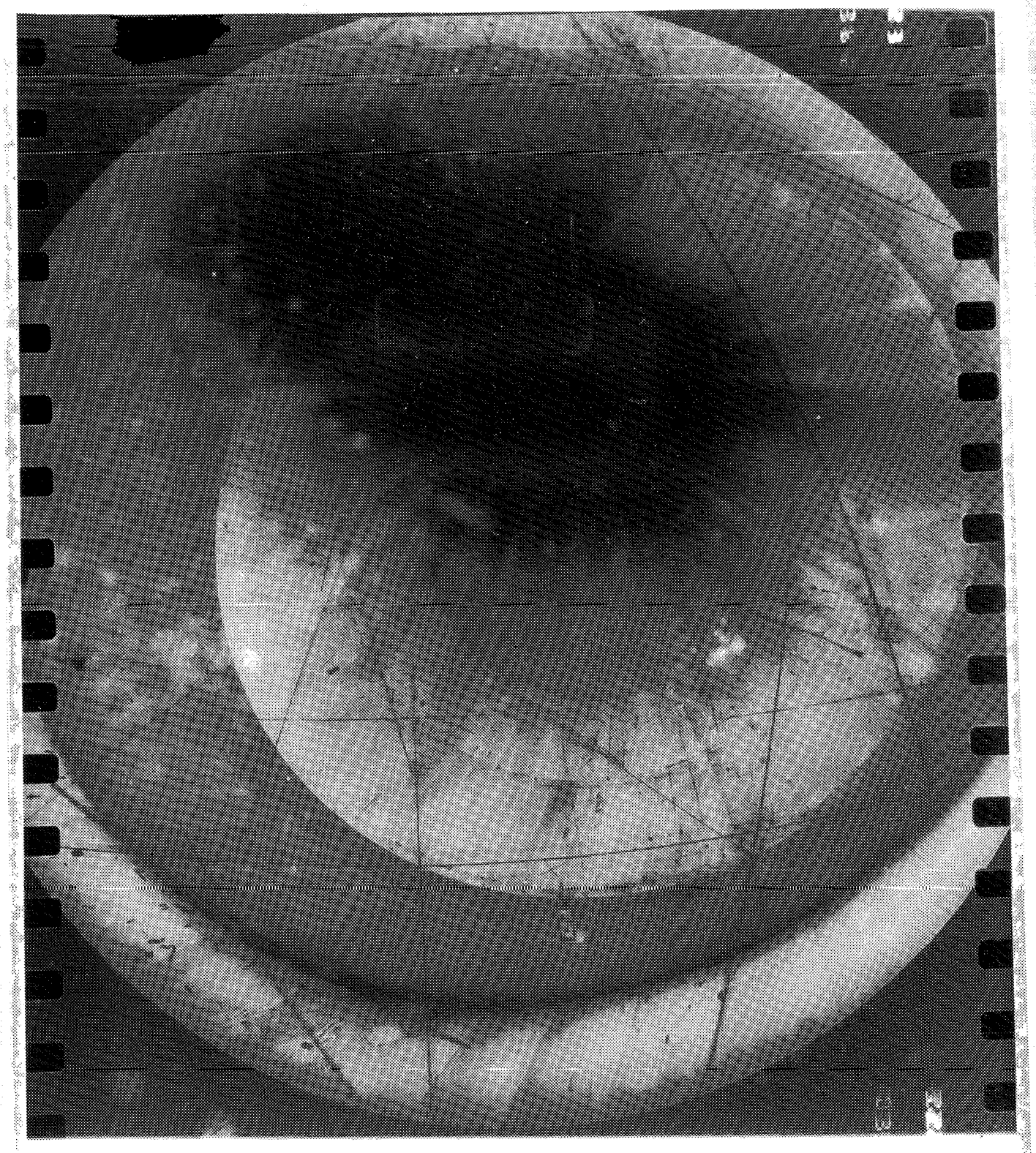

Fig. 23 (a)

Fig. 23 (b)

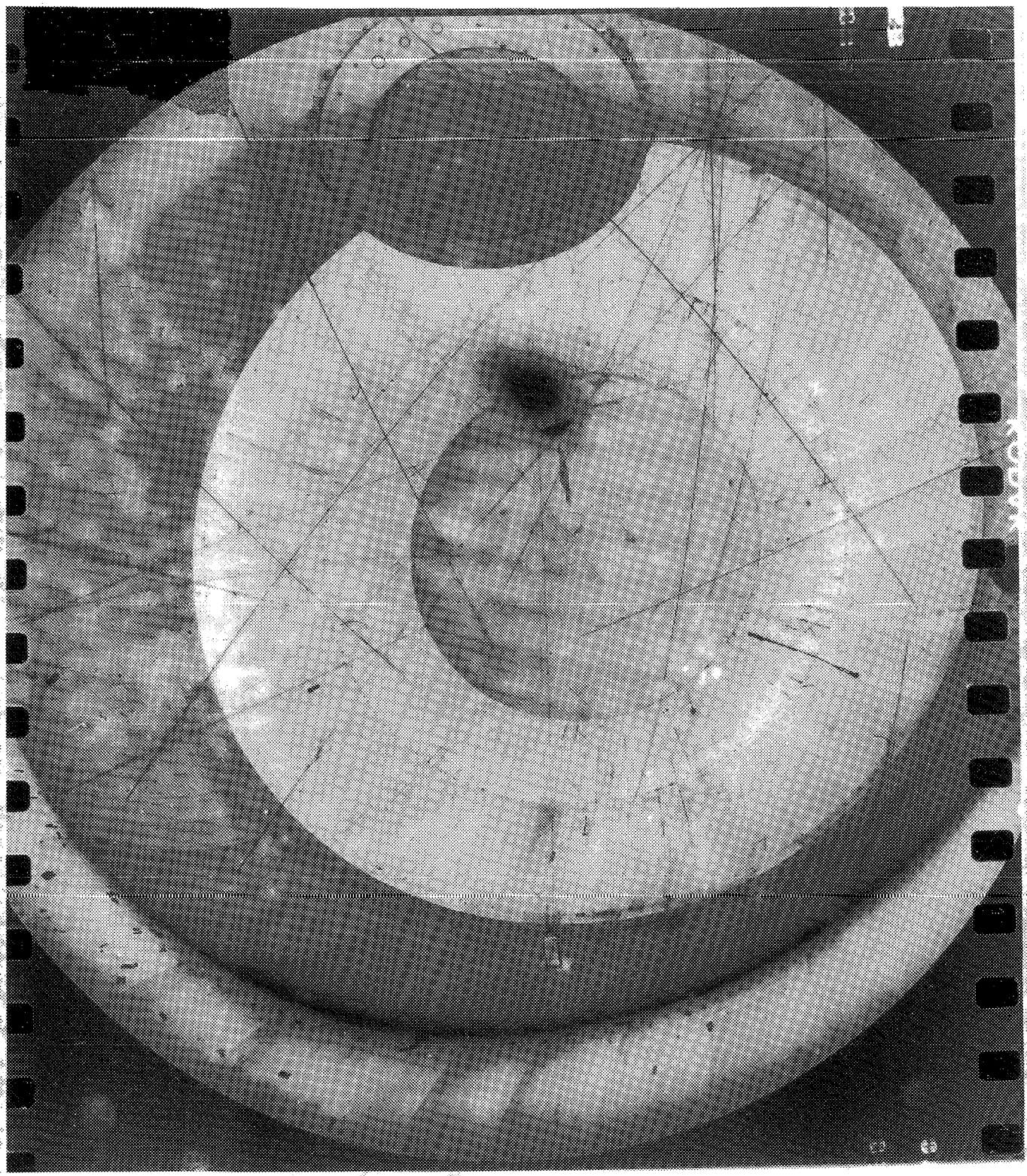

Fig. 23 (c)

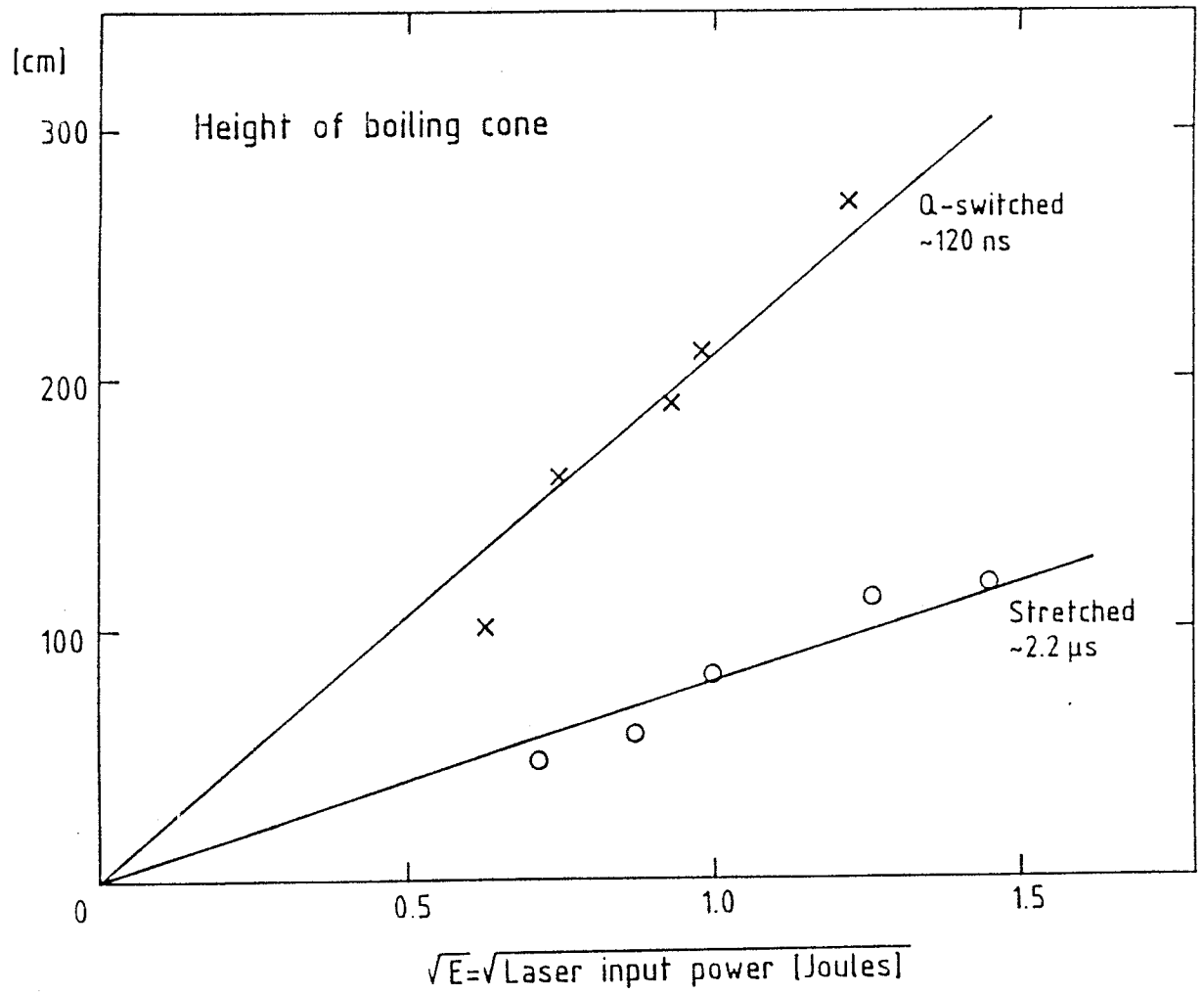
[cm]
Height of boiling cone
300
200
100
0
Q-switched
~120 ns
Stretched
~2.2 µs
0.5
1.0
1.5
√E=√Laser input power [Joules]

Fig. 24

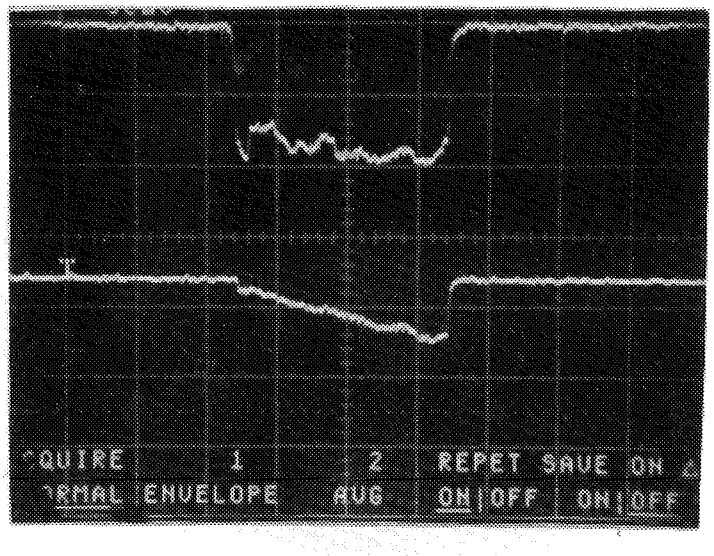

Fig. 25

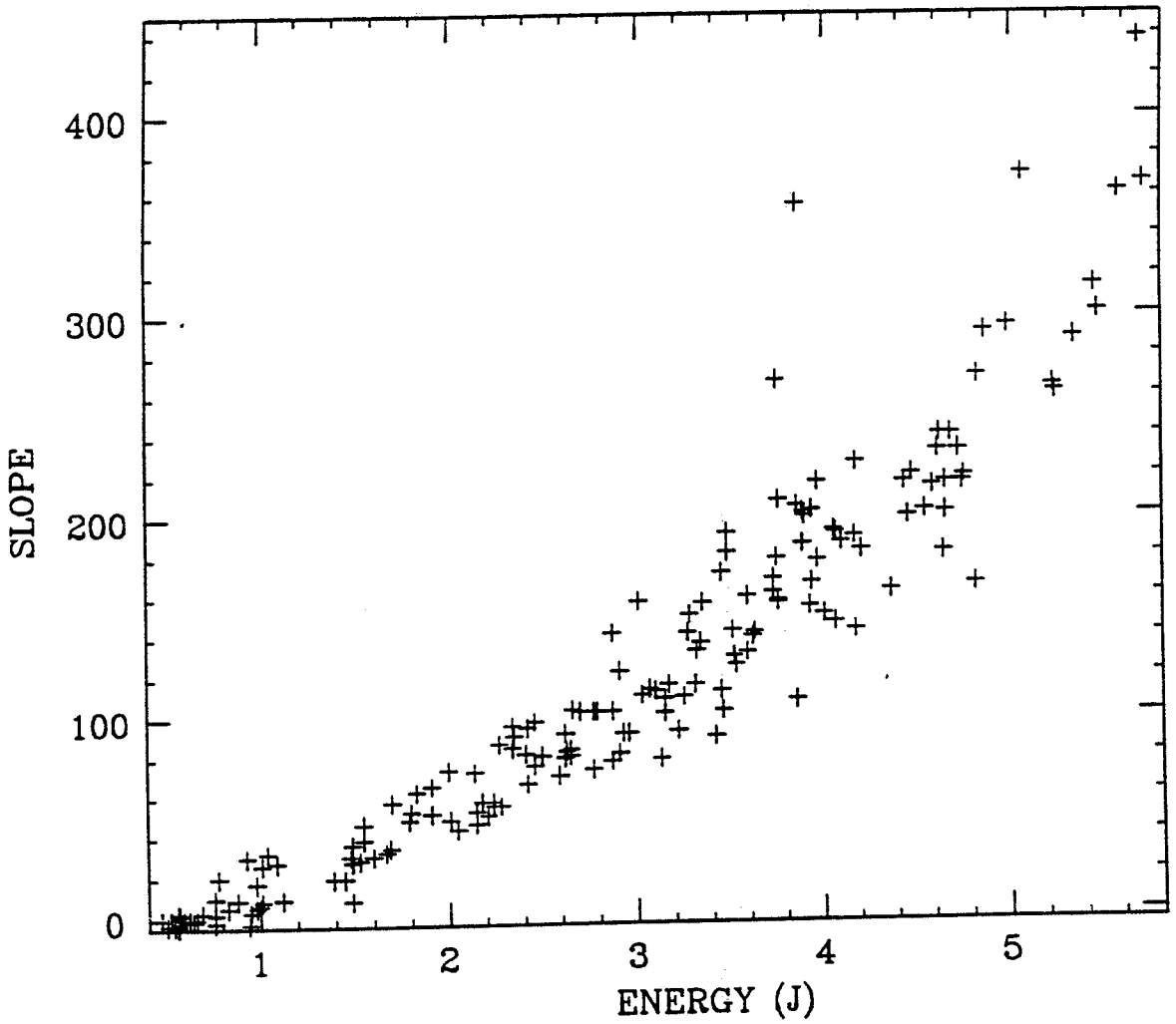

Fig. 26

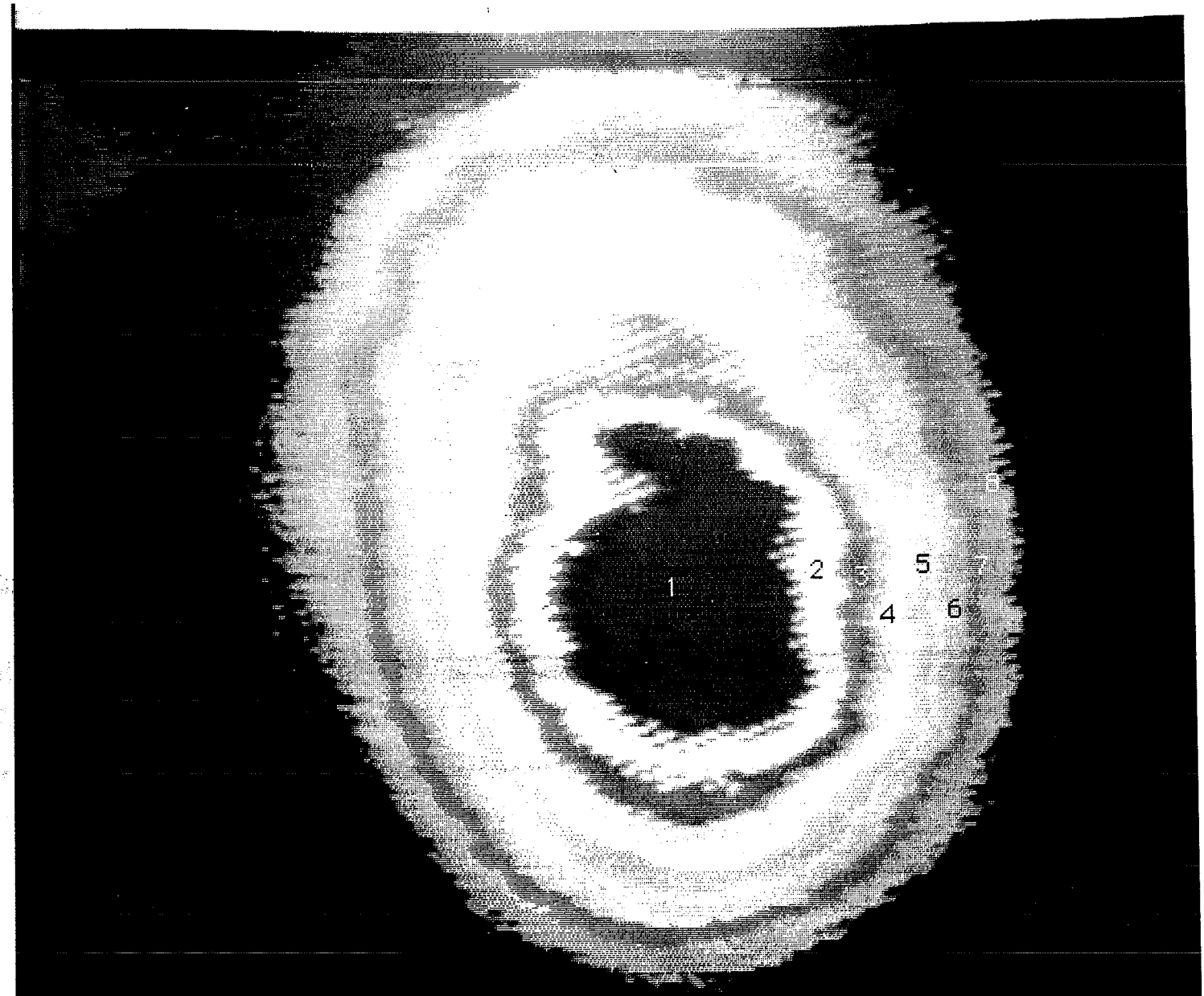

Zone #	1	2	3	4	5	6	7	8
Pixel-level	225 254	197 224	169 196	141 168	113 140	85 112	57 84	29 56

Fig. 27 (a)

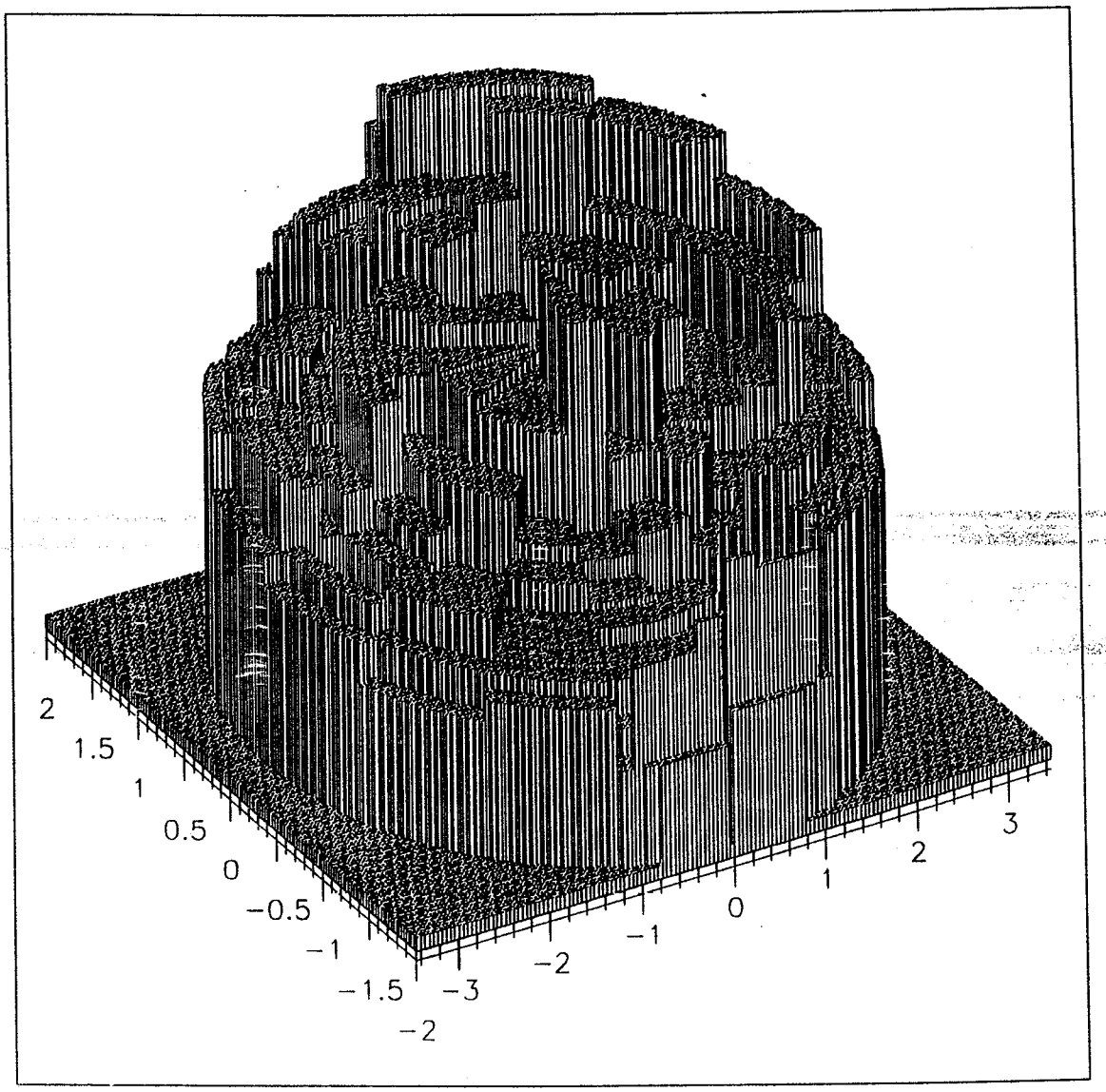

BEAM PROFILE

Fig. 27 (b)

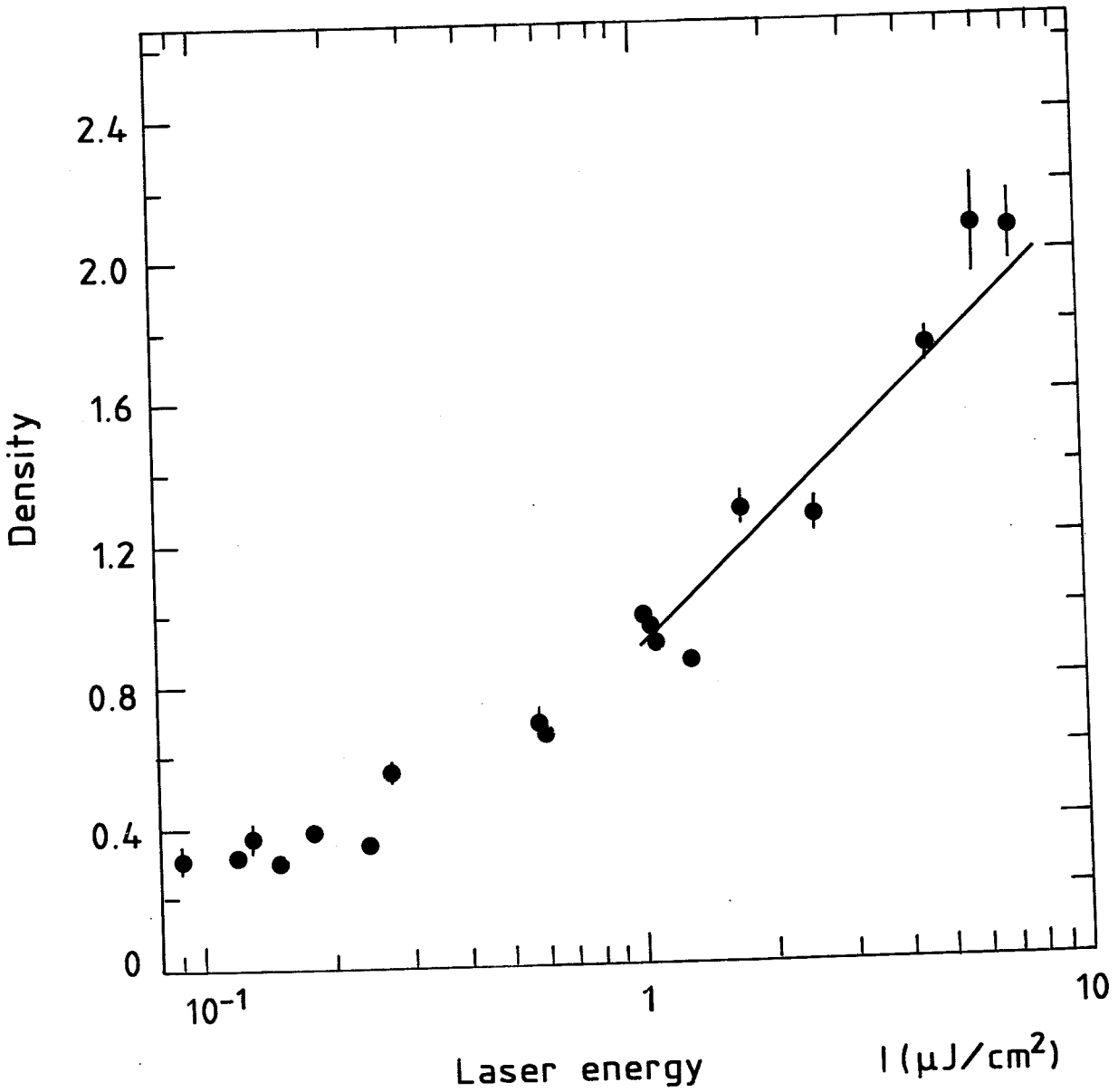

Fig. 28 (a)

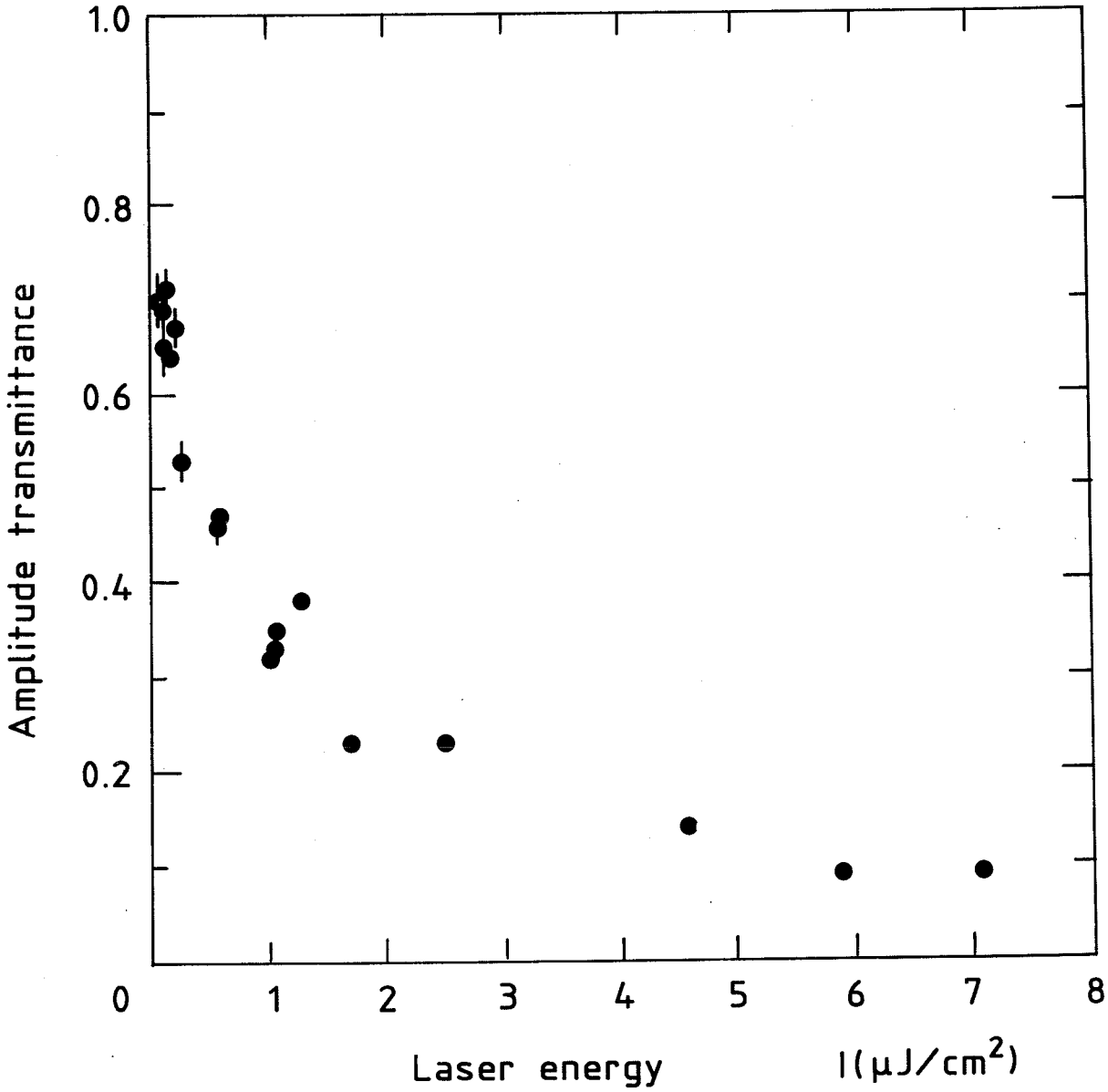
1.0
0.8
0.6
0.4
0.2
0
Amplitude transmittance
1
2
3
4
5
6
7
8
Laser energy
I(μJ/cm²)

Fig. 28 (b)

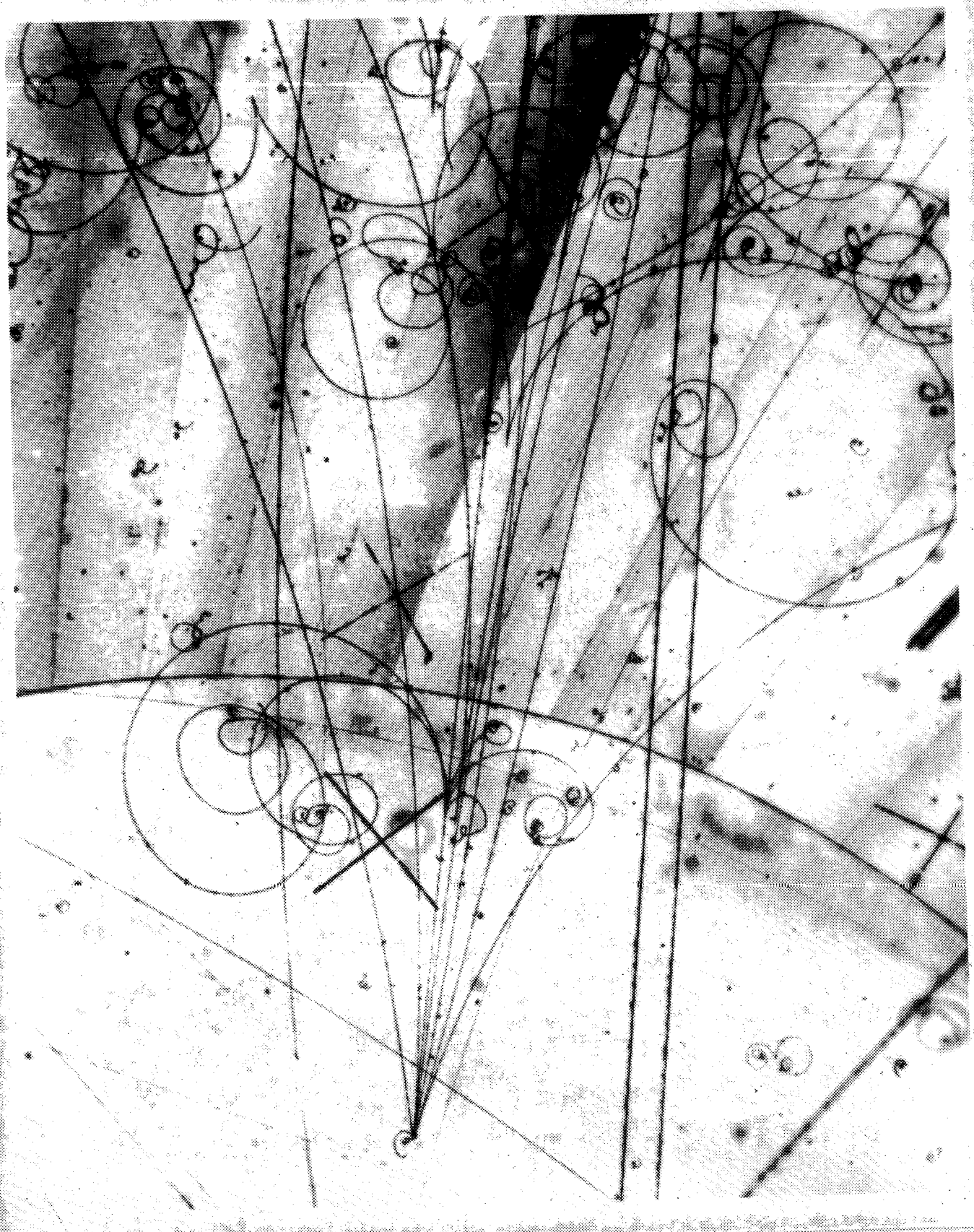

Fig. 29 (a)

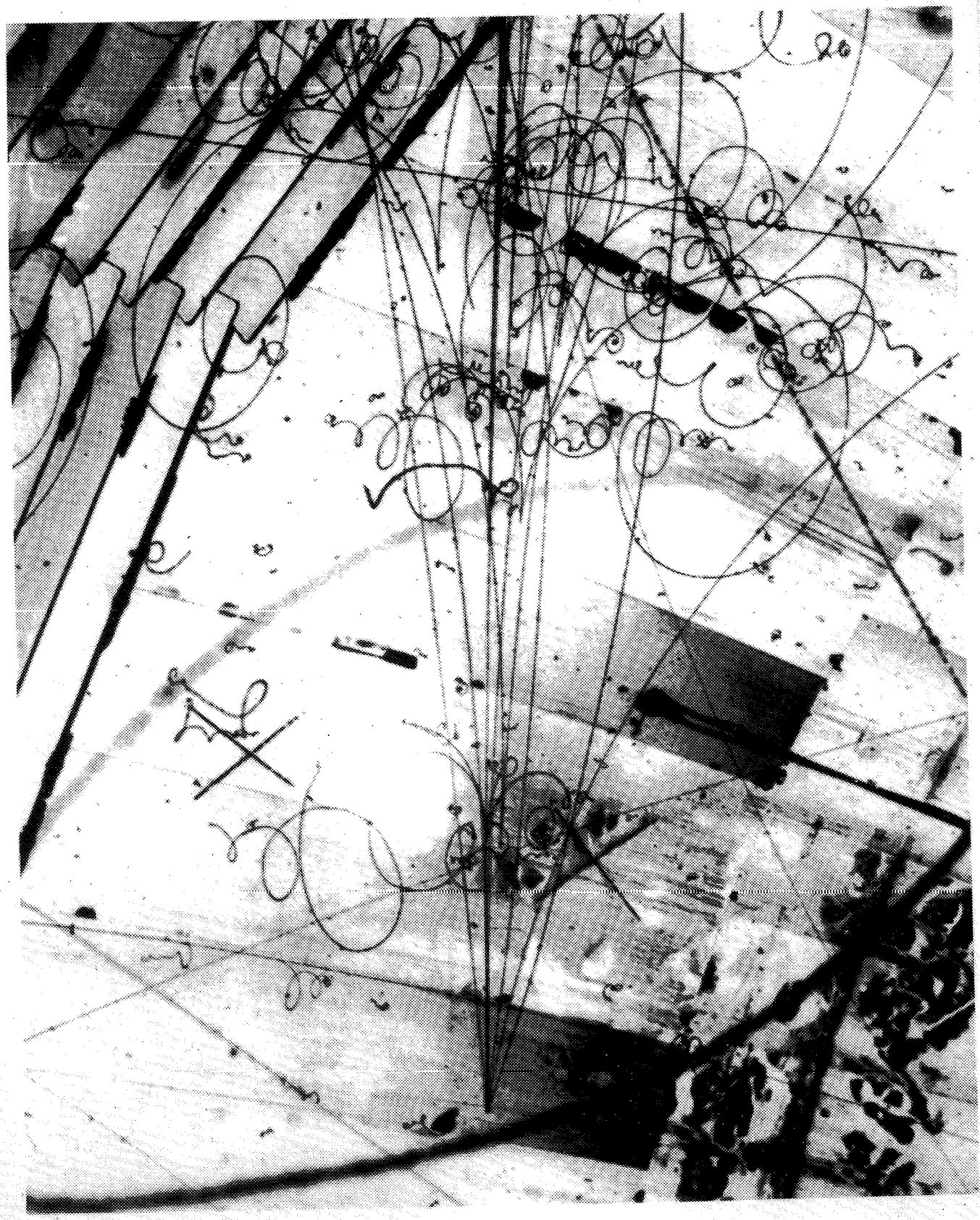

Fig. 29 (b)

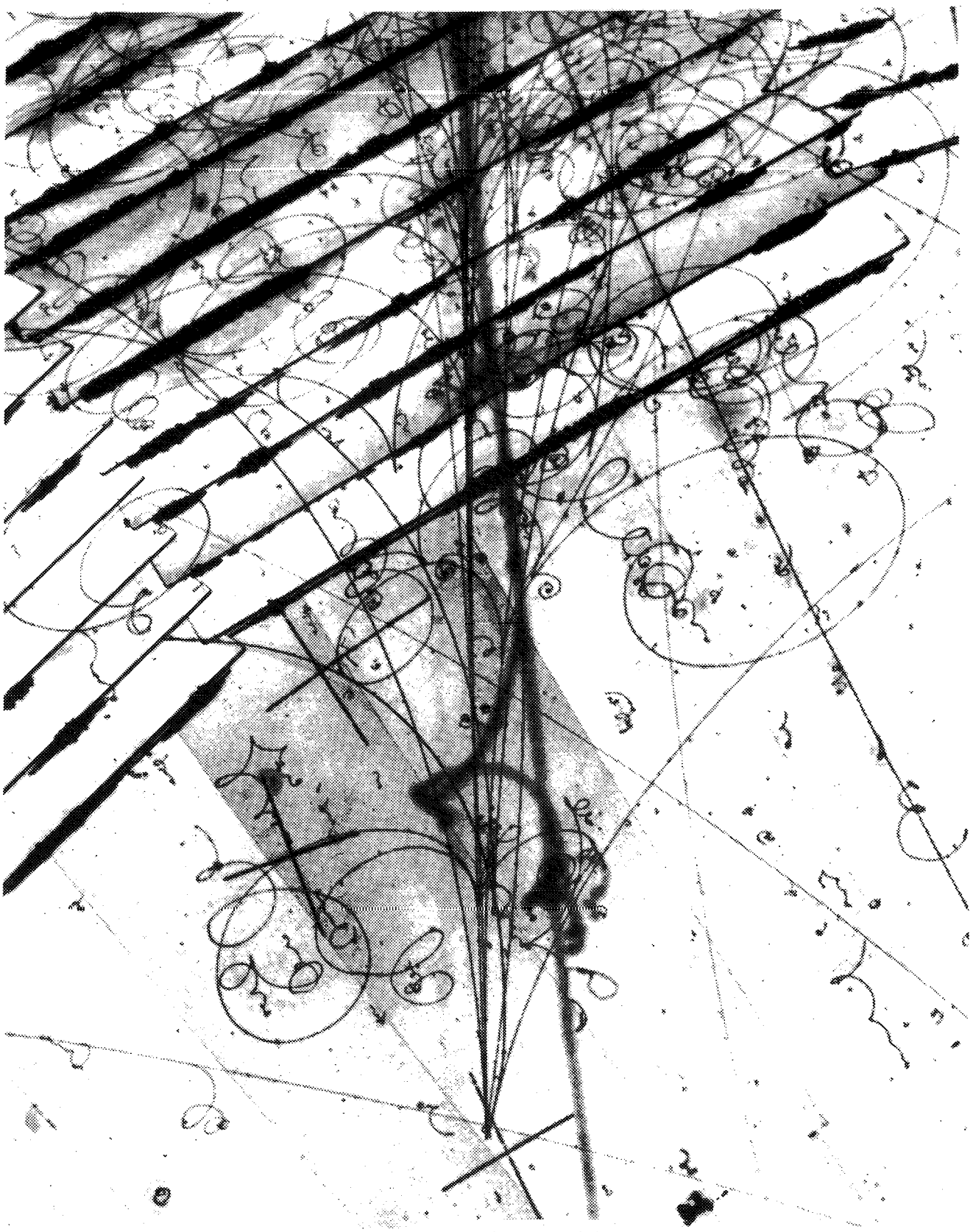

Fig. 29 (c)

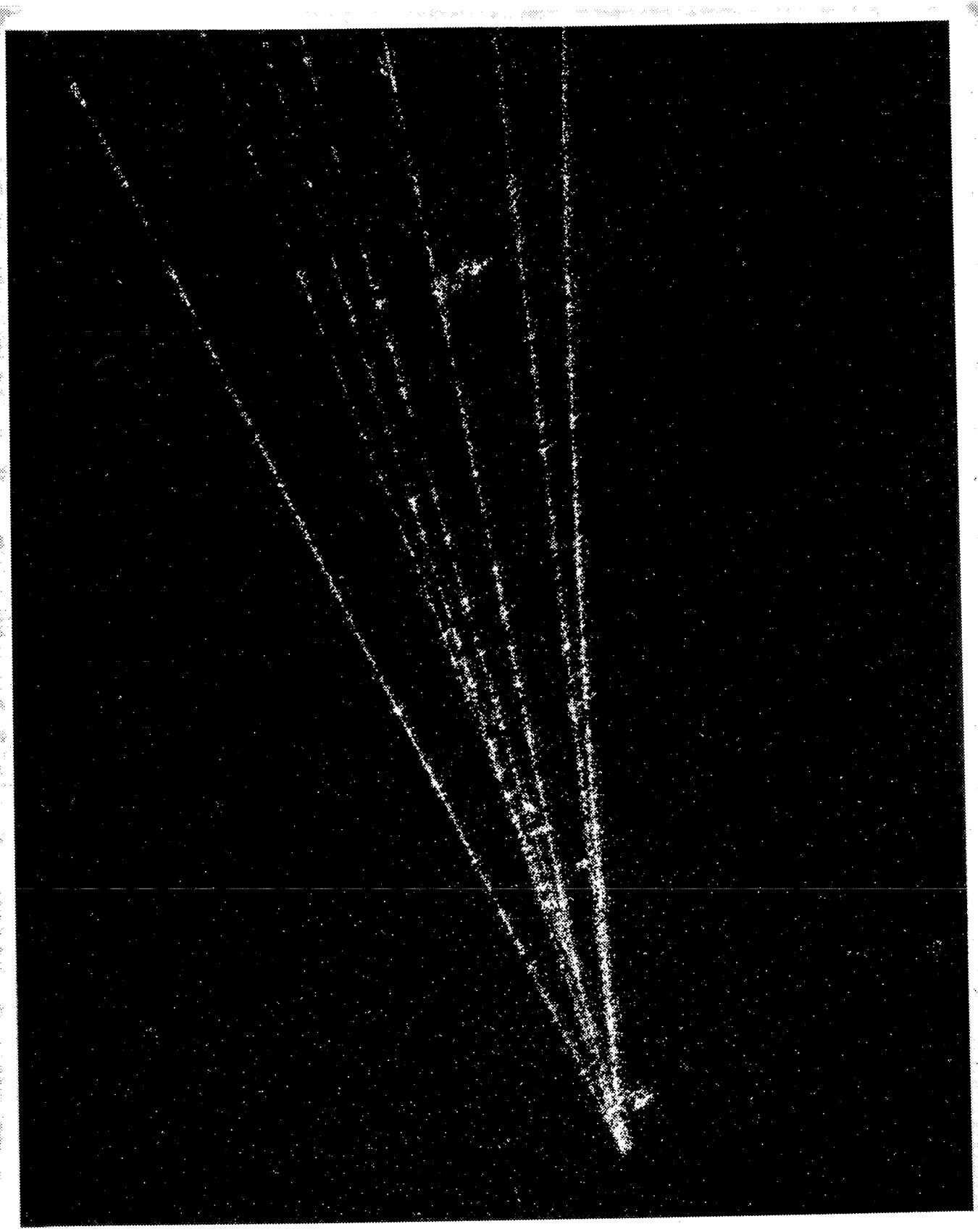

Fig. 29 (d)

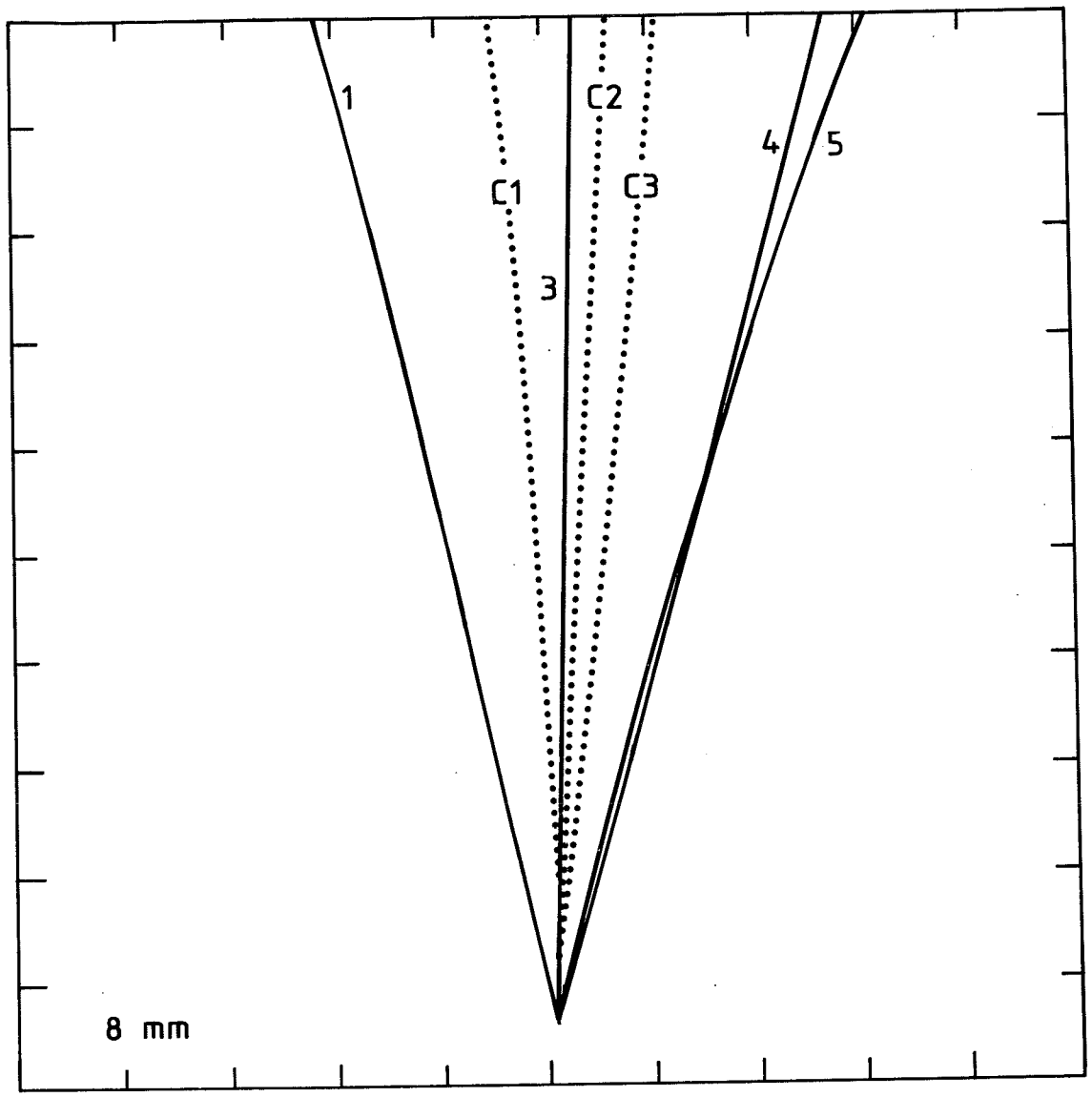

Fig. 29 (e)

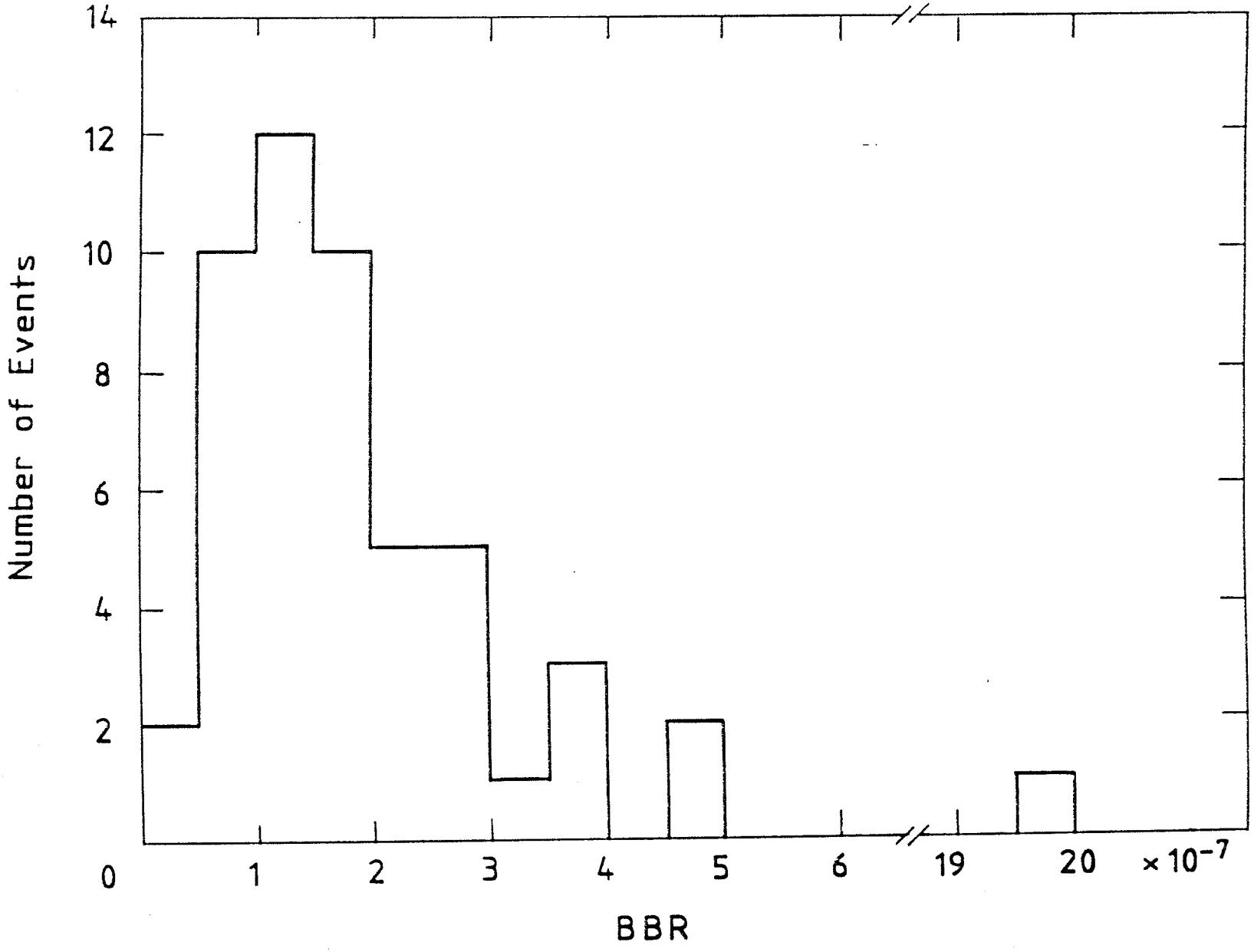

Fig. 30

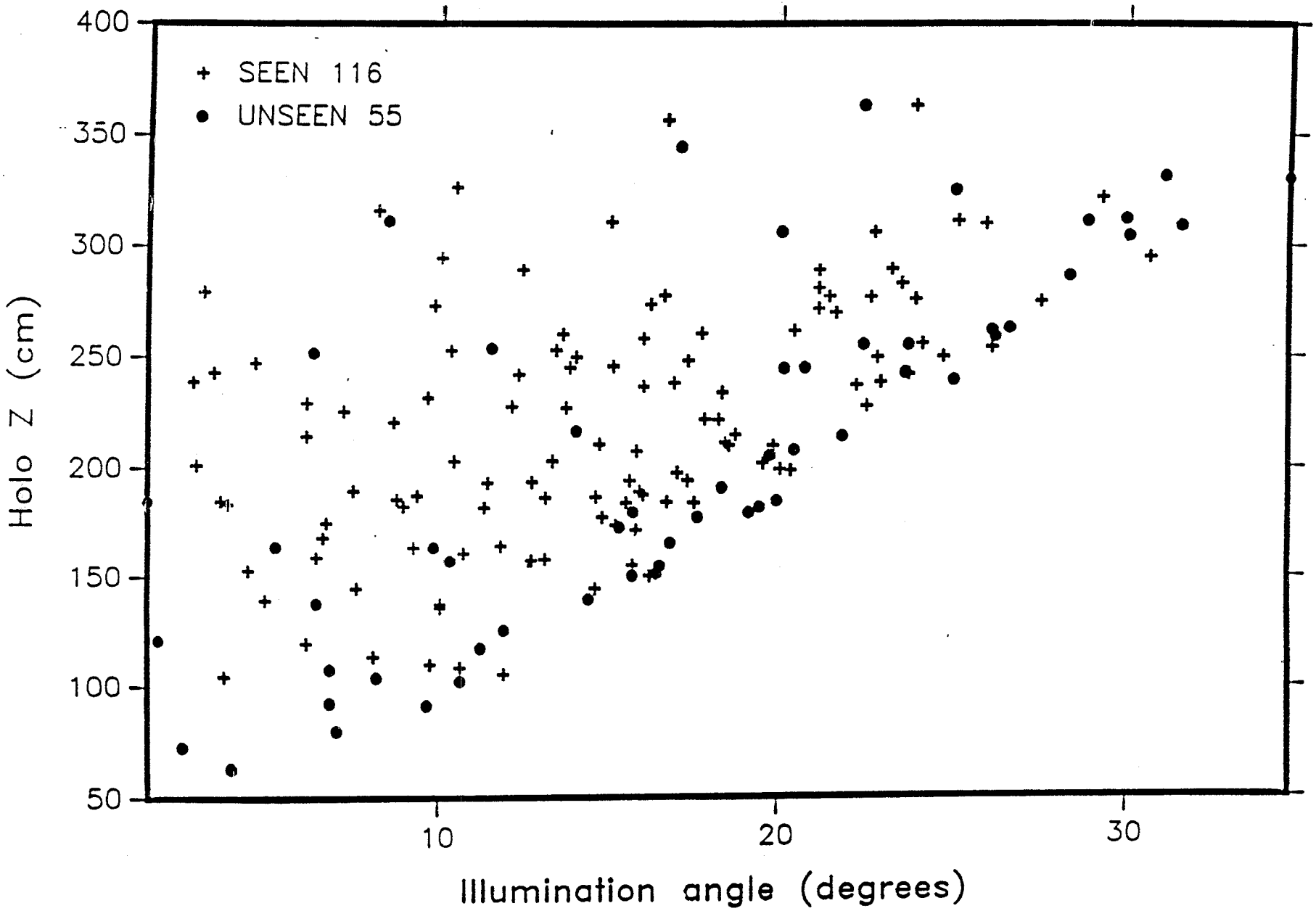
SEEN 116
UNSEEN 55
400
350
300
250
200
150
100
50
Holo Z (cm)
10
20
30
Illumination angle (degrees)

Fig. 31